North Carolina Agricultural and Technical State University

Aggie Digital Collections and Scholarship

2011

Development Of A Procedure For The Detection Of Subsurface Defects In Bridge Deck Joint Armor Using Ground Penetrating Radar And Seismic Properties Analysis

Jr. Larry Rickard
North Carolina Agricultural and Technical State University

Recommended Citation

DEVELOPMENT OF A PROCEDURE FOR THE DETECTION OF SUBSURFACE DEFECTS IN BRIDGE DECK JOINT ARMOR USING GROUND PENETRATING RADAR AND SEISMIC PROPERTIES ANALYSIS

by

Larry Lance Rickard, Jr.

A thesis submitted to the graduate faculty in
partial fulfillment of the requirements for the degree of
MASTER OF SCIENCE

Department: Civil, Architectural, Agricultural and Environmental Engineering
Major: Civil Engineering
Major Professor: Dr. Wonchang Choi

North Carolina A&T State University
Greensboro, North Carolina
2011

School of Graduate Studies
North Carolina Agricultural and Technical State University

This is to certify that the Master's Thesis of

Larry Lance Rickard, Jr.

has met the requirements of
North Carolina Agricultural and Technical State University

Greensboro, North Carolina
2011

Approved by:

_____   _____
Dr. Wonchang Choi   Dr. Taher Abu-Lebdeh
Major Professor   Committee Member

_____   _____
Dr. Miguel Picornell   Dr. Sameer Hamoush
Committee Member   Department Chairperson

_____
Dr. Sanjiv Sarin
Interim Associate Vice Chancellor for Research and Graduate Dean

iii

DEDICATION

This work is dedicated to the memory of my father, Larry Lance Rickard, who taught me the inherent value of the past. It is also dedicated to my nephew, Wyatt Colton Chapman Rickard, to whom the future belongs.

BIOGRAPHICAL SKETCH

Larry Lance Rickard, Jr. was born on 25 July 1968 in Lumberton, North Carolina. He grew up in Sanford, NC where he graduated from Lee County Senior High School in 1986. Mr. Rickard attended Campbell University briefly before beginning his career in the fields of civil engineering and land surveying. He worked in various capacities in the public and private sectors before earning his North Carolina Professional Land Surveying License in 1999. Mr. Rickard earned his Baccalaureate in Civil Engineering from North Carolina A&T State University in 2009 and became a Professional Engineer in North Carolina that same year. Mr. Rickard is a member of Tau Beta Pi and Phi Kappa Phi honor societies and the American Society of Civil Engineers. He is currently employed as a Civil Engineer with the North Carolina Department of Transportation's Location and Surveys Unit and lives with his wife in Asheboro, NC.

ACKNOWLEDGMENTS

If there is anything I learned during the process of writing this thesis, it's that I certainly wasn't working in a vacuum. It never escaped me that a multitude of people helped make this work possible - no matter how self-absorbed I seemed to get at times. It's clear I owe many people a debt I may never be able to repay.

My wife Elizabeth deserves first mention for twenty-four years' worth of love and encouragement. She's the one most responsible for goading me to complete my college education in the first place, and she's never failed to support my many ideas and schemes, no matter how daft or impractical. Only time will tell if this thesis is one of those; what is certain is that I could not have done it without her.

The rest of my family deserves some mention here, if only because I've been conspicuously absent from their lives for the past seven years. My mother, Lida Rickard and my brother, Robert C. Rickard were both in the background a lot more than I care to admit, yet still somehow managed to express their love and support - often when I need it most. I would also like to express my gratitude to my father and mother-in-law, Larry and Stella Hawk; I certainly put all that graph paper to good use!

I'm immensely grateful for the guidance and assistance I received from my faculty advisor, Dr. Wonchang Choi. He possessed an uncanny knack for making sense out of what seemed a Sisyphean task at times, and never failed to help me find the focus I needed with a unique blend of expertise, encouragement and good humor. It was indeed an honor to share this work with him; I'll miss our weekly status meeting.

The other members of my thesis committee - Dr. Taher Abu-Lebdeh and Dr. Miguel Picornell - also deserve a great measure of thanks, for both were very generous with their time and input. I would also like to thank Dr. Sameer Hamoush and the rest of the faculty, staff and students of the Department of Civil, Architectural and Environmental Engineering at North Carolina A&T State University, who have been a more or less constant part of my life for the past seven years.

I'd be further remiss if I didn't recognize the enormous amount of assistance I received from the North Carolina Department of Transportation. In the Location and Surveys Unit Charlie Brown, Joel Gulledge, Derek Bradner, Dave Langston and Mike Motsinger all provided me with crucial support at one point or another over the past seven years. Particular thanks go to Brian Flippin for his help in scanning the test structure, Matt Jones for access to the Greyhound Court Bridge, and Robert Spargo for his assistance during coring.

Finally, I consider it a privilege to have shared my graduate school experience with my friend and fellow student Jason Pontieri. During my life I've met very few people with a stronger work ethic, a sharper wit or a greater depth of common sense. While these attributes have certainly served him well, I'm not ashamed to admit that they've helped to sustain me at one time or another over the past several years. I'm proud to count him among my friends.

To all of you – and to those I've somehow failed to mention here – I give my most humble thanks. I have most definitely stood on the shoulders of giants.

TABLE OF CONTENTS

xi

LIST OF FIGURES

FIGURES **PAGE**

LIST OF TABLES

LIST OF SYMBOLS AND ABBREVIATIONS

AASHTO	American Association of State Highway Transportation Officials
ADOT	Arizona Department of Transportation
ADT	Average Daily Traffic
ASCE	American Society of Civil Engineers
ASTM	American Society for Testing and Materials
C	Capacitance (Farads)
C_o	Capacitance (Farads)
DFT	Discrete Fourier Transform
DSM	Digital Surface Model
E	Young's modulus (or modulus of elasticity)
FHWA	Federal Highway Administration
FO	Functionally Obsolete
ft.	U.S. Foot
GHz	Gigahertz
GPa	Gigapascals
GPR	Ground-Penetrating Radar
GPS	Global Positioning System
HDS	High Density Surveying
HERMES	High Speed Electromagnetic Roadway Mapping and Evaluation System
HMA	Hot-Mix Asphalt
in.	Inch

kg	Kilogram
kHz	Kilohertz
kph	kilometers per hour
ksi	kips per square inch (1 kip=1,000 pounds)
m	meter
MHz	Megahertz
mm	millimeter
mph	miles per hour
N/A	Not Applicable
NCDOT	North Carolina Department of Transportation
NDE	Non-Destructive Evaluation
NDT	Non-Destructive Testing
NDT/E	Non-Destructive Testing and Evaluation
PennDOT	Pennsylvania Department of Transportation
R	Reflection coefficient (unitless)
RC	Reinforced Concrete
SD	Structurally Deficient
SPA	Seismic Properties Analyzer
SR	Sufficiency Rating
SSM	StructureScan™ Mini
SV	Single vehicle weight limit
TDOT	Tennessee Department of Transportation
TIP	Transportation Improvement Program (NCDOT)
TTST	Tractor-trailer weight limit

USDOT	United States Department of Transportation
USW	Ultrasonic Surface Wave Analysis
VI	Visual Inspection
ε	Dielectric constant of a material (unitless)
v	Poisson's ratio
ρ	Mass density

ABSTRACT

Rickard, Larry Lance, Jr. DEVELOPMENT OF A PROCEDURE FOR THE DETECTION OF SUBSURFACE DEFECTS IN BRIDGE DECK JOINT ARMOR USING GROUND PENETRATING RADAR AND SEISMIC PROPERTIES ANALYSIS. **(Major Advisor: Wonchang Choi)**, North Carolina Agricultural and Technical State University.

The overall performance and longevity of highway bridges is highly dependent upon the integrity of their deck joints. The North Carolina Department of Transportation has experienced problems with bonding in the armored deck joints installed on many of its bridges. These defects have historically been detected using conventional NDT techniques such as visual inspection, chain-dragging and by detecting sounds made by the joint due to passing traffic. By the time these methods are effective the joint has usually failed, however, and must be replaced.

Future bridge maintenance challenges will demand the development of techniques and procedures to detect and monitor these defects before they become apparent. This research seeks to extend the use of three NDT/E techniques – High-Density Surveying (HDS), Ground-Penetrating Radar (GPR) and Seismic Properties Analysis (SPA) - to the detection and quantification of subsurface defects and anomalies in and around bridge deck armor. All three methods were employed on an abandoned bridge in Winston-Salem, North Carolina and their results evaluated against actual core specimens from the deck. Any challenges peculiar to these techniques with regard to armored deck joints were also investigated and documented, as was their potential as alternatives – or adjuncts to – conventional NDT/E techniques.

CHAPTER 1

INTRODUCTION

America's highway system is comprised of over 4 million miles of roadway of all types, of which bridges are a critical link. The number of highway bridges in service nationwide has grown steadily from approximately 578,000 in 1992 to 603,254 as of December 2009. Of this total, 78,468 – or 13 percent - were classified as Functionally Obsolete (FO), while 71,179 - or 11.8 percent - were classified Structurally Deficient (SD). While the total of SD structures has steadily decreased over the last twenty years, the number deemed FO has remained relatively steady (Figure 1.1). Overall, 24.8 percent of all bridges in the United States were considered in need of repair, rehabilitation or replacement [1].
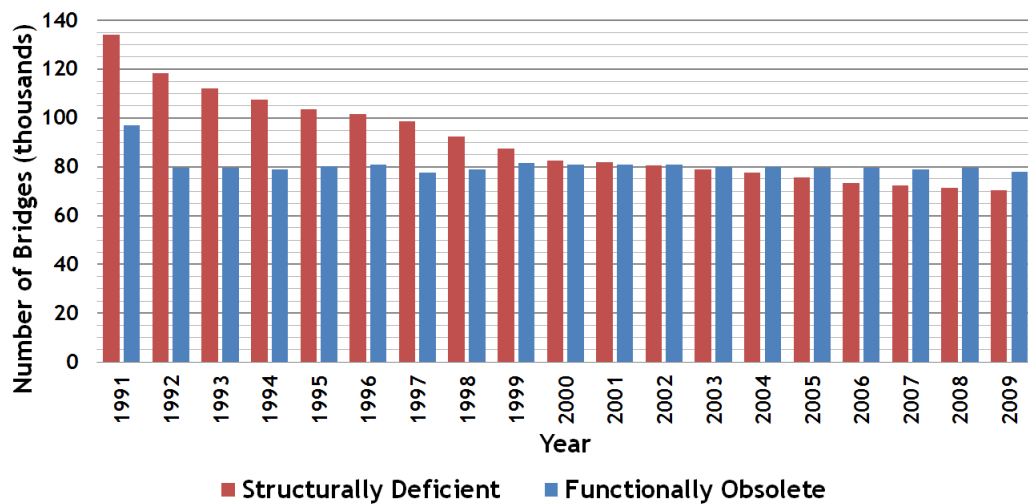
Figure 1.1. Structurally Deficient vs. Functionally Obsolete structures in the U.S.
(Adapted from "Our Nation's Highways 2010")

The American Society of Civil Engineers (ASCE) reported in 2009 that 30 percent of North Carolina's bridges were structurally deficient or functionally obsolete [2]. The North Carolina Department of Transportation's (NCDOT) own figures are less charitable. As of January 2010 there were 13,251 bridges in its inventory. Of these, 2,739 – or 20.6 percent - were deemed functionally obsolete, while 2,557 – or 19.29 percent - were considered structurally deficient [3]. A total of 39.9 percent of North Carolina's highway bridges were considered inadequate to meet the state's current or future traffic demands.

There are many factors which can affect the overall performance and longevity of highway bridges, including the integrity of its deck joints. They do not generally constitute a major portion of a bridge's construction cost, yet over time joints that are improperly designed, installed or maintained can cause damage that far exceeds their relative size and initial cost. This possibility has become a concern with the NCDOT, which has experienced problems with the bonding in the armored deck joints installed on many of its bridges. These bonding defects have historically been detected using conventional Non-Destructive Testing and Evaluation (NDT/E) methods, which generally include visual inspection (VI), chain-dragging, hammer blows and detecting the sounds made by traffic passing over suspect joints. The problem common to these techniques is that damage to the joint in question is usually severe enough to warrant its replacement by the time such methods are effective.

The use of advanced NDT/E technology - Ground-Penetrating Radar (GPR) and Acoustic methods such as Impact-Echo (IE) and Ultrasonic Surface Wave Analysis

(USW) in particular − is one possible solution to this problem. Their effectiveness in collecting quantitative data on delamination in bridge decks has been well established through decades of study and field use, and has been repeatedly verified with ground-truth data [**4**] [**5**]. In the majority of these works, the focus has been on whole deck assessment and not the examination of any particular area. There were several reasons for this, but the ones common to most of the technologies used were cost, cumbersome equipment and the lack of real-time data display.

NDT/E technology is advancing rapidly, however. The current generation of portable equipment is relatively inexpensive, exhibits improved diagnostic capabilities and is easily deployed by a small group or a single operator. They are particularly well-suited to studies of highly localized areas such as bents, approach slabs and deck joints. All of these attributes could make these newer technologies an attractive alternative to the conventional traditional NDT/E methods that are normally used during routine bridge inspections.

1.1 Functional Obsolescence vs. Structural Deficiency

The terms *Functionally Obsolete* (FO) and *Structurally Deficient* (SD) have thus far been used to describe a bridge's general status as a working transportation structure. They have become a part of the American lexicon in recent years, yet are often misunderstood and used interchangeably by the general public. This is understandable considering that they are not entirely independent of one another; there is some overlap in

3

their definitions. The distinction between the two is so important to the field of bridge management, however, that their further clarification is warranted here.

1.1.1 Functional Obsolescence

The NCDOT defines the term *functionally obsolete* thus [**3**]:

> A bridge is considered Functionally Obsolete if it is narrow, has inadequate under-clearances, has insufficient load carrying capacity, is poorly aligned with the roadway, and can no longer adequately service today's traffic.

Therefore, a structure is classified as *functionally obsolete* when certain aspects of its design fail to meet certain current criteria. Because a given structure was almost certainly considered adequate at the time it was built, it can be surmised that this failure is almost entirely due to changes in those properties extrinsic to the structure itself. Among those possible:

1) Changes in engineering standards or statutory requirements.

2) Changes in the nature of the obstacle being crossed.

3) Increases in loading due to traffic volume and/or gross vehicle weight.

For example, a bridge built with two 10 ft. (3.1 m) lanes in 1939 would almost certainly be considered FO today, simply because modern design practices dictate the use of wider lanes. Likewise, cumulative increases in runoff over time could raise the flood elevation at a given bridge, increasing the likelihood of scour or overtopping. It is important to note that a structure determined to be FO is not necessarily lacking in its original strength or structural integrity; it may be perfectly sound. On the other hand, certain aspects of a bridge that are deemed obsolete – older types of unsealed deck joints

4

for example – may contribute to the degradation of a structure over time to the point where it could classify as *structurally deficient*.

1.1.2 Structural Deficiency

A structure is classified as being *structurally deficient* when its intrinsic properties of strength and integrity have been compromised in some way. For example, a routine inspection may reveal excessive spalling on a bent that may cause a loss of section severe enough to warrant a reduction in load capacity. Section loss due to corrosion at the ends of steel deck girders is particularly common in regions of the United States where de-icing agents are used, and if severe enough can cause a corresponding reduction of shear strength. It is important to note that in its definition of structural deficiency, the NCDOT makes no distinction between a reduction in load capacity due to structural deterioration or that due to the limitations inherent to the original design. This overlap with the FO definition is the probable cause of confusion among the public at large.

1.2 Case Study: Church Creek Bridge, Rowan County, NC

NCDOT's Church Creek Bridge on Secondary Road (SR) 1004 in Rowan County (Figure 1.2) is a practical example of a structure that is both functionally obsolete and structurally deficient. It also serves to illustrate the potential for damage that may result from faulty or poorly maintained joints over time. Although the sealed butt-type joint likely used on this structure is not representative of the armored joints that are the focus of this study, the damage it had sustained is typical of that which may occur on bridges with defective joints of any type.

Figure 1.2. Church Creek Bridge looking east.

1.2.1 Background and Construction

The Church Creek Bridge carried the two lanes of Secondary Road 1004 (also known by the local name of Stokes Ferry Road) in an east-west direction over a small tributary of the Yadkin River known as Church Creek. It was built in 1946 as Federal Aid Project Number 7-351 by or for the North Carolina State Highway Commission, the forerunner of today's NCDOT. As of 2010 it was listed in the NCDOT bridge inventory as Rowan County Bridge Number 790143. Other than routine maintenance and deck resurfacing, the bridge had changed little since its construction.

Its superstructure was comprised of a series of three simply-supported spans; two approach spans of 25 ft. 6 in. (7.8 m) each and one 35 ft. 0 in. (10.7 m) center span, for a total length of 86 ft. (26.2 m) (Figure 1.3). Each span consisted of a reinforced concrete deck supported by four steel girders, the ends of which rested on simple steel bearing

plates. On either side of the deck protrusions known as parapets were cast at regular intervals. Reinforced concrete guardrails - known as parapet rails – were cast atop these. The end bents were reinforced concrete caps poured in place over steel piles and the two interior bents were of reinforced concrete post-and-beam construction. Over the previous decades the original concrete wearing surface had been overlaid with hot-mix asphalt concrete (also known as "bituminous surface treatment" by NCDOT). The construction details of the deck joints were unknown, but were assumed to be a type of sealed butt joint.

1.2.2 Functional Obsolescence

This is an example of a structure that was both functionally obsolete and structurally deficient. The last field inspection for this bridge was performed on September 24, 2010 and the resulting report listed its condition as "poor", with a sufficiency rating (SR) of 27.8. The posted single vehicle load limit (SV) was 22 tons (20 metric tons) and the tractor-trailer/semi-trailer load limit (TTST) was 28 tons (25.4 metric tons) [6]. Its FO status was determined by several factors, including deck width and deck elevation [7].

With regards to deck width, Figure 1.2 shows that the deck was only wide enough to accommodate the actual travel lanes. The problem wasn't the 12 ft. (3.7 m) width of the individual lanes - standard for most modern bridges - but the lack of additional clearance toward the barrier rails. This left little room for oversized vehicles and didn't allow space for water to drain during periods of heavy rainfall. The scuppers at the base of the rail were also prone to clogging with road debris, which also hindered drainage.

7
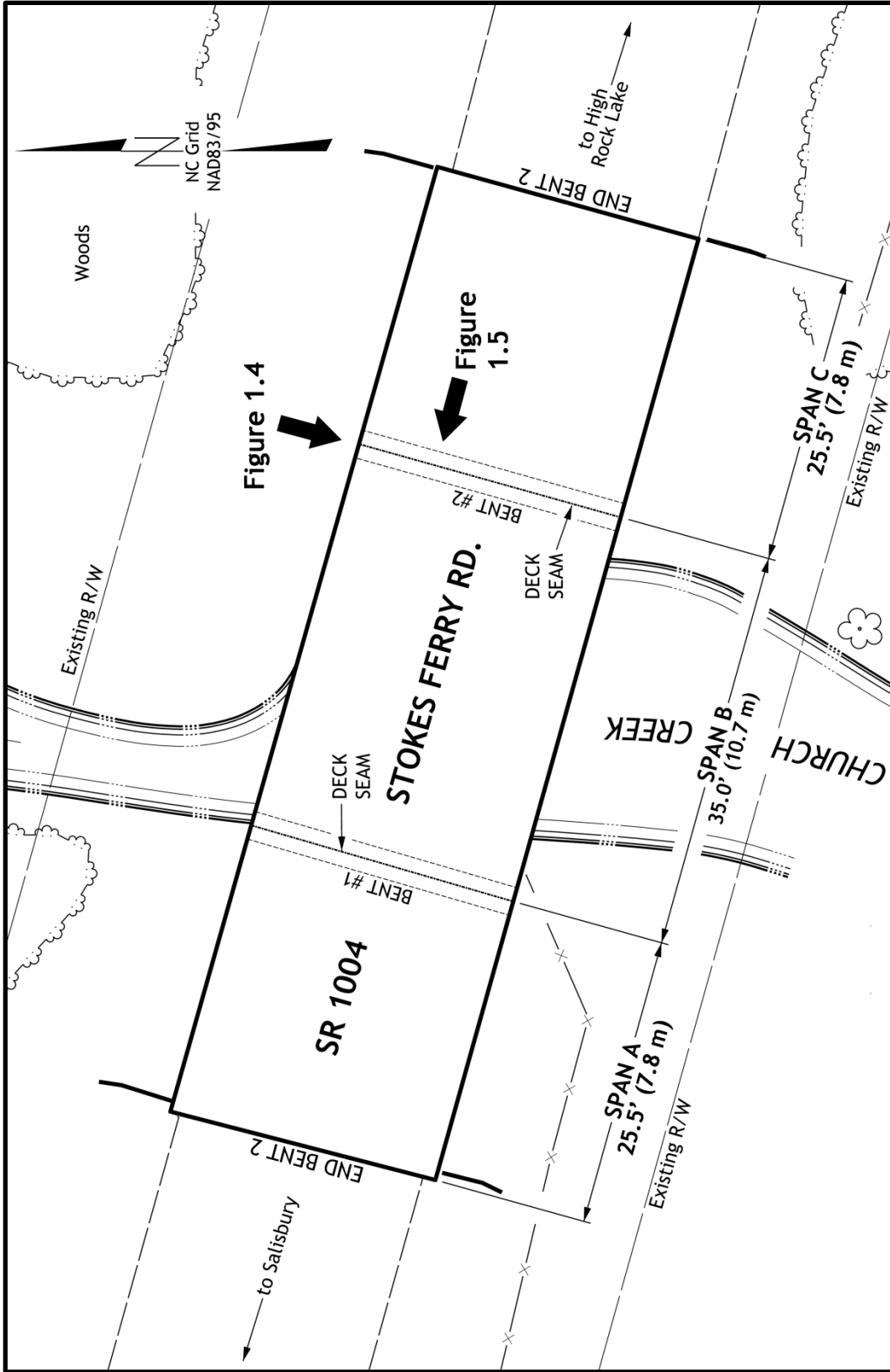
Figure 1.3. General arrangement of Church Creek Bridge. Figure not to scale.

8

The bridge deck was also relatively low, making it prone to overtopping during a major storm event. No evidence was found during research that this had in fact occurred, but the field inspection report did note that the waterway (Church Creek) had risen to within one foot of the bottom of the girders at some time in its recent history. This was of concern because the lowest bridge seat elevation was measured at 665.94 ft. (203.0 m); the 100-year flood elevation was 666.5 ft. (203.1 m). While a 100-year storm event would not have necessarily overtopped the deck, it is possible that extensive scouring damage could have occurred around the substructure.

Storms of this magnitude are also capable of moving large amounts of debris such as large limbs and small trees. These could have become lodged against the two center bents, creating a straining effect that would in all likelihood have exacerbated the flooding. The resulting forces produced by this combination could have significantly damaged or destroyed the structure.

Although it was not specifically noted in the report, it can be inferred from the NCDOT's own definition of FO that the structural complexity of the Church Creek Bridge was a third factor that severely limited its value as an active transportation structure. Three spans was a relatively high number for a structure this size by present-day standards. While this design was easily and cheaply built with the technology and methods then available, it also increased the number of structural members – including joints - to be inspected and maintained. A single-span replacement of modern construction would have far fewer structural elements than the original structure, and would eliminate the need for the two center bents and the two interior deck joints.

1.2.3 Structural Deficiency

Its SD status was determined primarily by evidence of extensive deterioration in several of the major structural members, a substantial amount of which was caused by apparent chloride intrusion due to seepage through the original joints. Some of this seepage undoubtedly occurred during the early life of the structure when its original bare concrete wearing surface was still exposed. As that surface deteriorated, at least one layer of asphalt concrete was applied. When fresh, this additional cover helped seal the original deck joints but decades of movement, freeze-thaw cycles, etc. caused cracks to appear, allowing further seepage.

Figure 1.4 illustrates the damage to the northeastern side of Bent 2 (see Figure 1.3 for the exact location). Apparent chloride intrusion had caused corrosion of the rebar, resulting in spalling of the exterior concrete (A). Years of direct exposure to water and de-icing agents had caused extensive corrosion of the girder ends, with a resulting loss of section on both. This loss was much more severe on the lower flanges of each girder, where water tended to accumulate. Delamination of the steel in the lower flange was evident at (B); this would likely exacerbate any reduction in shear capacity caused by section loss in the web, shown at (C). Corrosion of the bearing bolts (D) was so severe that only vestiges of them remained. There was little or no sound steel left to fix the girders in place.

Water infiltration from the unsealed deck joint above had also caused chloride intrusion of the concrete in the deck and the diaphragms (Figure 1.5). This resulted in rebar corrosion and spalling (E) just as severe as that found on the exterior girders. The

spalling along the diaphragm shown was extensive enough to have caused an almost complete loss of development length in the rebar (F), compromising this member's ability to carry tensile loads along its bottom half. This ultimately caused the shear cracking at (G).
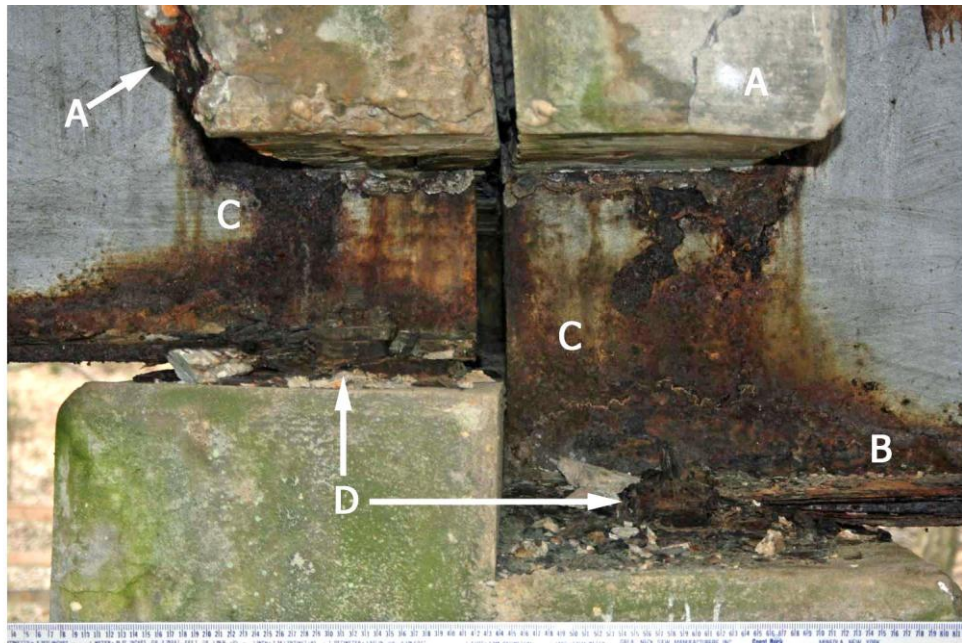
Figure 1.4. Damage to the northern end of Bent 2.

1.2.4 Candidate for Replacement

NCDOT bridge managers considered the factors described in the preceding paragraphs to be severe enough to warrant replacement of the entire structure. NCDOT Transportation Improvement Plan (TIP) project B-4257 called for the original bridge to be destroyed upon completion of a new structure to be built approximately 66 ft. (20.1 m) to the south. This design was a single span 100 ft. 4 in. (30.6 m) in length that eliminated the two center bents and two interior deck joints present in the original structure. The

reinforced concrete deck was designed with a total width of 32 ft. 7 in. (9.9 m), a centerline elevation of 683.14 ft. (208.2 m) and would be supported by three 72 in. (1.8 m) prestressed concrete bulb tees on elastomeric bearings. The increased deck elevation was further enhanced by improved grading and slope protection at the end bents, which was projected to reduce the 100-year flood elevation from its existing 666.5 ft. (203.1 m) to 666.1 ft. (203.0 m).

Figure 1.5. Damage to diaphragm.

1.3 Scope

The nation's overall bridge maintenance load will steadily grow as new structures are added and existing ones age. Spiraling labor and materials costs will complicate the equation even further. In light of these challenges, determining the mere existence and

location of a given defect will not be enough. The ability to quantify and monitor potential defects before they become apparent will assume much greater importance.

This research will investigate the extension of the use of handheld GPR units and the Portable Seismic Properties Analyzer to the detection of subsurface defects and anomalies in and around bridge deck armor. Particular attention will be paid to exploring the challenges peculiar to these techniques with regard to armored deck joints, and to their potential as an alternative − or adjunct to − conventional non-destructive testing techniques. In addition, this work will attempt to quantify the results found and to study the possible feasibility of their incorporation into existing bridge maintenance programs.

Chapter 1 provides an overview of the status of the bridge inventories of the United States and in the state of North Carolina. Also discussed is the importance of properly-functioning deck joints in maintaining the integrity of the bridge structures in which they are installed. The terms *functionally obsolete* and *structurally deficient* are both defined. A case study is provided to help illustrate the similarities and differences between them, and to stress the effects of improperly functioning deck joints. The scope and objectives of this study are also summarized.

Chapter 2 provides background information on the armored deck joints currently in use by the NCDOT. The problems commonly encountered with these joints are also discussed. Several studies regarding different NDT/E methods are summarized, including Visual Inspection, High-Density Surveying (HDS), Ground-Penetrating Radar, and Acoustic Techniques.

Chapter 3 includes a description of the NDT/E methods and equipment used in this study. The basic theory behind the operation of HDS (the Leica ScanStation), GPR (the StructureScan™ Mini by GSSI) and Acoustic equipment (the Seismic Properties Analyzer by Geomedia Research and Development) are discussed and illustrated. A listing is made of the equipment used and any operational details or other important specifications are noted.

Chapter 4 is a detailed chronicle of the process of choosing and verifying the test site for this study. Considerations regarding the condition of the existing structure, suitability of the joint and potential complications due to removal of one span are discussed. Finally, a brief summary of the deployment of HDS equipment is provided.

Chapter 5 is a detailed narrative of the actual process of deploying the StructureScan™ Mini (SSM) and Seismic Properties Analyzer (SPA) described in Chapter 3.

Chapter 6 is a discussion of the results found from the data gathered in Chapters 4 and 5. Maps of the area immediately adjacent to the joint under study illustrate the results of the GPR and SPA tests.

Chapter 7 outlines this study's conclusions. Included are specific details of the idiosyncrasies of the test equipment used and guidelines for their use in future research.

1.4 Objectives

This study was performed with the aim of achieving the following objectives:

1) To investigate the effectiveness of the current generation of portable and handheld GPR and Acoustic test devices in the detection of subsurface defects in the vicinity of deck joint armor.

2) To gain an understanding of any challenges or difficulties peculiar to these techniques with regard to testing concrete in the immediate vicinity of armored deck joints.

3) To lay the groundwork for the development of a protocol to ensure effective use of the portable GPR and SPA equipment currently available.

CHAPTER 2

LITERATURE REVIEW

2.1 Deck Joints in General

According to American Association of State Highway Transportation Officials (AASHTO), adequate expansion joints should [**8**]:

- Accommodate all structural movement

- Possess sufficient load capacity

- Possess good riding characteristics

- Not present a hazard to traffic of all types

- Not place unnecessary stresses on the structure

- Not vibrate and be relatively quiet

- Be corrosion-resistant

- Allow for maintenance

- Protect the structure below it by restricting leakage

- Be reliable throughout the range of temperatures expected in service

In addition, deck joints should not impede or be damaged by snowplowing operations and should employ anchorage systems that support the deck surface in their immediate vicinity [**9**]. This means that such anchorage systems should ensure a given joint's ability to sustain highly localized wheel and impact loads - repeatedly and without undue deflection – while remaining as maintenance-free as possible.

2.2 Armored Deck Joints

In North Carolina, bridges with an average daily truck traffic count of 2,500 or more are fitted with armored deck joints to sustain the repetitive loads described above. The type of joint to be installed is generally decided upon during the design stage. Two primary factors are considered: the length of expansion to be accommodated (measured normal to the centerline) and the bridge's skew angle [10]. There are three types of armored joints commonly found on NCDOT bridges.

The first is a type of closed joint that employs an extruded neoprene gland; Figure 2.1 illustrates the details of its installation. These joints are typically used for movements of 2.5 in. (65 mm) or less and consist of two parallel steel anchors fitted on opposite sides of the joint and placed below he finished grade. The gland is placed atop the anchors, and serves as the waterproofing member. It is held in place by two steel hold-down bars bolted in place at even intervals along the length of the joint. Installation details are covered in the NCDOT Standard Specifications, Project Special Provision 22 [11].

Figure 2.1 (b) illustrates the second type of joint, the armored Evazote seal. It uses anchors similar to those used in the gland type, except that the hold-down bars (and associated hardware) are omitted and the anchors are placed at or just slightly below the deck's finished grade. The waterproofing member in this case is a closed-cell compression seal of polyethylene copolymer foam (often referred to by the trade name "Evazote" in NCDOT literature). These joints are also typically used in members exhibiting movement of 2.5 in. (65 mm) or less. Installation details are outlined in the NCDOT Standard Specifications, Project Special Provision 21 [12].
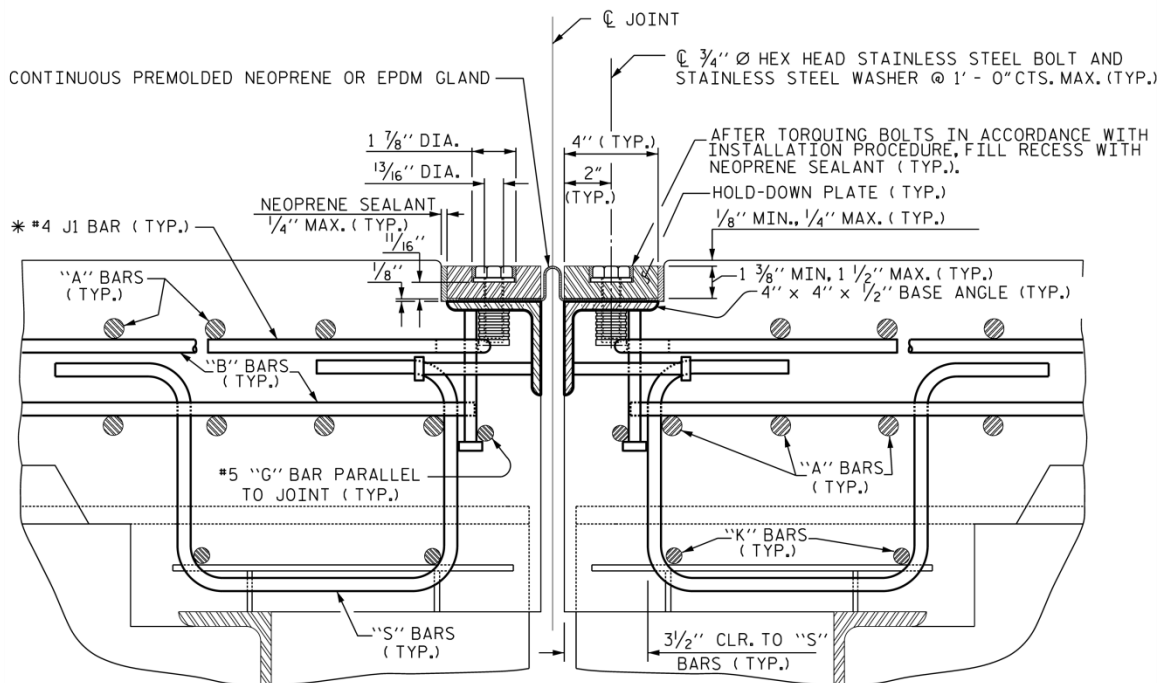
(a) Typical neoprene gland-type seal.
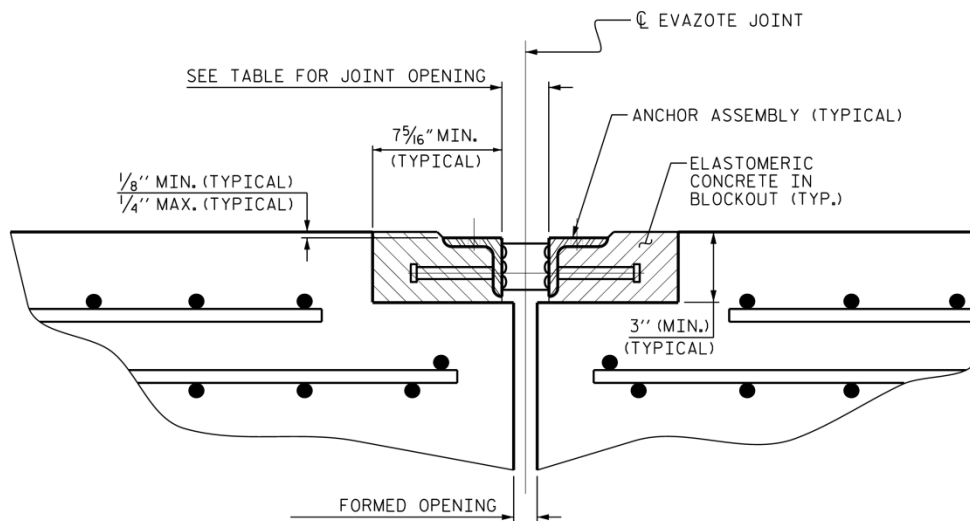
(b) Typcal Evazote seal.

Figure 2.1. Details of armored joints used by NCDOT (adapted from the NCDOT 2003 Standard Drawings).

The third type is the finger joint (Figure 2.2). It is usually considered a type of open joint and has historically been used to accommodate moderate to large structural movements of approximately 3 in. (76 mm) or greater. It is still found on some larger NCDOT bridges built during the mid-twentieth century. These joints were relatively inexpensive to install and tended to be very durable, experiencing few problems during their operational lifetime [10]. Some types did suffer problems with bonding and bent or broken fingers. While they are capable of withstanding heavy traffic loads, they are difficult to seal; modern installations are often fitted with a neoprene trough to prevent seepage. The lack of any reference to this type of joint in the NCDOT Standard Specifications suggests that it is no longer used in new construction; modular joints are used instead. The installation of modular joints is outlined in the NCDOT Standard Specifications, Project Special Provision 20 [13].

Figure 2.2. The finger joint used in this study. The empty spaces between fingers accommodate the fingers for the opposing half of the joint, which has been removed.

All of the joints described above rely on steel anchors to fasten them to the concrete deck and resist movement caused by traffic and other loads. These generally

consist of a standard AISC L4X4 section (or similar member) with studs welded perpendicular to their interior faces (see Figure 2.1). These studs are the primary mechanism for bonding with the surrounding concrete.

2.3 Problems with Armored Deck Joints

During the course of this study, a survey was conducted to gain insight into the particulars of armored joint defects in North Carolina. The Bridge Program Manager in each of NCDOT's fourteen geographical divisions was contacted via an email which contained a link to an online survey. This survey consisted of ten questions designed to determine: (1) the most common type of armored joint installed on NCDOT bridges, (2) the most common defects particular to each joint type, (3) the most common location of these defects and (4) the education and experience of each respondent.

Nine of the fourteen managers responded to the survey, yielding an overall response rate of 64.2%. Their individual experience in bridge inspection and maintenance ranged from under five to over twenty years, and half of all respondents possessed at least a four-year degree or equivalent. When asked about the type of joint most prevalent in their division, seven (77.8%) stated that armored Evazote seals were most commonly used, while two (22.2%) stated that the gland-type seal was more common.

The respondents were then asked three specific questions regarding armored Evazote seals. When asked about the most common failure mode, the responses were divided evenly between the three specific choices. The majority (85.7%) stated that both

visual and audible methods were used to detect failures for this particular joint type. The respondents were more evenly divided on when to replace the joint; 42.9% stated that the joint would be replaced at the first visible sign of failure, while the remaining 57.1% deferred joint replacement until failure was imminent.

A series of three questions were then asked that pertained specifically to armored gland-type joints. The vast majority (80.0%) of respondents stated that the most common failure mode was breakage of the bolts that fasten the "hold-down" bars. Another 60% stated that debonding of the anchoring concrete from the surrounding deck was a problem. Only 20% of respondents cited the actual debonding of the anchor studs as a major problem. When asked about failure detection methods, 100% stated that noise made by traffic passing over the joint was used as a detection method, while 60% also used visible evidence of failure. All respondents (100%) stated that the joint was replaced when the joint had failed completely and presented a hazard to traffic.

A significant finding was the location of damage to armored joints of both types. All respondents (100%) stated that the majority defects occurred within the immediate vicinity of the paths taken by traffic. The complete survey and its results are shown in Appendix D.

In 2003 the Transportation Research Board issued a report that reflected the current "state of the practice" with regard to the various deck expansion joint systems then in use [**10**]. Information for the report was gathered through responses from a survey sent to transportation officials in 34 states - including North Carolina - and 10

Canadian provinces. Topics covered by the survey questions included construction practices, maintenance, joint use and any problems experienced in these areas.

Responses to the survey tended to vary depending upon the geographical locations of the respondents and the type of joint covered by a given question or topic. Nonetheless, several important generalizations were determined from the information provided. For example, while all respondents cited numerous problems with nearly every joint type, the strip seal was found to be the least problematic of all those currently in use. Another discovery was the fact that the majority of those surveyed avoided all open joint types such as finger joints. Some respondents did consider finger joints with neoprene troughs to be a type of closed joint, however. The report also noted that deck joint problem areas included failures in the welds, anchor systems, support beams and the various sealing methods.

Another study of several joint types was performed by the Pennsylvania Department of Transportation (PennDOT) during the mid 1980's. This FHWA-sponsored project was in response to an earlier study that found 76 percent of joints in use in that state were either leaking or completely unsealed. The latter study investigated a wide range of joint types that included armored neoprene and preformed neoprene seals. Engineers discovered a high rate of failure in the anchorage systems of these joints, especially those on bridges with skewed decks. To minimize these failures, it was recommended that future joint anchorages be cast integrally with the surrounding concrete and tied to the reinforcing steel [**8**].

2.4 The Case for Joint Elimination

The case study presented in Chapter 1 illustrated the importance of the watertight integrity of deck joints. Their constant exposure to impact loading and environmental factors render closed joints of all types vulnerable to leakage, however. As a result, most deck joints – no matter their construction-are relatively short-lived in comparison to the rest of the structure. For example, in the UK it was found that most expansion joints that operate from 0-80 mm (0-3.1 in) have a life of approximately 5-10 years. [**14**]

Because of their critical nature and in light of their numerous maintenance difficulties, their possible elimination in both new and existing structures has merited serious consideration. During the late 1980's the Tennessee Department of Transportation (TDOT) undertook a program to reduce or eliminate the number of deck joints on bridges of new design [**8**]. It established a limit of 800 ft. (245 m) for concrete bridges and 400 ft. (150 m) for steel bridges. New structures were designed with expansion joints placed at the extreme ends of the deck, behind the abutments. Deck movement was accommodated by using appropriate bearings on the abutments themselves. While the results overall were reported to be satisfactory, some problems were noted with the asphalt paving on the approaches of some structures. This was addressed by adding elastic material to the problem areas.

This approach was not limited to bridges of new construction [**15**]. Elimination of joints from existing bridges is obviously a major undertaking, as an improper approach can compromise the entire structure. Since the role of deck joints is to relieve the stresses generated by dimensional changes in the structure, it follows that the elimination of any

joints from an existing bridge will cause those stresses to reappear. A thorough engineering study should be performed of the structure in question to determine the magnitudes and locations of these additional loads, and to insure that the members involved are capable of withstanding them.

2.5 Bridge Deck Inspection Using NDT Methods

While there have been numerous studies regarding the investigation of entire bridge decks using NDT methods, very little research was found regarding their use specifically around deck joints or other limited areas on bridges. The reasons for this seem to vary depending upon the technology. In those instances involving GPR for example, many of the systems involved truck-mounted arrays intended to be operated with the regular flow of traffic. Likewise, works that focused on gathering and interpreting IE and USW data often noted that deployment of the equipment proved relatively cumbersome and time consuming.

Regardless of the technology used, advanced NDT/E equipment has historically tended to be specialized and costly in terms of money, equipment and manpower. As a result it has been more economically feasible to test entire decks (or groups of decks) than to focus on small areas like deck joints. In addition, these methods usually required skilled operation and interpretation of the collected data. This apparent scarcity of NTE/E studies specifically focusing on the problems regarding deck joints obviously shifts the focus on those whole-deck studies and those that attempted to increase the accuracy of analyzing the data. Several such studies are presented in this chapter.

2.5.1 Visual Inspection

The use of non-destructive methods for in-situ testing and evaluation of transportation structures is not new. Visual Inspection (VI) is the most basic form of NDT/E, having been in existence as long as engineering itself. Until the year 2000, there had not been a comprehensive study major study regarding the efficacy of VI since the adoption of the National Bridge Inspection Standards in 1971. This was somewhat of a curiosity since VI remains the most prevalent NDT/E method and the one against which most of the latest technologies are compared. That study listed three primary objectives [**16**]:

1) To measure the overall accuracy of routine inspection programs in which VI was a major part.

2) To measure the overall accuracy of in-depth inspection programs in which VI was a major part.

3) To investigate the influence of several crucial VI factors on in-depth and routine inspections.

The study gathered a group of practicing bridge inspectors from various State Departments of Transportation. The inspectors then completed a series of realistic inspection tasks on test bridges the FHWA Nondestructive Evaluation Validation Center in McLean, Virginia. Extensive data was gathered on the effects of environmental and psychological factors on the reliability of VI. The potential benefits cited by the study included improved confidence in the results of routine and in-depth inspections, the

ability to quantitatively measure inspector performance and an understanding of how environmental and human factors influence in-depth and routine inspections.

2.5.2 High-Density Surveys

One study by Curtin University of Technology in Perth, Australia demonstrated the effectiveness of using High-Density Surveys (HDS) in the detection and measurement of structural deformation [**17**]. The primary tool used in the study was the Cyrax 2400 Laser Scanning System manufactured by Cyra Technologies (since 2001 a part of Leica Geosystems) of Oakland, California. This system used a green light source with a central wavelength of 532 nm to collect data at a rate of 800 Hz. The scanner's maximum spatial resolution was stated as 0.5 mm at a distance of 50 m (164 ft.).

The study involved two separate scanning sessions. The first was a simulation exercise that involved the monitoring of a subsiding building face on the campus of Curtin University.   Five separate scans or "epochs" were conducted of the building façade with the scanner mounted on a "precision, vertical translation stage".   The scanner's optical center was stationary for the first two scans, called "control epochs". The remaining three scans were performed after raising the scanner head in 8.5 mm increments, which simulated a progressive subsidence of $\Delta Y1 = $ -8.5 mm, $\Delta Y2 = $ -17 mm and $\Delta Y3 = $ -25.5 mm; the results detected vertical motions of -10.9 mm, -21.2 mm and - 29.6 mm. Each epoch also exhibited a horizontal systematic error that was believed to have been caused by a lack of vertical axis compensation.

The second scanning session was an actual field scan of an old wooden bridge in Toodyay, Australia. The separate point clouds were georeferenced, registered, and

converted into a 3D database of structural components. This data was used to create models for finite element analysis. The article also mentioned that the bridge under study would be monitored during a controlled loading fieldwork experiment at some point in the future.

The study concluded that HDS may possess an advantage over traditional survey methods. This is due to the large volume and high density of the information gathered, which might help uncover areas of local deformation that would otherwise be overlooked. This study also highlighted the importance of instrument calibration, the filtering of raw data in the point clouds to remove redundant or superfluous data, and the importance of recognizing data "holes" due to the poor reflectivity of certain materials.

2.5.3 Ground-Penetrating Radar

A search of ASTM International's website listed numerous procedures for the use of GPR in various fields, but only one specifically pertaining to bridge inspection [18]. This document (ASTM Standard D6087 − 08) primarily describes the procedure for using GPR in the evaluation of asphalt-covered bridge decks. These methods are also valid for bare concrete decks or those with a concrete overlay, however. Procedures for the proper use and calibration of both air and ground-coupled GPR systems are listed. Also documented are two different algorithms for calculating the extent of any delamination present. One particularly noteworthy item is the attention paid to ensuring that passes made by the GPR unit are perpendicular to the top layer of reinforcing steel.

One study that illustrates the effectiveness of GPR in the assessment of bridge decks was performed by the Arizona Department of Transportation (ADOT). That

agency conducted a statewide survey that compared GPR results to those obtained by conventional NDT/E methods [**4**]. A total of 1.5 million square feet of deck area on 134 bridges was surveyed between December of 1998 and April of 1999. These bridges represented five different construction methods, which are summarized in Table 2.1.

All but three of the decks in this survey had bare concrete wearing surfaces; the remainder had an asphalt concrete overlay. Attenuation of a given GPR signal is greater through concrete weakened by chloride intrusion or delamination than in intact concrete. Therefore, deterioration in the bare concrete decks was detected by measuring the attenuation of the radar signal either through the entire thickness of the deck or through the concrete cover over the top layer of reinforcing steel.

Table 2.1. Bridge construction types studied in ADOT survey. Table was adapted from Maser and Bernhardt.

Description	Number Surveyed
Concrete deck on steel girders	65
Concrete deck on concrete "T" girders	14
Concrete deck on prestressed girders	15
Concrete Slab	33
Concrete box girder	7
Total	134

The radar equipment used in this particular study was manufactured by Pulse Radar, Inc. of Houston, Texas. It consisted of a dual-horn antenna array mounted on the front of the scan vehicle. The system operated at a center frequency of 1 GHZ, and the antennas were rotated so that the signal polarization radiated perpendicular to the line of travel. This was done to measure the concrete cover depth by maximizing the signal received from the transverse layer of reinforcing steel.

INFRASENSE's DECAR® software was used to analyze the collected data. This involved the estimation of deterioration quantities through mapping areas exhibiting high signal attenuation and high dielectric constant. The results of the GPR surveys were compared with those from more traditional methods such as chloride sampling, half-cell corrosion potential tests and coring. A reasonably good correlation was found between these conventional techniques and the GPR results, enough so that the study concluded that GPR effective enough for use as an initial inspection tool. GPR identified seventeen of the decks as requiring extensive rehabilitation, requiring either an overlay or complete deck replacement.

Attempts have been made to increase the accuracy of interpreting GPR data. One study conducted at Dalhousie University in Halifax, Nova Scotia was an effort to determine the effects of concrete cover on the GPR signal [19]. A combination of GPR, half-cell potential surveying, chain-dragging and visual inspection was used to evaluate the decks of six Nova Scotia bridges. The test structures were from 8 to 36 years old and exhibited deck delamination that ranged from 0% to 18.4% of the deck area.

The exact GPR model was not specified; the study's authors described it as a "GSSI 1500 MHz center frequency ground-coupled radar system." Data was collected in the direction of traffic along longitudinal lines spaced 1.64 ft. (0.5 m) apart. GSSI's RADAN software was used for data post-processing, which converted the normally hyperbolic rebar signatures into representations of discrete points.

Half-cell testing was performed by placing copper-copper sulfate electrodes at 3.3 ft. (1.0 m) intervals along the GPR paths. Surfer (a software package used to generate

contours) was used to create a 0.5 ft. (0.15 m) grid and interpolate the -0.35V contours. The area within this curve represented portions of the subject deck with a chance of corrosion greater than 90%.

Chain-dragging was used to determine the extents of audibly-detectable delaminations. Once found, they were physically drawn on each deck surface in rectangular form. This was done to simulate the method used to mark repair locations in actual practice.

One of this study's most significant findings was the extent to which interpretation of GPR data can be materially affected by signal attenuation through the concrete covering the transverse bars. Both the cover depth and the concrete's chloride content were determined to contribute to this phenomenon. Overall correlation to the traditional NDT/E methods was found to improve when a structure-specific regression model was created and used as a calibration curve for the data. The regression model charted the 90th percentile signal amplitudes versus the range of two-way travel times encountered on the structure. This improved correlation was also expected on decks with an asphalt concrete overlay.

2.5.4 Acoustic NDT/E Methods

As mentioned in Chapter 1, acoustic methods such as chain-dragging and hammer blows have been used for decades to detect delaminations in bridge decks. One of the newer tools is the Seismic Pavement Analyzer (SPA). This instrument combines the capabilities of Impact-Echo (IE) testing and Ultrasonic Surface Wave Seismic Analysis (USW) in one unit. A more detailed description of the SPA is given in Chapter 3.

Acoustic testing of concrete by electromechanical methods (electrically operated seismic methods) is currently outlined in two ASTM standards [20] [21]. The first (C1383 – 04) involves the measurement of P-wave speed and concrete plate thickness. The second (C1740 – 10) outlines procedures for evaluating the actual condition of concrete plates. A third standard is available for the analysis of concrete using Ultrasonic Surface Waves (USW), but the method of excitation covered in this document was incompatible with the equipment used in this study.

The SPA was employed in one study to investigate debonding in concrete slabs on Texas Route 225 southwest of Houston [22]. Field records in the form of time records and frequency spectra were gathered; scrutiny of this data confirmed the shortcomings of using time-domain analysis of the reflected waves in IE testing. It also confirmed the long-standing use of the Fast Fourier Transform (FFT) and the effectiveness of frequency–domain analysis in detecting marginally-delaminated slabs.

One potential problem with FFT in the analysis of concrete slabs lies in the fact that their boundaries are inherently finite. This can present a problem in the interpretation of the results since reflections from the slab boundaries can obscure crucial portions of the reflected signal. The study's authors demonstrated that:

> …a fast Fourier Transform-based IE spectrum can provide only averaged spectral amplitudes. When surface waves are not very strong, the structure is simple (ambient noise is minimal), and the reflections are clearly recognizable, the spectrum is sufficient to distinguish the frequency peaks of target echoes. However, large-amplitude incident surface waves and echoes from geometrical boundaries of the structure may obscure the frequency of the desired target echoes or reflections from the bottom of the slab or debonding.

31

An additional potential problem in frequency-domain analysis is that the reflected signal may not always be separated from ambient noise, a problem very likely to be encountered when using the SPA on a bridge deck. While not specifically noted in the study, it could be inferred that such noise could not only be caused by traffic actually on the structure under test, but also immediately adjacent to it.

An improved method of analysis was introduced to address these difficulties. The normalized spectral amplitudes (the FFT of each reading) were plotted against their corresponding time signals to create a series of time-frequency scalograms. These scalograms were found to combine the benefits of the FFT with the preservation of the data contained within the initial time-based waveforms. This allowed the researchers to reach conclusions based on more nuanced aspects of the data that would have otherwise been obscured by boundary reflections. Through the use of these scalograms and ground truth data, IE records from the SPA were found to be sufficient to differentiate between intact and fully delaminated slabs but were still inconclusive for those that were marginal.

Another recent study involving the SPA was conducted in 2010. This study investigated the effectiveness of several different NDT methods in detecting debonding of hot-mix asphalt (HMA) layers in airport runways [**23**]. While this study did not specifically address issues with concrete bridge decks, it was nonetheless informative because the GPR and the SPA both proved effective despite the complications inherent to HMA as a test material. Among those difficulties cited:

1) PCC slabs are typically thicker than compacted HMA lifts.

2) The cement paste in PCC bonds with the aggregate to form an almost homogeneous material, while HMA essentially remains a particulate substance bound by a viscoelastic fluid.

3) Tack coats between HMA lifts act as a bonding agent, which may complicate detection of debonding.

4) The mechanical properties of HMA vary with temperature.

Four different NDT methods were compared: GPR, Impulse Response (another name for Impact-Echo or IE), Ultrasonic Surface Waves (USW) and Infrared Thermography. Ten test sections were constructed for this study, each 9 ft. (2.7 m) long by 10 ft. (3.2 m) wide. The pavement cross-section of each consisted of approximately 8 in (200 mm) of HMA placed in three lifts on a sandy-silt subgrade. The debonding agents included talcum powder, grease, clay slurry and oil-soaked paper, with a tack coat being used as a control. Direct shear tests were done on each to determine its effectiveness in debonding.

The IR method was the most effective with 59 percent of debonded areas detected. The SPA in USW mode detected 53 percent of all debonded areas tested and was the most effective at detecting shallow debonding. GPR detected 33 percent of the debonded areas, primarily when clay or talcum powder was the debonding agent. The study noted that GPR could be used quantify severe debonding in HMA, especially when moisture was present. This could have a positive impact on the use of GPR and SPA on older concrete decks with HMA overlays.

2.5.5 *Studies Combining GPR and Acoustic Techniques*

As powerful a tool as individual testing methods can be, the evaluation of a bridge using a combination of techniques can reap even greater rewards. One such study was performed in 2001 [**5**]. A comparison of GPR, Impact-Echo (IE) and the chain drag method was performed on the Van Buren Road Bridge across Quantico Creek in Virginia. The primary objective of the test was to assess each method in its ability to search for deck delamination due to rebar corrosion. Another stated goal was to test the overall reliability of the chain-drag method. The use of a single bridge for the test allowed the GPR and IE results to be compared to one another then verified with ground truth data obtained by chain dragging and coring.

The GPR testing was performed on the bridge's center span using two different instruments. One was an off-the-shelf GPR unit, the SIR-2000 system by Geological Survey Systems, Inc. (GSSI) of Salem, NH. This was a portable GPR unit with a ground-coupled antenna pair centered at 1.5 GHz. Scans with the SIR-2000 system were conducted by pushing the GPR unit "lawnmower style" along reference lines spaced 2 ft. apart on the deck surface. The raw data produced by the SIR-2000 scan was typical of that gathered by GPR units in general; a two-dimensional plot with hyperbolas denoting the reinforcing steel and subsurface anomalies.

The other GPR unit was a Federal Highway Administration (FHWA) prototype bridge inspection vehicle called the High Speed Electromagnetic Roadway Mapping and Evaluation System (HERMES). Built by Lawrence Livermore National Laboratory, HERMES was a trailer-mounted array of 64 transmitter/receiver pairs tuned to a radar

frequency band centered on 2.4 GHz. It was capable of scanning a path 16.2 ft. (1.9 m) wide while being towed at normal highway speeds. While the data gathered by HERMES was similar in many respects to conventional GPR data, its broad bandwidth and large antenna array allowed three-dimensional images to be generated by a method called wavefield-backpropagation.

The instrument used for IE testing on the Van Buren Bridge was the Docter IE system by Germann Instruments of Copenhagen, Denmark. It consisted of a handheld piezoelectric transducer unit with a resonance frequency of approximately 1 kHz connected via cable to a computer data acquisition/signal processing unit. A 2 ft. by 2 ft. grid system was used to mark test locations on the deck.

The study found that the acoustic methods (IE and chain-drag) were generally comparable in their ability to detect delamination. The IE method did reduce the likelihood of subjective testing errors when compared to the chain-drag method, but was extremely slow and did not always produce conclusive results. Another finding was the inability of the IE method to detect delamination in decks with an asphalt overlay.

The two GPR systems studied proved much faster and easier than the acoustic methods at gathering data. The state-of-the-art GPR systems of that time still did not produce consistent results, however. At the time of the study the FHWA was sponsoring the development of a newer system dubbed HERMES II that was hoped to have better delamination detection capability and the ability to detect delamination in asphalt-overlaid decks.

CHAPTER 3

NDT EQUIPMENT AND THEORY

3.1 High-Density Surveys: The Leica ScanStation

High-Density Surveying (HDS) is a relatively new method in the fields of Civil Engineering and Geomatics. While it is not strictly speaking an NDT method, it does possess capabilities that may enhance the ability of researchers to draw conclusions based upon other equipment and techniques such as GPR, IE and USW. Because much of the technology involved with HDS methods is "black box" – i.e. the internal processes are not open to inspection or intervention by the user – only a cursory explanation of the technique will be presented here.

HDS involves the use of a computer-controlled laser rangefinder to rapidly read and generate an extremely high-density dataset known as a *point cloud* (Figure 3.1). A given point cloud may contain thousands – or even millions – of discrete three-dimensional points, which may be spaced as closely as 0.02 in. (0.5 mm) apart (this measure of a given scanner's ability to discern these discrete points at small angular distances is known as its *spatial resolution*). A mathematical algorithm is used to develop the point cloud into a computer model of the scanned surface with the desired degree of detail. This stands in contrast to data collected using conventional survey techniques, which as noted in Chapter 2 is usually rather sparse and may overlook details such as localized deformation in structural members.
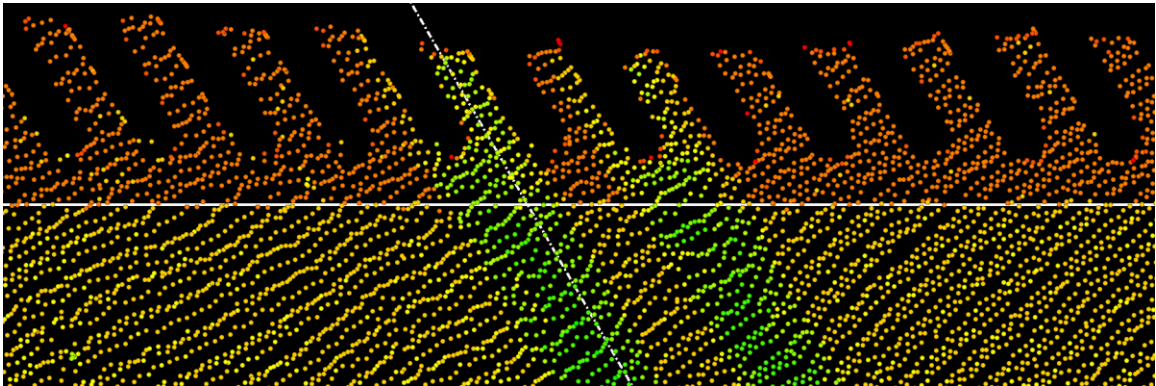
Figure 3.1. Typical HDS point cloud. Different colors reflect the varying albedo of the scanned surface. The horizontal white line represents the joint interface; the diagonal white line represents the bridge's centerline.

The laser scanner used during this study was the Leica ScanStation, manufactured by Leica Geosystems of Heerbrugg, Switzerland (Figure 3.2). It uses a visible green laser to read a maximum of 4,000 points per second at a maximum range of 984 ft. (300 m), depending upon the reflectivity or *albedo* of the scanned surface. Positional accuracy of any individual point was approximately 0.019 ft. at 164 ft. (6 mm at 50 m); distance accuracy was approximately 0.013 ft. at 164 ft. (4 mm at 50 m). This particular model required an external user interface - in this case a laptop computer - to set the parameters of the survey and store the collected data (the NCDOT Location and Surveys Unit has since purchased an updated model).

The entire apparatus as deployed in the field was comprised of (1) scanner head (2) tripod assembly (3) portable gasoline generator, (4) wireless 802.11g router, (5) power supply, (6) equipment case and (7) registration point target assembly. Not shown in the figure is the laptop used to control the scanner head. Also, only one registration target is shown in the figure; a minimum of four targets are required when scanning.

Figure 3.2. The Leica ScanStation.

The ScanStation was capable of gathering data in all directions (including directly overhead) except for the area directly beneath the scan head. This range is called the *scan field*, and is illustrated in Figure 3.3. Its limits are defined by a cone with an angle of 45 degrees below the unit's horizontal axes; the unscanned area will have a radius (r) equal to the height (h) above the surface. This "cone of silence" makes multiple scans necessary if the instrument is mounted directly upon the surface to be scanned.
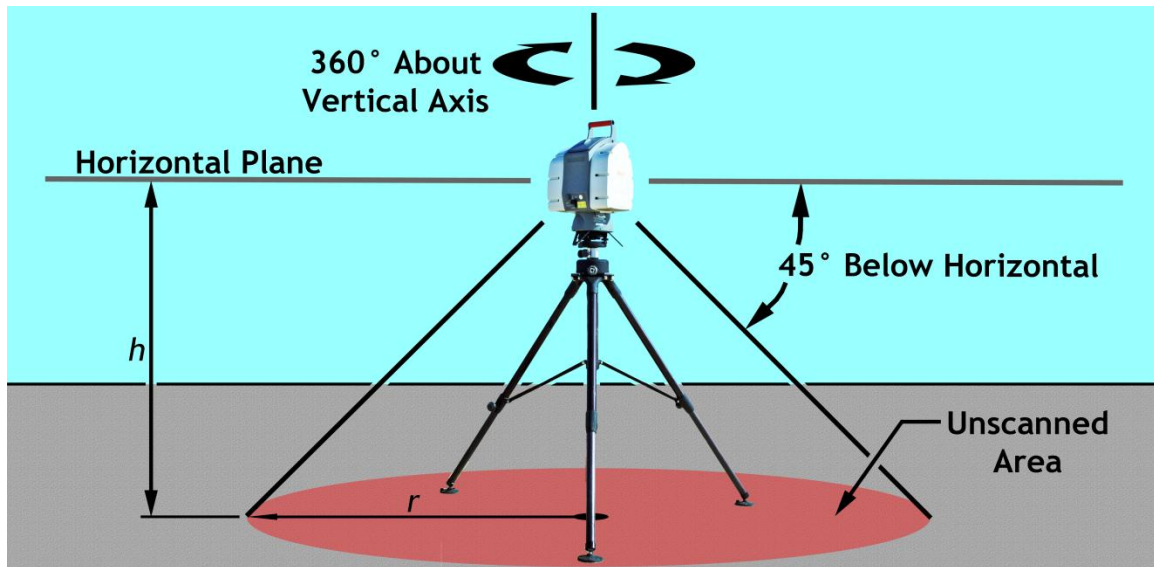
Figure 3.3. The scan field of the Leica ScanStation. The "cone of silence" results in the unscanned area beneath the scanner itself.

A typical scanning session usually begins with the placement of the scanner atop its tripod assembly at some convenient point. Up to four control points are then established within the range of the scanner. These are typically nails driven into the ground or pavement, and may or may not be georeferenced depending upon the survey requirements. Registration targets are then placed atop the control points. Finally, the survey parameters –including point density and scan limits - are established using the laptop control unit before beginning the actual scan.

Complex or large objects may require multiple scans (Leica's term is *scan worlds*) from several different instrument locations. If so, the scanner assembly is moved to another convenient point within the scanner's range and within sight of the registration targets, which are turned about their vertical axes to face the scanner's new position (their original *mounting* positions are maintained between successive scans). The survey

parameters are then re-established for the new position before beginning the second scan. This process is repeated until the required number of scans is attained.

After the field scanning is completed, the point clouds are then manually post-processed to remove extraneous objects outside the areas of interest and/or anomalies that are not part of the original scanned object. Examples of such objects include stray gravel, retreads thrown from truck tires and other debris. Individual point clouds with common control points may be merged to create a composite point cloud through a process known as *registration*. A complete three-dimensional model of the scanned surface can then be created from the merged scans and used for further analysis.

3.2 Ground-Penetrating Radar: The StructureScan Mini™

The GPR unit used in this study is the StructureScan™ Mini (SSM), made by Geophysical Survey Systems, Inc. (GSSI) of Salem, New Hampshire. It is a compact, lightweight handheld unit designed expressly for the location of subsurface objects in concrete structures. The scanner itself consists of a radar transmitter and receiver, onboard computer, color LCD display, targeting lasers and carriage assembly in one relatively lightweight unit.

The SSM is shown in Figure 3.4. It includes (1) the scanning unit with lithium-ion battery, (2) spare battery, (3) battery charger, (4) Quick-Start Guide, (5) DVD with instructional video and support materials, (6) USB cable, (7) power supply for battery charger and (8) carrying case. The SSM's built-in software and 16GB SD card allow for an approximate total of 7,400 ft. of scans at high resolution.

Figure 3.4. The GSSI StructureScan™ Mini.

The SSM works by calculating the relative differences between the dielectric constants in the material being scanned. The dielectric constant of a material is defined by GSSI as the ability of a material to hold an electric charge. In Physics, a material's dielectric constant (ε) is defined as the degree to which an insulator is polarized by a surrounding electrical field. It is calculated by the following equation:

$$\varepsilon = \frac{C}{C_o} \qquad (3.1)$$

where C_o is the capacitance between two parallel plates separated by a vacuum and C represents the capacitance between the same two parallel plates *under identical conditions* when separated by the dielectric material in question. Table 3.1 lists the dielectric constants for materials likely to be found in concrete structures [**24**].

Table 3.1. Dielectric constant ε for materials commonly found in concrete.

Material	ε	Material	ε
Vacuum	1.00000	Polyvinyl Chloride (PVC)	3.18
Air (at 1 atm)	1.00059	Plexiglas	3.40
Teflon	2.1	Glass	5-10
Polyethylene	2.25	Neoprene	6.70
Mica	3 to 6	Water	80.4

According to the table, air has a ε of 1.0 for all practical purposes while water has a ε of around 80.4 (the manual rounds this up to 81). The ε of concrete can vary depending upon its age, chemical composition and environment; the effect of chloride intrusion was outlined in Chapter 2. Generally speaking, however, fully cured concrete has a nominal ε of around 6. Because the SSM is optimized for subsurface analysis of concrete structures of all ages, it is necessary to identify ε for concrete in different stages of curing. These are summarized in Table 3.2.

Table 3.2. Dielectric constant ε for concrete in various stages of curing.

Concrete Age/Environment	Approximate ε
Less than 2 months/wet environment	9+
Less than 12 months/outside	7-8
More than 12 months/dry	5-6

All materials present in concrete will absorb the RF energy produced by the scanner to some degree. As a result, the scanner's dominant colors will be "Black-White-Black" or "White-Black-White", depending on whether ε for the target object beneath the surface is higher or lower than that of the surrounding concrete. This difference is called the reflection coefficient (R) which is defined thus [25]:

$$R = \frac{\sqrt{\varepsilon_2} - \sqrt{\varepsilon_1}}{\sqrt{\varepsilon_2} + \sqrt{\varepsilon_1}} \qquad (3.2)$$

Returns on the screen are also dependent upon the orientation of subsurface objects with respect to the path taken by the unit. A more exact estimate of a target's location is obtained when the object in question lies perpendicular to the scanner's path (Figure 3.5). For example, the path of the unit taken by '*A*' (shown in red) is optimal for detecting the red rebar labeled 'a'. Likewise, the blue rebar labeled 'b' will be detected best when the unit follows path 'B'.

From the standpoint of detecting the actual rebar pattern, the path represented by C illustrates a less desirable scenario; the unit's path is oblique to both the axes of both the "a" and "b" bars. This will result in a more rounded (or "less peaked") hyperbolic signature, making it more difficult to locate the actual center of the rebar or other target. This difficulty increases as the angle between the scan path and the target axis becomes more acute. The worst-case scenario would involve the SSM's scan path running parallel to and directly over the rebar or other target.
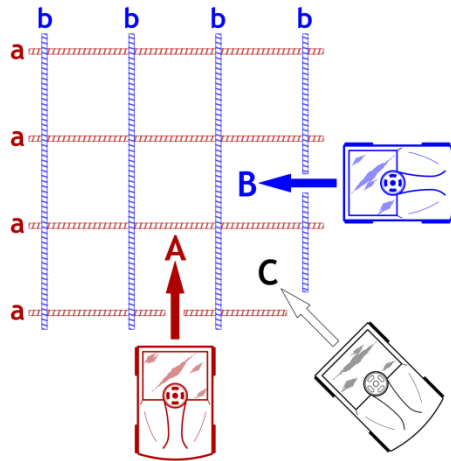
Figure 3.5. Orientation of SSM with respect to subsurface targets.

Typical output from the SSM is shown in Figure 3.6. This particular scan clearly shows the both the location and depth of the reinforcing steel within the structure. In this example the penetration depth was set to 8 inches to eliminate the possibility of receiving return echoes from anything other than the outer reinforcing steel, which is shown as a series of black-white-black hyperbolas. This hyperbolic signature is typical of most point targets detected by GPR units in general, and is a function of the forward motion of the scanner and the time taken by the signal between transmission and reception. The SSM software also includes an algorithm that converts the radar signatures into discrete points.

In the figure, the approximate depth is determined by noting the center of the *first dominant color* of the hyperbola in question; in the case of the first hyperbola to the left, the first dominant color is black, and its center lies at a depth of approximately 1.75 in. (44 mm). This is within the minimum of 1.5 in. (38 mm) normally considered as adequate cover for reinforcing steel. Approximate spacing of the rebar is taken from the distance scale at the top, which shows the center of the first hyperbola at approximately

1.35 ft. (0.41 m) and the second at approximately 2.70 ft. (0.82 m). The difference between the two is 1.35 ft., or 16 in. (0.41 m) for practical purposes.
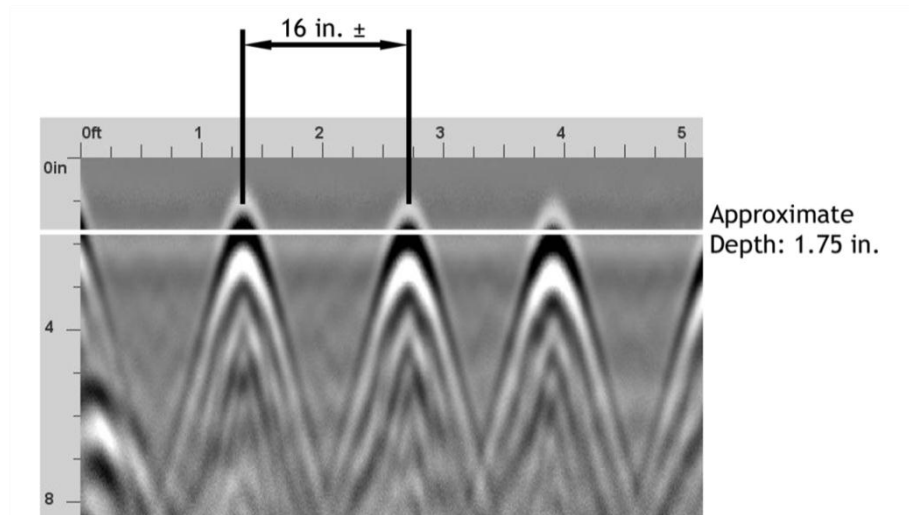
Figure 3.6. Typical SSM scan showing hyperbolic rebar signature.

3.3 Acoustic Methods: The Seismic Properties Analyzer

The portion of this study involving acoustic methods was conducted by using the Portable Seismic Pavement Analyzer (SPA), manufactured by Geomedia Research and Development of El Paso, Texas. It combines the capabilities of IE and USW in a single unit, allowing the user to simultaneously detect delamination and measure the dynamic modulus of a given point. Unlike the StructureScan™ Mini, this is not a self-contained NDT tool; it is actually a peripheral device connected to a computer via a USB port. The SPA is shown in Figure 3.7. It consists of (1) the SPA unit, (2) ruggedized laptop, (3) USB cable, (4) spare parts and rubber foot pads and (5) carrying case. While not as compact as the SSM, it is nonetheless very portable and easily deployed in the field.
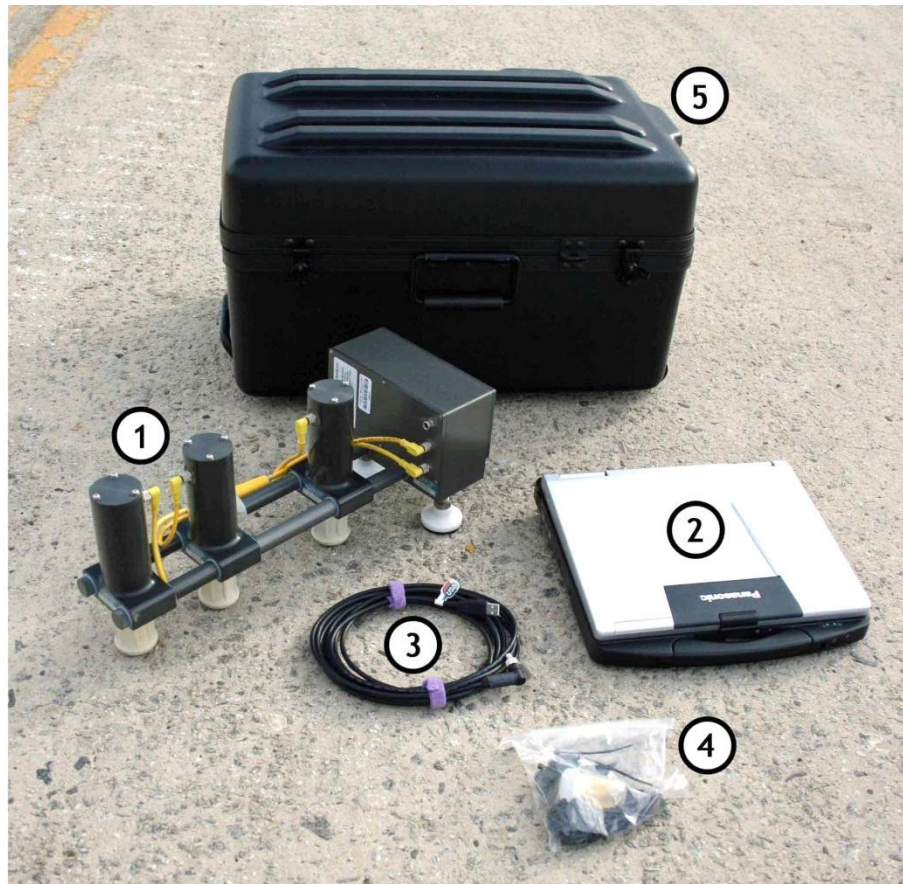
Figure 3.7. The Seismic Properties Analyzer (SPA).

The SPA itself consists of ten major parts. The first is a solenoid-operated hammer called the *source;* it is powered by the USB port and activated by the software in the attached computer. Two accelerometers are mounted at precisely 4 in. and 10 in. from the source. They are called the *near receiver* and the *far receiver* respectively and are visually identical to the source. The source and receivers are connected together with four precision *extension rods* which are designed to maintain the distances required for proper operation. This assembly is connected to the *electronics box* by two additional short extension rods. The electronics box contains the necessary control and analog-to-

digital conversion hardware necessary for operation and waveform conversion. The general layout of the SPA is shown in Figure 3.8.
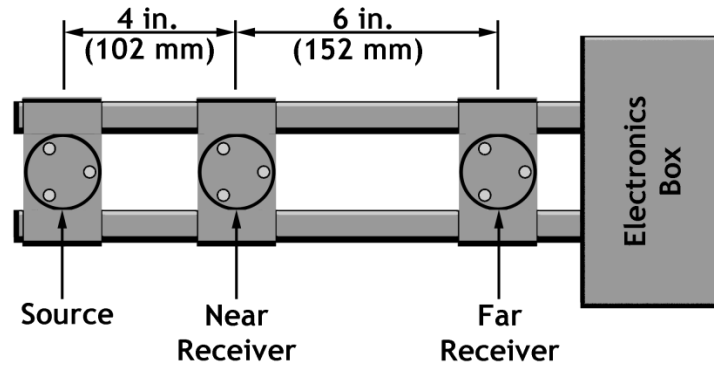
Figure 3.8. General arrangement of the SPA (top view). Connecting cables have been omitted for clarity.

The SPA is specifically designed to measure the dynamic modulus and overall quality of a variety of materials including concrete, asphalt, base materials and compacted soil. It works by repeatedly actuating the source, which generates a series of pulses in the material under test. The near and far receivers then receive these pulses after they have propagated through the test material at a given test point. The accelerometers in the receivers then convert the received energy into an analog electrical signal. Conversion of this signal into a digital waveform takes place in the electronics box before being sent to the computer.

Until this point the signals produced by the SPA are in the time domain. Analysis of the material, however, requires their conversion into the *frequency domain.* This is done via the included software (SPA Manager), which performs a Discrete Fourier

Transform (DFT) on the detected waveform. This develops the frequency signature and the dispersion curve from which the dynamic modulus of the material is determined.

The procedure outlined above requires that the SPA apparatus detect three distinct types of waveforms [26]. *P-waves*, also called *Primary* or *Dilatational* waves, are illustrated in Figure 3.9 (a). These propagate horizontally and cause purely tensile stresses or "peaks", and compressive stresses or "troughs" in the material under test. Relative particle motion is back-and forth, parallel to the direction of propagation. P-waves possess the fastest velocity of any of the three wave types outlined here; their theoretical velocity is dependent upon the material's elasticity and density, thus:

$$C_P = \sqrt{\frac{E(1-v)}{(1+v)(1-2v)\rho}}$$ (3.3)

where C_p is the theoretical P-wave velocity, E represents the material's modulus of elasticity, v represents Poisson's ratio and ρ the material's density.

A diagram of the S-wave is shown in Figure 3.9 (b). The energy in this waveform is transferred by causing a ripple effect that is uniform at all levels of the material; any one particle within the material moves in a vertical line, creating shear stresses within the material. Its theoretical velocity is determined by the equation:

$$C_S = \sqrt{\frac{E}{2(1+v)\rho}} = C_P\sqrt{\frac{1-2v}{2-2v}}$$ (3.4)

where C_s is the theoretical S-wave velocity.

R-waves, also known as *Rayleigh* or simply *surface waves* are illustrated in Figure 3.9 (c). These are primarily surface waveforms and can be considered a combination of the P- and S- waves. The energy of the wave's propagation imparts both horizontal and vertical components to the motion of a given particle, which moves in a circular path. Where the R- wave differs from the previous two is the fact that energy within the wave is not distributed evenly. The majority of the wave's energy is toward the material's surface; as a result, relative particle motion decreases linearly with depth. The theoretical velocity of the Rayleigh wave is given by the equation:

$$C_R = C_S \cdot \frac{(0.87 + 1.12 \cdot v)}{(1 + v)} \qquad (3.5)$$

Where C_R is the theoretical R wave velocity.

The SPA uses R-waves to perform USW analysis. It determines the dynamic modulus of a given material by the equation:

$$E = 2\rho(1 + v)[C_R(1.13 - 0.16v)]^2 \qquad (3.6)$$

where E represents the material's dynamic modulus. Poisson's ratio (v) for concrete typically falls between 0.15 and 0.20; 0.18 will be assumed for this study. Likewise, the density of concrete (ρ) will be assumed to be 150 lb/ft^3 (2,402.8 kg/m^3). It is important to note that the R-wave velocity C_R is not calculated from Equation 3.5, but from the dispersion curve mentioned earlier in this chapter.
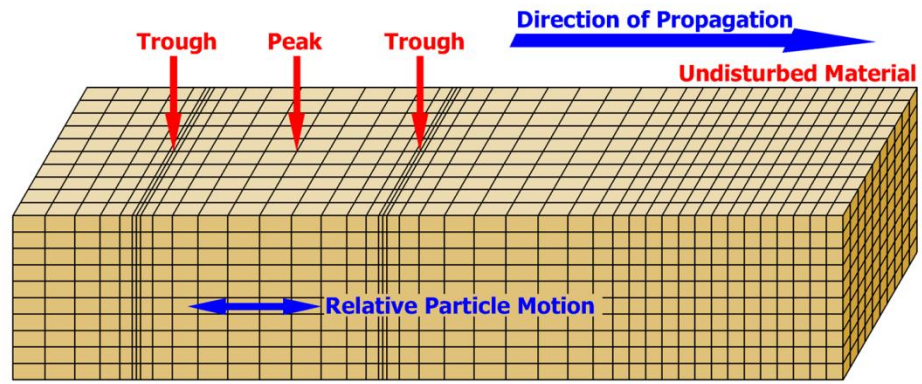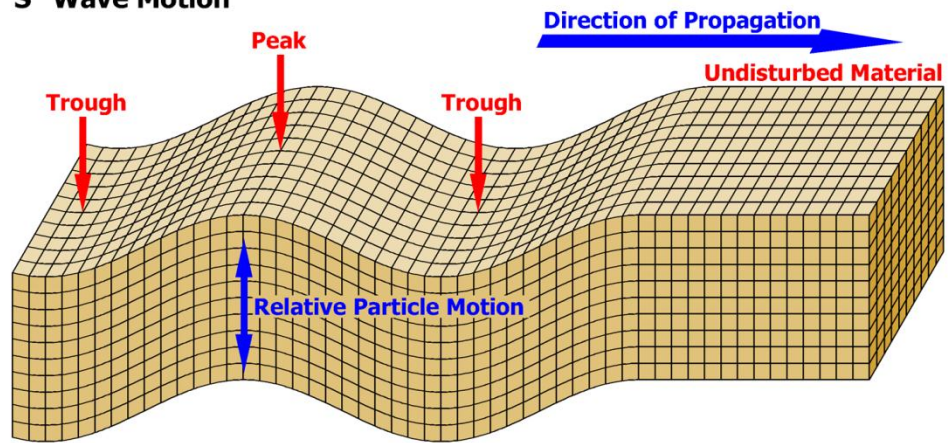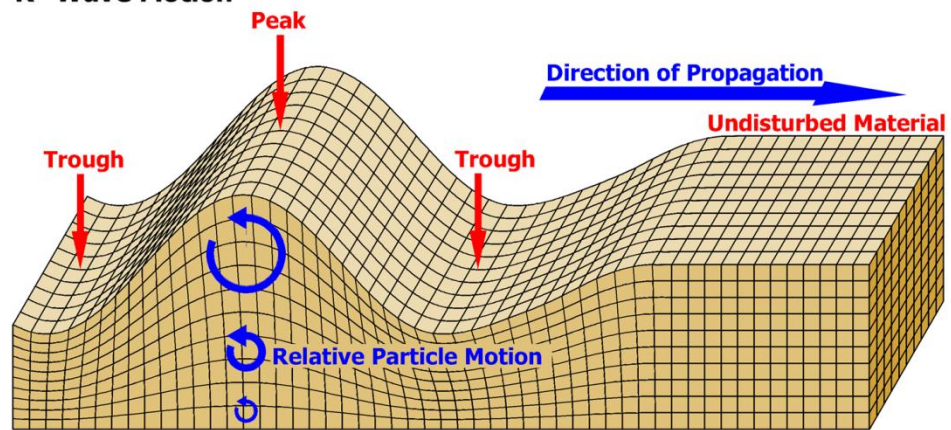
Figure 3.9. P-, S- and R- waves illustrated.

A schematic diagram illustrating the relationships between P-, S- and R-waves in an ideal concrete plate is shown in Figure 3.10. Energy from the source against the plate surface causes shear forces in the form of S-waves to propagate through the material from the point of impact. R-waves are formed as the S-waves interact with the surface. As the initial S-waves propagate, their behavior becomes more like that of P-waves, particularly after reflecting off of the lower boundary. The amplitudes of all three wave types are attenuated as they travel from the source; the degree to which this occurs is largely dependent upon the physical properties of the material.
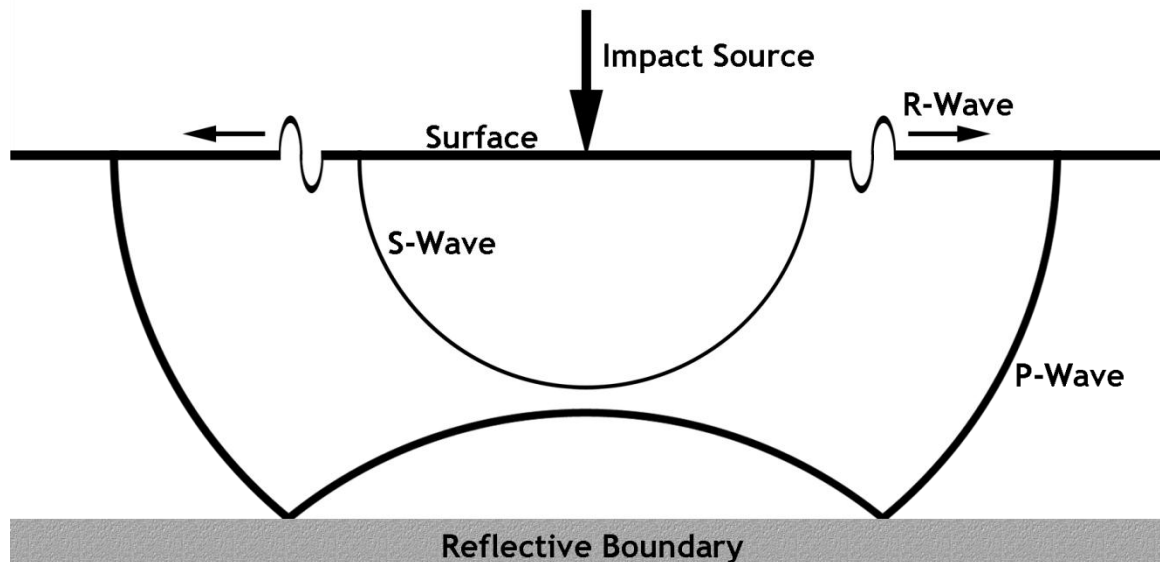
Figure 3.10. Relationship between P-, S- and R-waves in a concrete plate.

The SPA is controlled − and its data processed - by a program called SPA Manager. This software runs in the attached computer and performs the necessary DFT on each waveform and interprets the results. SPA output for a given measurement is presented visually using two different tabbed windows. Both windows display data

regarding the location of the test point and its flexural strength, dynamic modulus and thickness. Data from the SPA can also be output as waveform files and in report form.

The first window displayed is the "Waveforms" window, illustrated in Figure 3.11. This is a standard amplitude-versus-time plot of three separate signals. The original pulse initiated by the source is shown as a red line on the plot. Signals detected by the near and far receivers are shown as black and green lines, respectively. One item of interest is the relatively rapid attenuation of the source signal over time when compared to the two receiver signals. Also noteworthy is the time shift between the near and far receiver peaks.
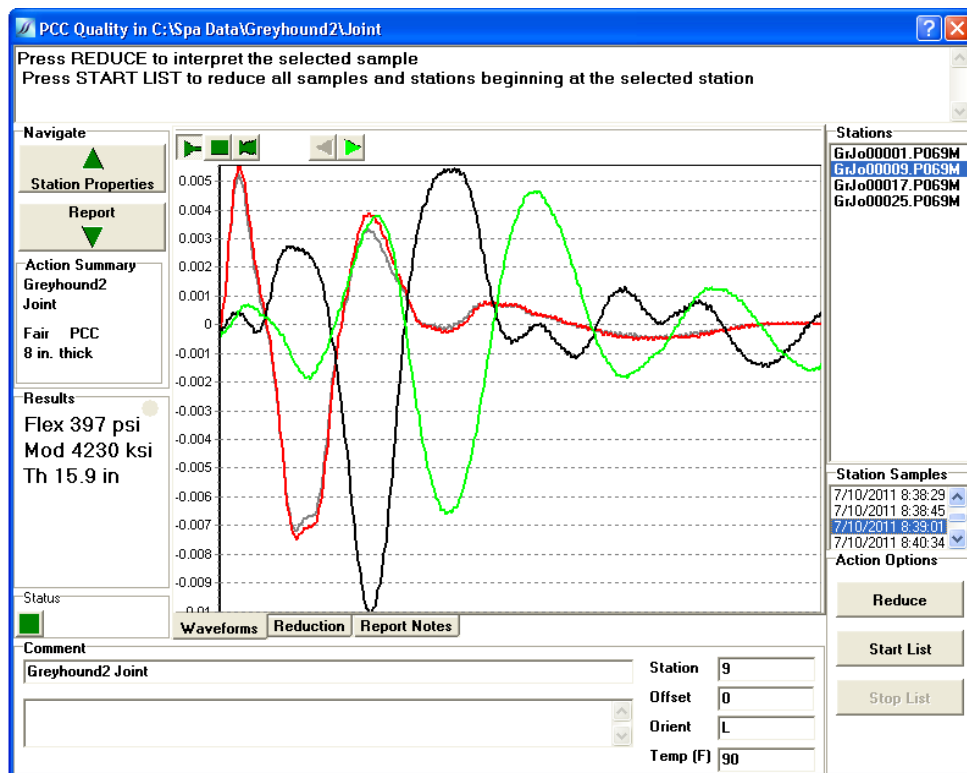
Figure 3.11. Typical SPA waveform window.

The second visual output display is the "Reduction" window, which is illustrated in Figure 3.12. This is an interpretation of the waveform values shown in the previous figure and is divided into four separate graphs. The top graph displays amplitude versus frequency, essentially the Discrete Fourier Transform (DFT) of the signals shown in the waveforms display. This example shows the dominant frequency of the test point to lie somewhere around 23 kHz, with a minor peak around 18.5 kHz.

The second graph, located toward the center of the window, illustrates the relationship between depth and dynamic modulus. It is produced by measuring R-wave velocity through the material using data received from both receivers. Green squares signify the discrete modulus values at various depths within the slab. The vertical red line represents the slab's average modulus value. In general, closer horizontal spacing of these points is indicative of more sound material. The individual points shown in the example suggest that the strength of the concrete at the test point decreases with depth.

Toward the middle right of the display window is the IE graph. The data represented here is a product of the P-waves measured between the source and near receiver. Echo amplitude is measured on the graph's horizontal axis, while its depth is registered on the vertical. Significant echo amplitudes indicate areas of possible delamination or other deterioration at the indicated depth.

The final graph is the phase diagram, located at the bottom of the Reduction window. This is a plot of the phase of the received signal as a function of frequency. Raw data is represented by the green line, while the best-fit line is shown in red. The example indicates a poor correlation between the two; ideally, these should lie roughly

atop one another. The horizontal yellow bar denotes those frequencies used to calculate

wave velocity.
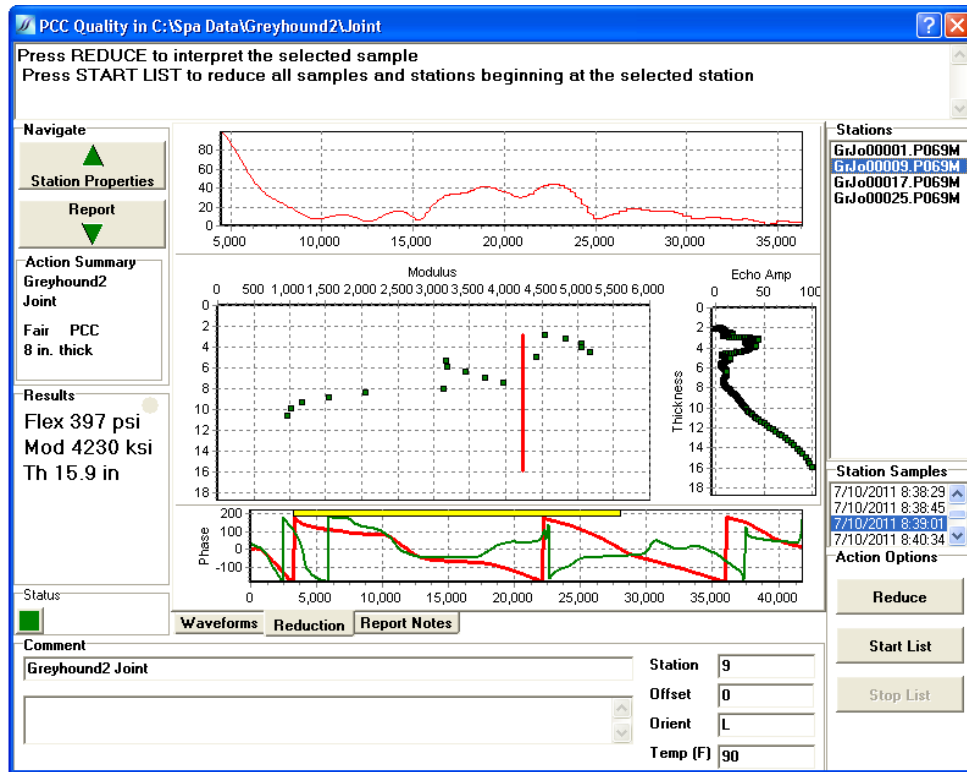
Figure 3.12. Typical SPA reduction window.

CHAPTER 4

FIELD TESTING: SITE SELECTION AND ASSESSMENT

4.1 The Greyhound Court Test Site

The candidate structure chosen for field testing was the Greyhound Court Bridge, an abandoned partial-interchange bridge located in the City of Winston-Salem, North Carolina. Its primary attraction as a test site was the likelihood that it would possess at least one of the joint types described in Chapters 1 and 2. The bridge's age and repair status also indicated the likely existence of cracking, spalling and delamination in the immediate vicinity of that joint. An additional benefit was the lack of traffic afforded by its recent closure. This allowed a variety of field procedures to proceed in relative safety and without the need for repeated lane closures.

This bridge originally carried the two lanes of Greyhound Court, (a Winston-Salem city street outside the NCDOT system) in a southwest-northeast direction over U.S. Highway 52. It was built in 1959 as part of Federal Aid Project Number 8.17375, and as of 24 July 2008 was listed in the NCDOT bridge inventory as Forsyth County Bridge Number 330171. It provided direct access to the industrial area immediately to the west for vehicles northbound on U.S. 52. This traffic consisted primarily of buses to and from the Greyhound bus station (for which Greyhound Court was named), but it also included heavy truck traffic generated by the R.J. Reynolds Tobacco Company (now Reynolds American) and automobile traffic bound for the predominately residential areas

to the east. Pedestrian traffic was accommodated by 5 ft. (1.5 m) sidewalks on each side of the deck. The structure in its original configuration is illustrated in Figure 4.1.

During its last routine inspection, the bridge was found to have suffered extensive deterioration due to years of use and neglect. This fact, combined with planned improvements to U.S. 52 for the Interstate 74 corridor, closure of the bus station and redevelopment of the property immediately to the west, rendered the bridge surplus to the needs of the NCDOT. The bridge was closed in April of 2010 and the southwest span was removed the following May. Concrete barriers and chain-link fencing were placed at both ends to prevent unauthorized vehicular and pedestrian access. Afterward, all access between downtown Winston-Salem and U.S. 52 was accommodated by the Third/Fourth Street and Martin Luther King Drive interchanges to the north. The Greyhound Court Bridge was slated for demolition in late 2011 or early 2012.

4.1.1 Structural Details

The bridge originally consisted of one simple 32 ft. (9.8 m) span (span A) and three continuous spans of 62, 80 and 58 ft. (18.9, 24.4 and 17.7 m) (spans B, C and D respectively), for a total length of 232 ft. (70.7 m) (Figure 4.2). All spans were built on a 30-degree skew and consisted of a reinforced concrete deck supported by 9 steel girders, with the ends of each supported by rocker bearings. Non-armored poured-in-place seals were installed at the two end bents, with a steel finger joint installed between spans A and B. The end bent caps were reinforced concrete cast in place over concrete piles. The three interior bents were of the reinforced concrete post-and-beam type with four columns per bent, positioned as shown in Figure 4.2.
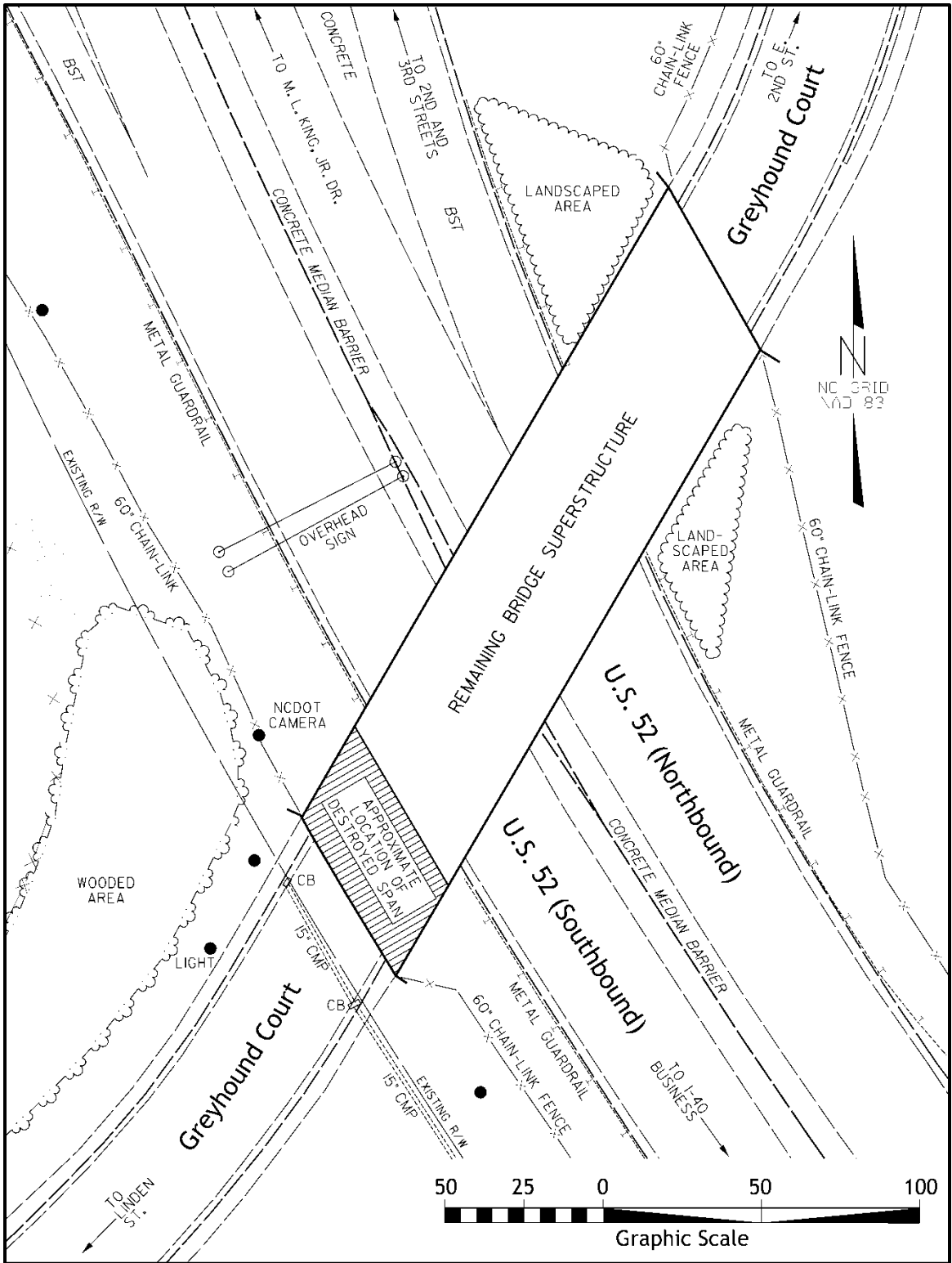
Figure 4.1. The Greyhound Court Bridge and its environment.

57
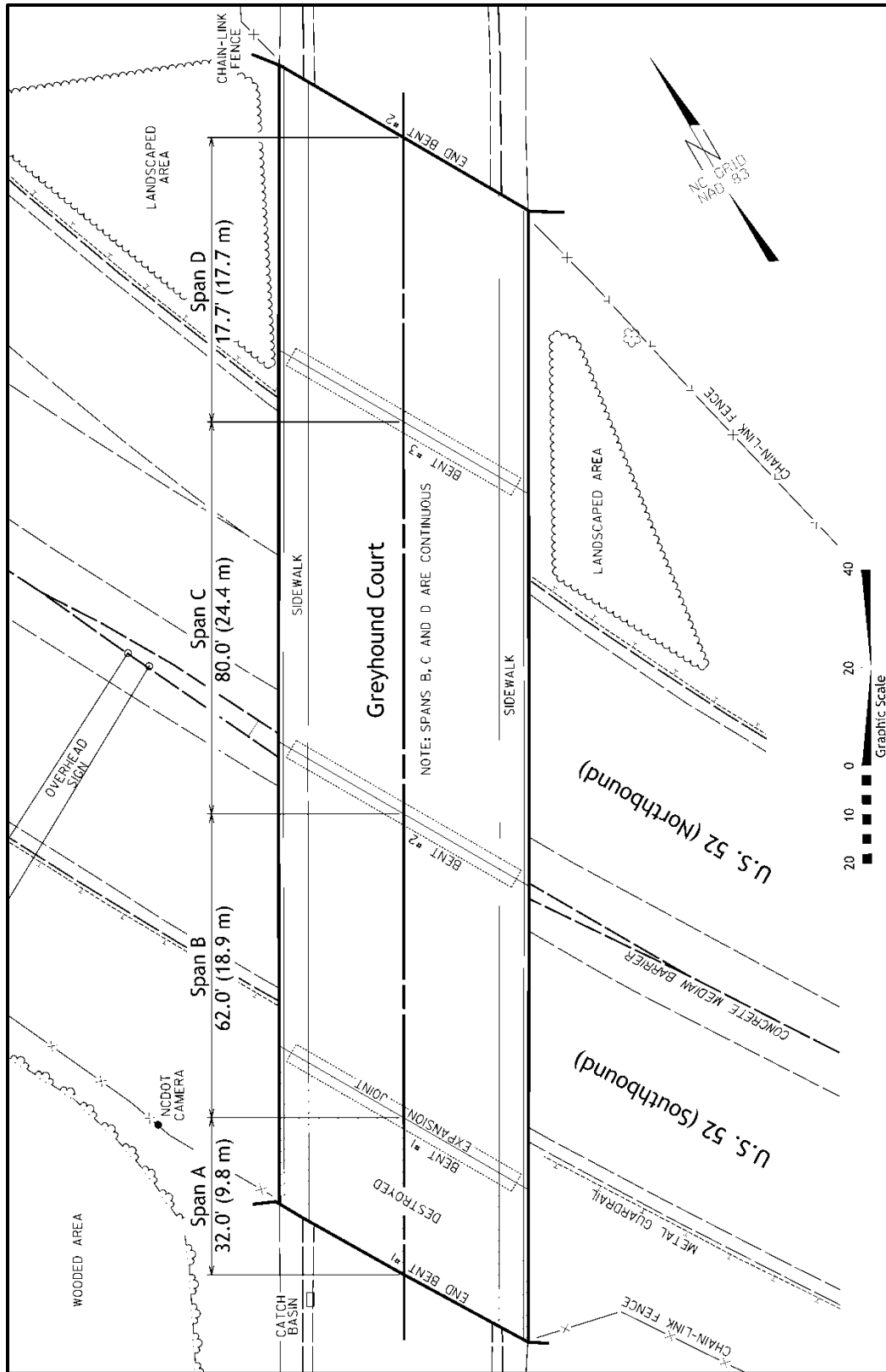
Figure 4.2. Greyhound Court Bridge details and dimensions.

4.1.2 DOT Inspection Summary

The bridge's final inspection report dated July 24, 2008 described its condition as "poor" [**27**]. Among the problems listed was extensive surface rust and scale on all of the girders, with section loss of $^1/_8$ to $^1/_4$ in. (3 mm to 6 mm) noted on those portions directly beneath the expansion joints. Corrosion was even more severe on the remaining portions of the superstructure steel, with section losses of approximately $^1/_8$ to $^1/_2$ in. (3 mm to 12 mm) noted on the rocker bearings and diaphragms.

The concrete portions of the bridge also showed signs of deterioration. A horizontal hairline to $^1/_8$ in. (3 mm) crack was noted at end bent 1, with delamination evident on some of the bridge seats. End bent 2 exhibited a hairline to $^1/_{16}$ in. (2 mm) horizontal crack, and map cracking was noted throughout its surface. The caps of the interior bents proved to be in surprisingly good shape, with few cracks and only minor delamination noted.

From the standpoint of this study the area of greatest concern was the deck, which was found to exhibit extensive transverse and map cracking in its surface. These cracks were characterized as "fine to hairline". Span A had suffered severe delamination in the past, evidenced by two large patches: one 2 ft. (0.6 m) in diameter, the other 6 ft. (1.8 m) wide by 3 ft. (0.9 m) long. Further delamination was noted in spans C and D, with spalling up to $^1/_2$ in. (12 mm) deep. All of the butt-type deck joints were found to be cracked and leaking; the sealing material in the joint between span D and end bent 2 was discovered to be missing entirely. The report did not note the condition of the finger joint between Spans A and B.

The sufficiency rating and any proposed vehicle weight limits were also not listed in this report. These figures were noted in a document dated June 6, 2010 found on NCDOT's website [**7**]. It listed the "Greyhound Street" bridge as structurally deficient, with a sufficiency rating of 57.9. The SV and TTSV limits were each noted as being 40 tons. The bridge was not considered functionally obsolete.

4.2 Initial Test Site Assessment

Once a suitable test site was found, an initial assessment was performed of the structure and its environment. This procedure consisted of two phases: visual and virtual. The primary objective of both was to ensure the existence and viability of at least one of the armored joint types listed in Chapters 1 and 2 (armored gland, armored poured-in-place, or finger). They would also provide a record of the structure as it existed during this study and help determine the nature and extent of any damage that may have occurred to the remaining structure during the removal of span A. In addition, any peculiarities affecting safety or impeding access to the site could be identified. Both phases of the initial site assessment are described in detail in the following pages.

4.2.1 Visual Inspection and Assessment

The visual assessment was performed first. Its main purpose was to determine if the physical condition of the remaining structure differed appreciably from that noted in the final inspection report. The chief concern was that removal of span A may have caused visible or latent damage to the remaining portion of the finger joint. Another concern involved any restriction of access to the structure caused by the span removal

and subsequent installation of the physical barriers noted previously. These could cause difficulties with the deployment of the test equipment in addition to being potential safety hazards. The visual assessment focused primarily on:

1) The environment surrounding the structure.

2) The condition of the remaining portion of the deck joint.

3) The condition of the concrete immediately adjacent to the deck joint.

4) The overall condition of the remaining portion of the structure.

This part of the initial site assessment proceeded in three stages. First, any major changes to the structure or other deviations from the inspection report were noted, including their nature and extent. Next, an attempt was made to quantify the combined impacts of these changes to both the physical state of the structure and its accessibility. A decision was then made based upon this assessment regarding the suitability of the test structure for this study.

4.2.1.1 Environmental assessment

The word "environmental" in this case refers to the physical state of the bridge within the context of its surroundings. In the case of the Greyhound Court Bridge, the very aspects that made it attractive as a test site (a decommissioned structure that was closed to traffic) also negatively affected its accessibility and safety – two areas of vital concern. The bridge would be useless as a test subject if it were unreasonably dangerous or difficult to transport and deploy the test equipment. For this reason it was necessary to note any specific safety hazards or problems with access to the structure. The site conditions as they existed during the time of this study are illustrated in Figure 4.2.

The removal of span A and the placement of physical barriers meant that traffic would pose essentially no danger to those performing the field tests, but it also brought with it several trade-offs. First, the missing span created a situation whereby all reasonable access to the deck was restricted to the bridge's northeast approach (Figure 4.3). This created a dead-end condition that made escape difficult for anyone confronted with a dangerous situation (the residential area to the east was considered high-crime and the areas between the girders at the end bents of many bridges are commonly inhabited by the homeless). This concern was addressed by performing all testing as early in the day as possible and by having more than one person present during testing.

Figure 4.3. Greyhound Court Bridge, southwest approach. View from end of span B.

The most likely danger, however, was the falling risk posed to anyone working in close proximity to the deck joint under study. Carelessness could have resulted in a fall of nearly 20 ft. to the toe of the concrete slope protection below. It was determined that

this could be mitigated by working carefully in this area, even to the extent of installing a safety line if necessary. The vigilance of the extra team members mentioned previously could also help prevent falls from the structure.

The chain-link fence and concrete barriers erected across the northeastern approach (Figure 4.4) presented another minor difficulty in accessing the bridge. The concern here was the deployment of test equipment, all of which would have to be lifted over the guardrail behind the fence. Because of the guardrail's height, anyone involved with the field testing could suffer lifting-related injuries. The SPA in its case, for example, weighs approximately 37 pounds (16.8 kg). Damage to the equipment could also occur if it were inadvertently dropped. Both of these possibilities could be mitigated by having two team members involved with the transfer of all equipment, with one person handing items to the other. This was one more argument in favor of additional manpower.

Figure 4.4. Greyhound Court Bridge, northeast approach.

None of the concerns outlined in the preceding paragraphs was considered to present any undue danger or difficulty in performing the NDT/E work involved in this study. Nor were they unique to the test site; real-world inspections of bridges in service – whether or not NDT/NDE techniques are used - necessarily require that those performing them be exposed to the dangers of live traffic in addition to the difficulties outlined above.

4.2.1.2 *Overall condition of the remaining structure*

Once the validity of the immediate test area was established, the next step was to assess the condition of the remainder of the structure. This was not an in-depth study, but rather a cursory visual examination done mostly with the naked eye and simple tools (Figure 4.5). The bridge's close proximity to live traffic made it necessary to inspect much of it – particularly the girders and rocker bearings - from a distance. This was performed using a pair of 7×50 binoculars. Not all structural members were visible; views of the girders at the bridge's northeast end were hampered by the lack of a safe vantage point. Invisible portions notwithstanding, the condition of the remaining portion of the bridge appeared to have changed little since the final inspection date.

4.2.1.3 *Condition of the finger joint*

Particular attention was paid to the condition of the remaining half of the finger joint, since any obvious physical damage in this area would materially – and negatively – affect the concrete to which it was attached. For example, a significant deformation in the remaining armor plate during removal of span A could have severely stressed its bond with the surrounding concrete; significant damage in the form of delamination and
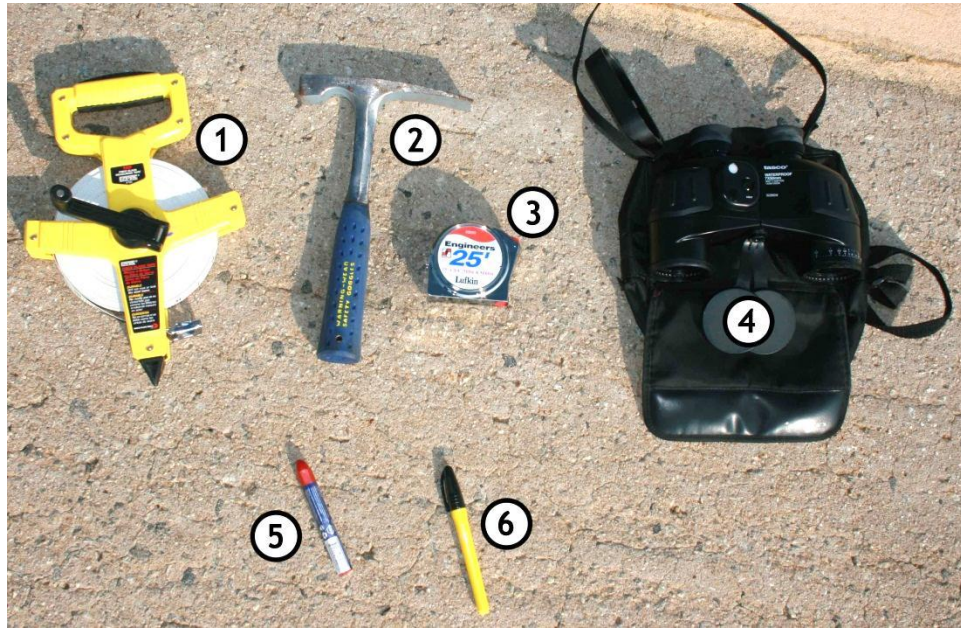
Figure 4.5. Visual inspection tools. (1) fiberglass engineer's tape measure, (2) rock hammer, (3) steel engineer's tape measure, (4) 7x50 binoculars, (5) lumber crayon or "keel", (6) felt-tip marker.

spalling could have occurred as a result. This type of damage is inconsistent with that caused by normal traffic and would thus change the test parameters, possibly to the extent of invalidating the structure as a test site.

The finger joint on the Greyhound Court Bridge was typical of those used on NCDOT highway bridges built during the mid-twentieth century (Figure 4.6). It originally consisted of two interlocking steel plates, the wearing surfaces of which were manufactured with a diamond pattern to increase traction. These "finger plates" are analogous to the joint armor described in Chapter 2, and were attached to anchor plates, which were in turn bonded to the concrete comprising the deck. In addition to their bonding function, the anchor plates for each half of the joint also served as a bearing surface for the fingers of the opposite half. This meant that the ends of the fingers were

fully supported and not cantilevered as with some designs, in effect creating a hybrid finger/sliding plate joint.
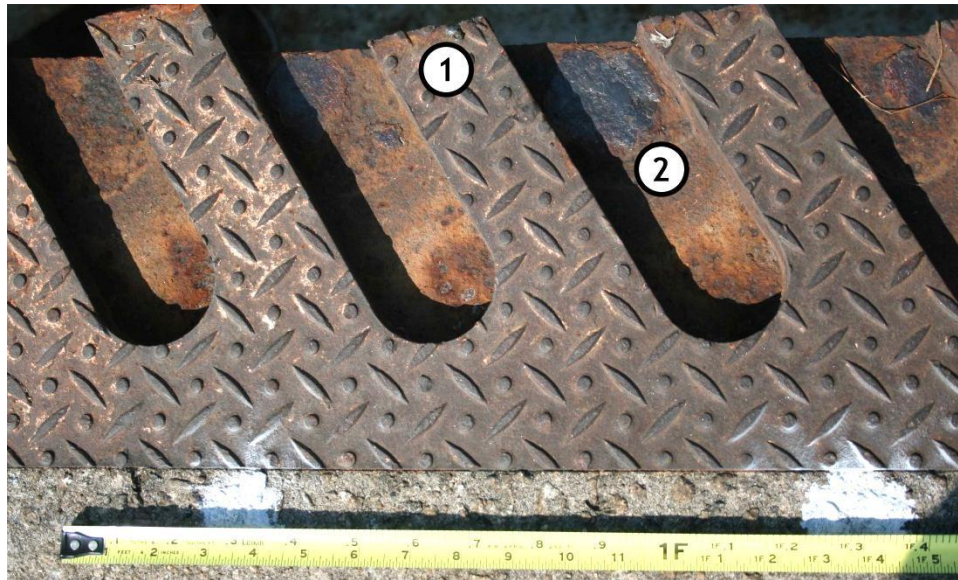
Figure 4.6. Finger joint detail. Note the rough cutoffs at the ends of the fingers (1) and the wear on the anchor plate troughs caused by the opposing fingers (2).

Field assessment of the joint revealed that the process of removing span A did cause some damage to that portion remaining on span B. Some of this damage was inevitable given the nature of structure demolition, but some also occurred because the two halves of the joint were interlocked. The fact that spans B, C and D were to remain standing over a major urban thoroughfare - albeit for a limited time - mandated that their structural integrity be maintained. Some means of separating the two halves of the joint before the demolition of span A was therefore necessary, as any significant damage to the southwestern end of span B could have caused a severe reduction in the shear strength of

that span, possibly to the point of collapse. Separation in this case was apparently achieved by using a cutting torch to sever the ends of the fingers. This was viewed as a relatively benign procedure for the purposes of this study since it didn't involve the extensive use of any heavy impact tools (jackhammers and the like) and because it left the joint's remaining half mostly intact.

Of greater concern was the vertical displacement evident in several of the fingers. This was evidence of one or several strong upward forces sufficient to exceed the elastic limit of the material, possibly a prying action caused by the collapse of span A during its demolition. The severity of these forces was especially noteworthy considering the cross-section of each finger (2 $^3/_8$ in. wide by 1 in. thick). Although the energy involved in bending these members was undoubtedly distributed somewhat by the anchoring steel, the mechanism by which the two were attached was unknown. The nature of the forces (e.g. one or a series of sudden impacts, a slower prying action, etc.) was also a mystery. Therefore, the displaced fingers were mapped, and a decision regarding the joint's suitability was deferred pending inspection of the concrete immediately adjacent to the joint.

4.2.1.4 Condition of the joint concrete

Because the condition of the deck joint itself was in question, the focus of the inspection shifted to the condition of that portion of the concrete deck to which the joint was bonded. This area was also scrutinized very closely for the same reasons listed above. Particular attention was paid to assessing the quality of the wearing surface because major defects in this area would also present difficulties when using the test

equipment. The SSM, for example, requires that the surface under test be relatively uniform, because it is essentially a wheeled vehicle with very little vertical clearance. Any major discontinuity (i.e. surface voids caused by spalling) could cause the unit to "bottom out", resulting in anomalous readings or damage to the unit. This effect is further described in Chapter 5.

The quality of the surface in this area was found to be quite typical of the deck as a whole, exhibiting the weathering, map cracking and evidence of chloride intrusion noted in the report [**27**]. There was very little spalling in this area, and there was no visible evidence of damage due to removal of span A. Tapping with a masonry hammer produced hollow sounds in some areas immediately adjacent to the joint, however. This was potential evidence of delamination, and tended to be more prominent toward the joint ends at the sidewalks, particularly the southern end.

4.3 Virtual Inspection

Virtual inspection of the Greyhound Court Bridge consisted of a High-density Survey using the Leica ScanStation described in Chapter 3. While the entire deck was scanned for future reference, its use in this study was limited to the assessment of the deck area in the vicinity of the joint. All scanning was performed during March of 2011 and had three primary objectives:

1) To build a three-dimensional computer model of the deck surface on which to base accurate measurements away from the field.

2) To provide an accurate record of the surface under test in the event of the structure's demolition.

3) To determine the existence of any rutting or other degradation of the surface caused by traffic during the structure's service life. If extant, a correlation could possibly be drawn to the results of the GPR and SPA testing.

4.3.1 Scanner and Control Placement

Because the bridge deck itself proved to be the only feasible place to position the scanner, two separate scans were necessary to model the entire deck surface (this was a direct result of the "cone of silence" described in Chapter 3). This in turn required that control points be established to allow registration between the two scans, called "Scan Worlds" in the Leica processing software. Control points are normally referenced to some coordinate system (NCDOT uses the NAD 83, NC 3200 coordinate system). Georeferencing was not considered necessary for this study however, since only *relative* deck elevations were needed. As long as the X-Y plane was not rotated about those axes, the point clouds generated during scanning could be rotated to any angle about the Z axis and set at any elevation considered most convenient.

Four control points were set prior to scanning. Control points 1 and 2 were "PK" masonry nails set at opposite ends of a transverse construction joint approximately 35 to 45 ft. (10.7 to 13.7 m) from the actual expansion joint under study. Control points 3 and 4 were also "PK" nails and were set at opposite ends of the expansion joint between Span D and End Bent 2. A registration target was placed atop each control point after it was set.

4.3.2 Scanning of the Deck Surface

For the first scan, the scanner was placed in the approximate center of the bridge at a point approximately 50 ft. (15.2 m) from the expansion joint under study. Once the scanner was switched on, it took a series of digital photographs that were merged into a single panorama. This was used to align the scanner with the registration targets before scanning, and could also be superimposed on the point cloud during post processing.

Before scanning was begun, it was necessary to establish the scan density for different areas of the deck. This was because the time required to complete a given scan is directly proportional to the amount of data gathered. For example, a 10 ft.^{2} (0.93 m^2) area scanned at 10 points per ft. (33 points per m) would result in a point cloud of around 10,000 points. The same area scanned at 100 points per ft. (330 points per m) would return approximately 1 million discrete points. It was therefore decided to scan the area in the immediate vicinity of the joint at a density of approximately 4 points per in. (1 point per 6.4 mm) at 50 ft. (15.2 m). The remainder of the deck was scanned at a density of approximately 1 point per in. (1 point per 25.4 mm) at 50 ft. (15.2 m). This would allow the maximum amount of data to be gathered in the immediate vicinity of the joint while still gathering a reasonable amount of data for the remainder of the deck.

Scanning began immediately after setting the scan density and was completed in approximately 20 minutes. The scanner was then moved to a second position approximately 100 ft. (30.5 m) from the first. Scanning from this position took approximately 10 minutes. The positions of the scanner and the registration targets are shown in Figure 4.7.
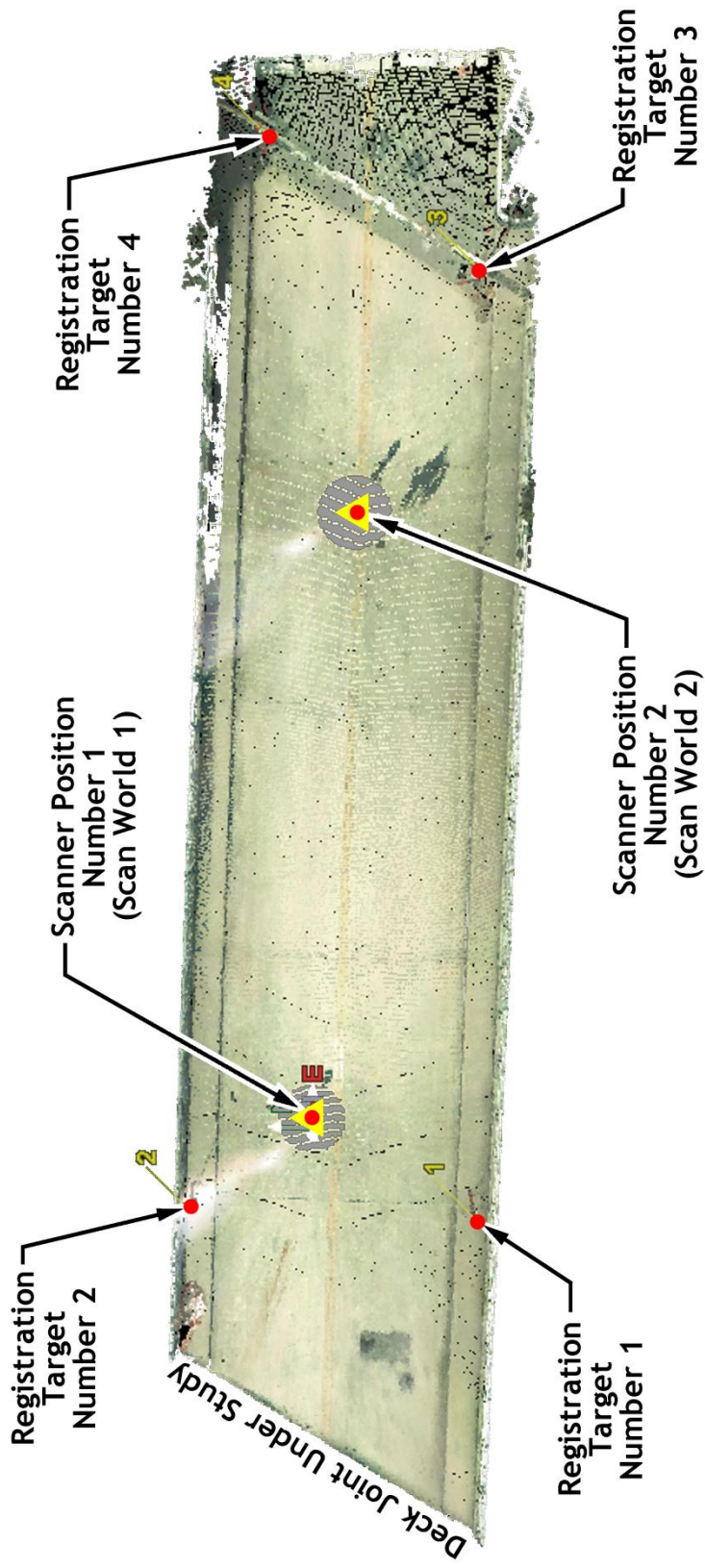
Figure 4.7. HDS scanner and target positions used during the course of this study.

71

CHAPTER 5

FIELD TESTING: EQUIPMENT DEPLOYMENT

5.1 Field Test Procedure Overview

Because two different NDT methods were to be used, it was necessary to lay the proper groundwork for their effective use. This necessarily involved the development of an integrated approach to equipment deployment prior to the actual testing. Such a system would help ensure that (1) equipment deployment would proceed smoothly, (2) the data gathered would be accurate, (3) the procedure could be repeated if necessary and (4) there would be an adequate overlap of data from the two test methods. The development of this procedure involved six tasks:

1) Establishment of test area limits.

2) Determination of test equipment parameters (limitations and capabilities within the context of the test site).

3) Determination of test equipment orientation.

4) Development of a coordinate system suitable for the test site.

5) Marking the test area.

6) Actual deployment of the test equipment.

Each of these methods involved procedures unique to both the equipment used and the test site. The steps involved in the deployment of this equipment are described in detail in the following pages.

5.2 Establishment of the Test Area

Early in the course of this study it was decided to limit the tests to that area of the deck within 2 ft. (0.61 m) of the joint/concrete interface. The main reason for this was to ensure that the joint itself would remain the focus of the testing and reduce any chance of "scope creep". A further consideration was the nature of the damage. Any delaminations or other subsurface defects located further than two feet from this interface was likely to have been caused by factors other than joint debonding.   An added benefit was a reduction of the time and effort necessary for data acquisition.

5.3 Determination of Test Equipment Parameters

5.3.1 SSM Parameters

Establishment of SSM parameters began by determining the closest practical distance it could operate without interference from the steel finger joint. A series of six trial or "proximity" scans were performed with the SSM running parallel to the joint interface. A control scan was run first, with the antenna directly over the top of the steel. The next scan was performed with the antenna directly over the interface. Four more scans were conducted at $^1/_4$, $^1/_2$, $^3/_4$ and 1 in. (6, 12, 18 and 25 mm) from the interface. The resulting data showed little difference between the control and interface scans. Likewise, there was little difference noted between scans taken at any distance from the joint. It was therefore concluded that for the purposes of this study, the minimum distance from the joint interface should be established at 1 in. (25 mm). This would

allow the SSM to scan as close to the joint as possible without interference from the joint itself, while allowing for minor variations and corrections to the scan path.

Surface uniformity was another consideration. Although not expressly stipulated in the SSM instructions, it could be inferred that any surface under test needed to be reasonably smooth. The unit's low clearance – approximately $^1/_8$ in. (3 mm) - combined with the relative non-uniformity of the test surface made it imperative that the scanned area be clean and free of major spalling, small stones, pieces of concrete and other debris. Any object between $^1/_8$ in. (3 mm) and $^1/_4$ in. (6 mm) diameter was a matter for concern. Aside from causing cosmetic damage to the unit, these objects could lodge beneath it and act as a fifth "wheel". This would cause erroneous readings by increasing the unit's clearance above the test surface or by causing it to veer off the designated scan path (Figure 5.1).

(a)   (b)
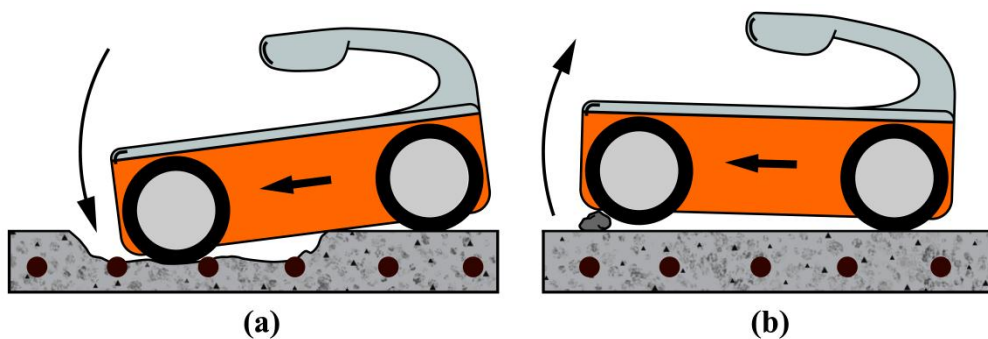
Figure 5.1. Effects of surface damage and debris on the SSM.

Another limiting factor for the SSM was the width of the deck. While the SSM is capable of storing over 7,400 ft. (2,255 m) of scan data, the maximum length of any one scan is limited to 34.1 ft. (10.4 m) – far less than the 46.2 ft. (14.1 m) joint length. Two

separate scans were therefore necessary to gather a single line of data for the entire length of the joint. The accurate mating of these two scans would depend upon the establishment of at least two reference lines. It was decided to use the deck centerline and southeastern gutterline for this purpose. These lines would be established during the marking of the test area.

One final factor regarding the SSM was the physical location of its measurement point, which was just forward of the center of the unit. The existence of the two curbs at the extreme ends of the joint meant that some of its length could not be scanned. While this was not a problem that could be directly solved, it was decided to use these curbs as start and stop points for scanning. The actual length of the unscanned portions of the joint were measured and subtracted from the actual joint length as appropriate (Figure 5.2).
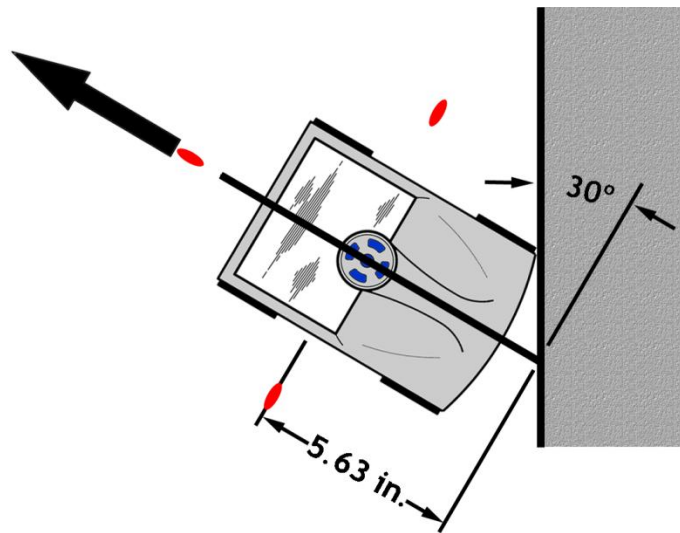
Figure 5.2. Measurement of index laser offset with the SSM against curb.

5.3.2 SPA Parameters

The general capabilities and limitations of the SPA were outlined in Chapter 2. There were several parameters to consider with regards to the test site, however. These involved the nonexistence of an infinite surface, the existence of a large amount of ambient noise at the test site, and proper coupling of the emitter and receiver units.

Because the theories behind the SPA's operation assume an infinite test surface, the deck's physical dimensions became a concern. This was exacerbated by the fact that the majority of SPA testing was to take place in the immediate vicinity of one edge. There was very little that could be done in this regard, with the possible exception of paying attention to the orientation of the instrument during actual testing.

Another consideration was the SPA's susceptibility to ambient noise. The location of the test site was above a busy four-lane urban freeway. Noise from passing traffic was actually felt by the study's author as vibrations within the deck itself; heavy trucks and motorcycles were particularly severe in this regard. Additionally, any movement of those performing the test work could cause further anomalies. It was decided to mitigate these effects by performing as much of the SPA work during off-peak traffic periods and by having the equipment operators remain still during SPA operation.

The weathered deck surface also presented challenges. The exposure of relatively large pieces of aggregate created extremely localized "bumps" in the surface that could prevent proper coupling of the emitter and receivers (Figure 5.3). As with the infinite surface problem, there was little that could be done. Effects of improper coupling could be minimized, however, by (1) following the procedure for placement in the provided

documentation, (2) ensuring that each foot rested upon a reasonably level surface and (3) taking repeated measurements at each test point.

(a)   **(b)**
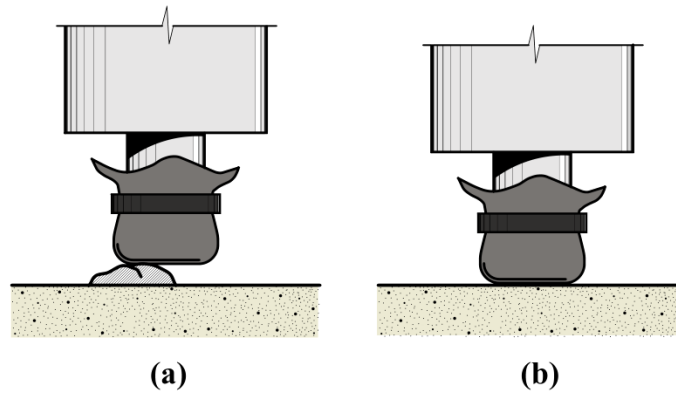
Figure 5.3. Effects of surface on the proper coupling of SPA feet.

To establish the SPA parameters, a series of trial tests was run on the actual deck surface. This had three objectives: (1) to establish the time required to test each point, (2) to gain experience with the instrument under actual field conditions and (3) to verify that the deck's weathered surface would not have a negative impact on the ability of the SPA to gather valid data (see Section 5.3.2). It was found that the mean time required to complete a series of three repeat measurements was approximately 90 seconds; effects of the deck's surface condition would have to be countered by monitoring each set of data.

5.4 Test Equipment Orientation

5.4.1 SSM Orientation

Because it was decided to operate the SSM on paths parallel to the joint under study, there was little to decide with regards to its orientation other than the direction of

scanning. A decision on the scan direction was therefore deferred until the actual reference system was developed.

5.4.2 SPA Orientation

SPA orientation was more problematic due to the proximity of the testing unit to the edges of the deck. The worst-case scenario involved placing the SPA as shown in Figure 5.4 (a), with the instrument's longitudinal axis perpendicular to the joint and the two receivers near the joint itself. Aside from ensuring maximum multipath interference from reflected waves, this position was physically impossible. Testing of those points immediately next to the joint would require that the feet supporting the control box hang off the end of the joint.

The next alternative is shown in Figure 5.4 (b). This also placed the unit's axis perpendicular to the joint, but in this case the source is resting on the joint itself. This would also be unacceptable for testing since the source would be improperly supported and the waves would have to propagate through dissimilar materials. Additionally, there was still the possibility of unacceptable multipath interference from the joint interface.

The third alternative – and the one chosen for actual deployment - was to position the SPA with its axis parallel to the joint as shown in Figure 5.4 (c) and (d). These two orientation options ensured the ability to gather data from those points nearest to the joint. They also helped somewhat to minimize interference from reflected signals. The actual direction the SPA faced would depend upon which side of the centerline the test point lay; that decision was deferred pending the establishment of a reference system.

78
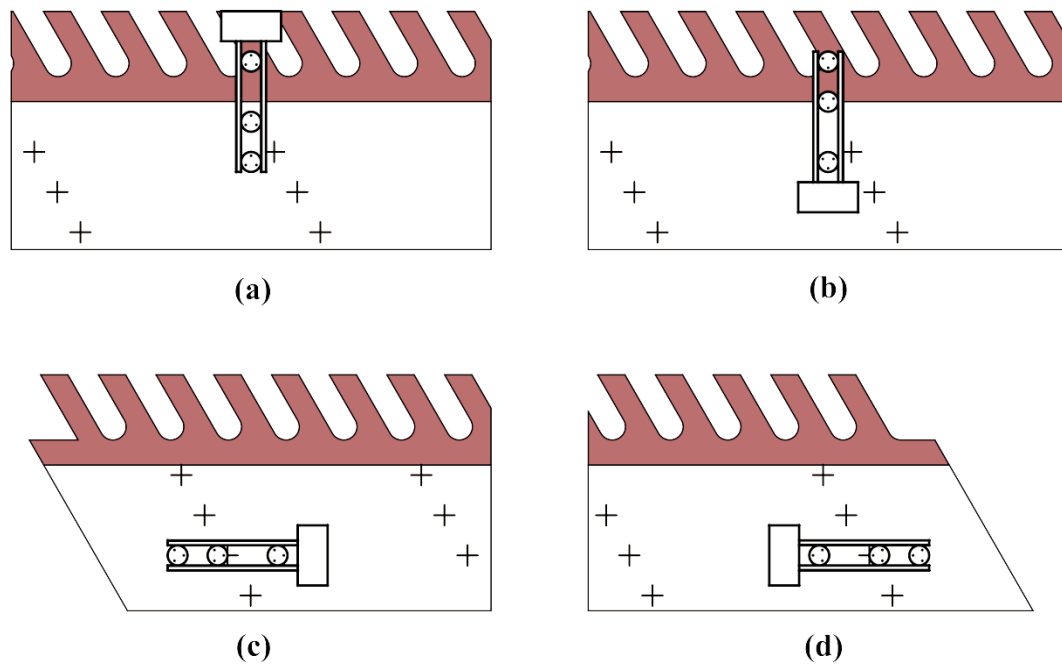
Figure 5.4. SPA orientation options.

5.5 Reference System Development

Two decisions were reached at the beginning of this study. First, all paths to be taken by the test equipment should be parallel to the joint interface under test. The primary reason was simplicity; the interface is easily seen, relatively straight and therefore a logical point of reference for anyone performing these tests in the field. Another reason was that delaminations or other bonding defects were not likely to be localized, but spread out over a considerable length of the joint. Operating the NDT equipment in this manner would increase the likelihood of detecting these anomalies. An additional benefit was speed, particularly with regard to the SSM deployment; it was faster to conduct a few 23 ft. (7.0 m) scans than a multitude of 2 ft. (0.61 m) scans.

The other decision was to use an initial spacing between paths of 4 in. (0.10 m). The reasoning here was flexibility; the 2 ft. (0.61 m) test limit was divided evenly by 3, 4 and 6 in. (76, 102 and 152 mm). Path spacing could be reduced to 3 in. (76 mm) if the data gathered during the initial testing was determined to be insufficient. The spacing could likewise be widened to 6 in (0.15 m) if too much data were gathered, or if data acquisition became too time-consuming.

The system traditionally used in Transportation Engineering and Route Surveying is the horizontal alignment, essentially a number line that follows the centerline of the route taken by a given project. Even stations are numbered in hundreds of feet (or meters), with objects and sites of interest located by perpendicular offsets to the left (negative offset) or right (positive offset) of the alignment. This method was determined to be too unwieldy for this study for three reasons: (1) the test area itself was relatively small, (2) the joint itself was used as a reference and (3) the missing span made its use inconvenient and perhaps even dangerous.

A hybrid system was therefore developed. The alignment followed the traditional route, which in this case was the bridge's centerline. This was easily determined in the field by direct measurement. Stations were then marked at 1, 5, 9, 13, 17, 21 and 25 in. (25, 127, 229, 330, 432, 533 and 635 mm) from the joint interface. Offsets in feet were then taken with reference to these stations and parallel to the joint under study. Offsets Left and Right were oriented as one faced the joint from the deck. A schematic of the hybrid reference system is illustrated in Figure 5.5.
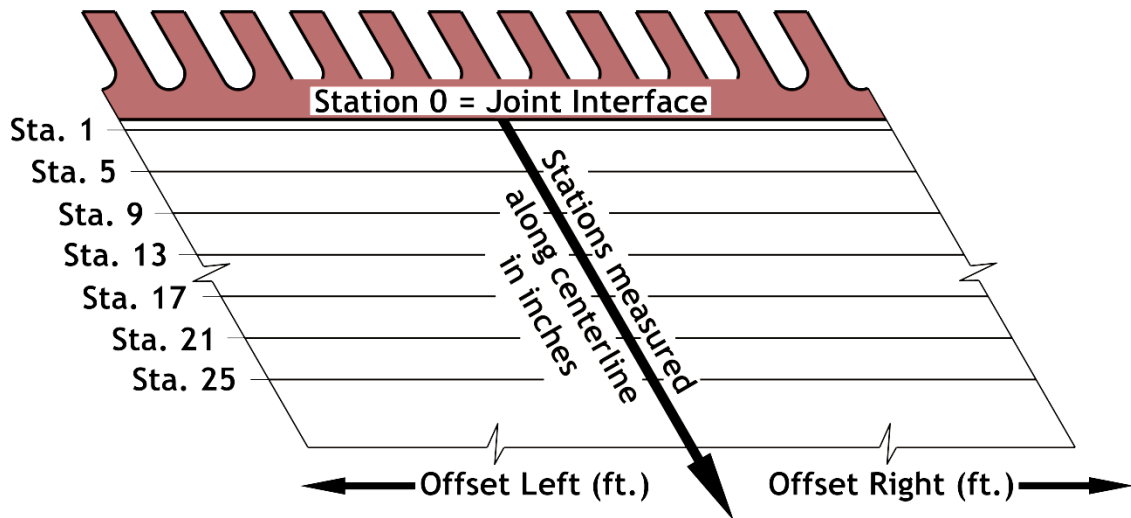
Figure 5.5. Hybrid reference system schematic.

5.6 Marking the Test Area

Accurate marking of the test area was necessary for the proper use of the test equipment and to ensure the reliability and repeatability of the results obtained. This proceeded in two phases: (1) chalk line marking for the SSM and (2) paint marking for the SPA. The SPA paint marking was done after scanning with the SSM to avoid aberrations in the GPR results due to any dielectric variation of the paint (the pigments of many paints contain metallic compounds that could affect the reflectivity of the GPR signal). Although each marking phase was completed prior to its corresponding test, both procedures will be outlined in this section.

Figure 5.6 illustrates the deck marking procedure. The centerline of the bridge was marked first, since the deck's crown could interfere with the chalk line. A fiberglass Engineer's tape measure was stretched across the deck at the joint interface, the distance

noted and a "crow's foot" mark drawn at the halfway point with a felt-tip marker (a). Next, the stations points plus one point 3 ft. from the interface were drawn at each gutterline (b). The tape was stretched across the 3 ft. (0.91 m) points and a second centerline point marked as before (c). A steel Engineer's tape measure and felt-tip marker were then used to mark the station points at the centerline. Finally, the chalk line was stretched and snapped between corresponding pairs of station points (d). The resulting lines were then used to guide the SSM during joint scanning.

(a)

(b)

(c)

(d)
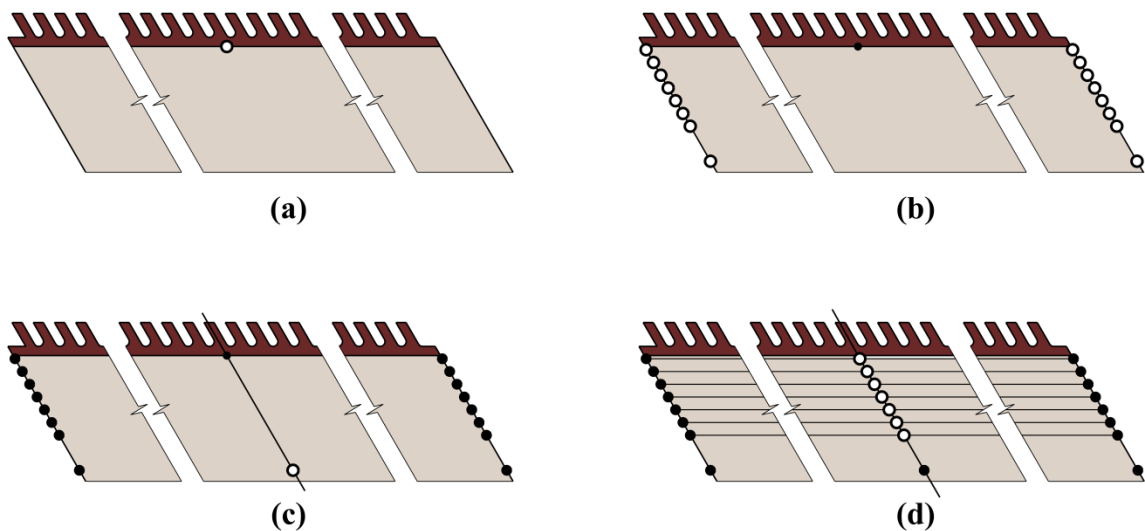
Figure 5.6. Deck marking sequence.

Paint marking for the SPA began after the GPR scans were complete and the results verified. This process began by stretching the fiberglass tape parallel to the chalk line for Station 1. The tape was shifted until an even foot on the tape corresponded to the centerline. A lumber crayon was then used to mark each offset from the centerline in 1 ft. (0.30 m) intervals. This was repeated for each station until the offsets for all stations

were marked. Marking paint in a spray can was used to "dot" the location of each offset (Figure 5.7). The paint was allowed to dry thoroughly before SPA testing was begun.

Figure 5.7. Painted SPA test points at the centerline.

5.7 Test Equipment Deployment

5.7.1 SSM Deployment

Three scan "sets" were used during the deployment of the SSM, all of which used the same system settings outlined in this section. The first set consisted of the Proximity Scans outlined in section 5.3.1. The second set was termed "Rebar Scans", which were used to detect the location of the upper layer of reinforcing steel in the vicinity of the joint. The third and final set was known as "Joint Scans". This was the set used to detect any potential delaminations or other subsurface defects.

Before the SSM could be deployed for this study, however, several housekeeping procedures needed to be performed. These were necessary to ensure that data acquisition proceeded rapidly and smoothly and to ensure the integrity of the gathered data. All

procedures were performed in accordance with the directions outlined in the Quick Start

Guide [**28**]. These included:

    1) Resetting the unit to the factory defaults

    2) Erasing the SD memory card

    3) Establishing the global settings to be used on all scans

Several additional SSM options had to be changed from the factory defaults before the

actual scanning could begin. The majority of these settings were located in the System

Main and Configuration menus.

Settings within the System Menu were checked first. The current date and time

were verified, and all files were cleared from the SD memory card. The Scan Density

was set to "High", which allowed for data to be collected at the rate of approximately 240

scans per ft. (8 scans per cm). The backlight was set to "100%" to make the display

easier to read in direct sunlight. Finally, the Save Prompt setting was set to "On". This

would allow each separate scan to be reviewed before saving to the SD card. Table 5.1

lists the System menu settings used in this study.

Table 5.1. SSM System menu settings used in this study.

Menu Item	Available Options	Test Setting
Date/Time	Direct User Entry	Current date/time
Configuration	N/A	See Table 5.2
Calibration	N/A	N/A
Clear	All files or specific files	All files
Scan Density	High/Normal	High
Backlight	25/50/75/100%	100%
Save Prompt	On/Off	On

The Configuration Menu was then entered and the appropriate options chosen. The Orientation option referred to the orientation of the SSM's built-in display when held in either the right or left hand. This was set to "Left" since the SSM's direction of travel would be from left to right, with the unit guided by the operator's left hand. The Language and Units options were both set to "English" for obvious reasons. The Laser option was set to "On" since the SSM's built-in lasers would be used to guide it along each scan path. They would also be used to position the unit over the deck centerline. The Sound option was set to "High" so that any warnings or notices could be heard above the traffic noise. Table 5.2 lists the Configuration menu settings used.

Table 5.2. SSM Configuration menu settings used in this study.

Menu Item	Available Options	Test Setting
Orientation	Left/Right	Left
Language	English/French/Spanish	English
Units	English/Metric	English
Laser	On/Off	On
Sound	High/Medium/Low/Off	High
Version	N/A	N/A

Calibration of the SSM was performed once the initial settings were complete. This was done not only to ensure the validity of the gathered data, but also to maximize the unit's performance in detecting both reinforcing steel and subsurface anomalies. This procedure was performed in accordance with the instructions outlined in the Quick Start Guide. It consisted of choosing the Calibration option in the SSM's main menu, holding the unit approximately 3 ft. (1 m) from any vertical surface, and pressing the Enter button. Calibration was completely automatic and took approximately two seconds.

Data collection began after completion of the housekeeping tasks and initialization of the global settings. Before each scan set, the options in the data collection menu were set (or confirmed) as shown in Table 5.3. A scan depth of 8 in. was chosen for several reasons, primarily because any delamination or other phenomena connected to the bonding of the joint was unlikely to exist any deeper than the actual depth of the joint itself. Another reason was to avoid any possible reflection from deep layers of reinforcing steel or from any other metal, such as the corrugated metal decking used as forms on modern construction. Although the actual dielectric constant of the concrete was unknown, the Dielectric option was set to 6.1 – considered to be a good estimate of ε for fully cured concrete [28]. The Auto Target option was set to "Off" and the display was set to "A+B" to allow the o-scope to show phase shifts in the signal that may not be obvious otherwise. Finally, the scan color was set to a smooth black-to-white gradient. This was done for two reasons: (1) the grayscale scan could be more easily seen and appraised in bright sunlight and (2) there was little advantage to be gained in using any of the color modes. The Data Collection menu options used during this study are listed in Table 5.3.

Table 5.3. SSM Data Collection options.

Menu Item	Available Options	Test Setting
Start Collect	Toggle On/Off	As needed
Depth	8/12/16 in. (20/30/60 cm)	8 in.
Dielectric	User selectable from 0 to 81 (in increments of 0.1)	6.1
Auto Target	On/Off	Off
Display	A (Data only) or A+B (Data + O-scope)	A+B
Color	5 different color schemes	B→W

The Proximity scans were performed first as outlined in section 5.3.1. The Rebar scans were performed next. The first of these was performed on the marked centerline since it intersected the upper layer of reinforcing steel at an angle of approximately 90 degrees. Scanning began by positioning the side laser index points just over the interface; the SSM was then pushed along the centerline until the lasers were just beyond Station 25. The scan data was then checked for completeness and accuracy before being stored. The procedure was repeated on both sides of the centerline at Offsets 22, 20 16, 12, 8 and 4. The Joint Scans were begun upon completion of the Rebar Scans. The procedure was used as that used for the Rebar Scans except for the scan pattern, which is illustrated in Figure 5.8. Stations to the right of the centerline were scanned first, followed by those on the left.
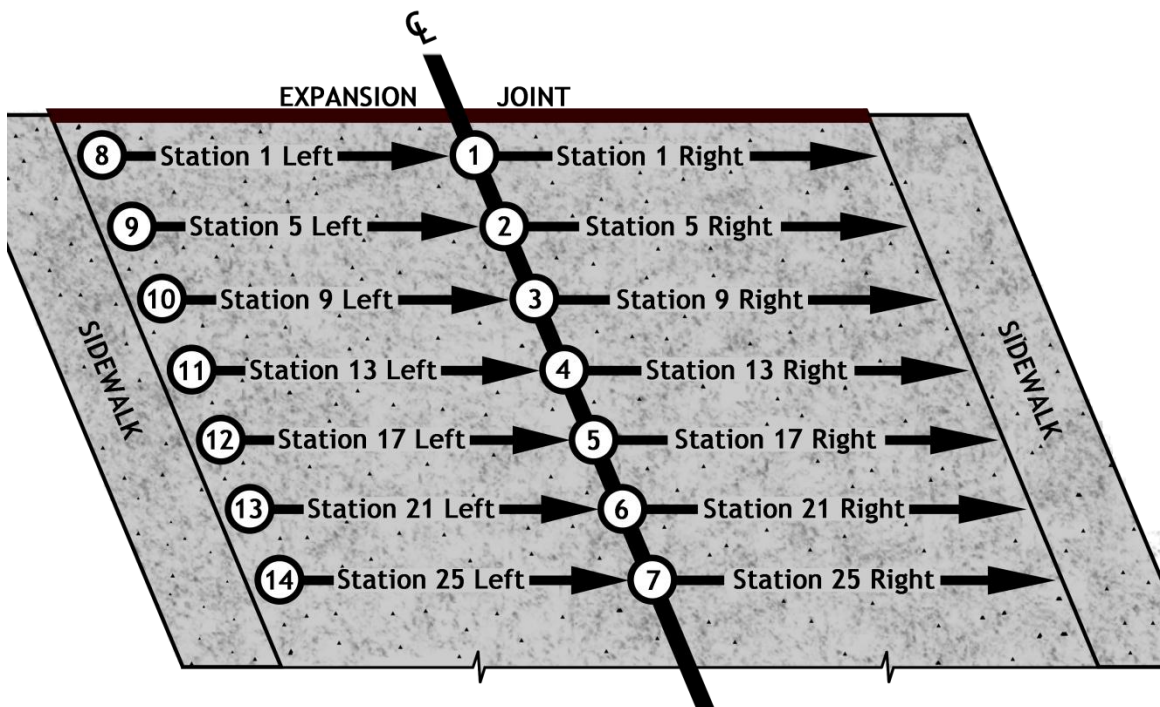
Figure 5.8. Schematic of SSM scan pattern.

87

5.7.2 SPA Deployment

Before SPA testing began, a balance needed to be struck between the amount of data needed for an accurate assessment and the time that would be required for data acquisition. This was determined by the following formula

$$T_T = \frac{\left[N\left(t_{mean} + t_{position}\right)\right]}{3600} \tag{5.1}$$

where T_T is the total time required for testing in hours, N is the number of points to be tested, t_{mean} is the mean time (in seconds) required to complete a series of three repeat measurements (approximately 90 seconds) and $t_{position}$ is the estimated time (in seconds) required to reposition the instrument between consecutive test points (approximately 45 seconds).

Testing all 315 marked points would have required an absolute minimum of twelve hours, which was considered to be time and cost-prohibitive. Furthermore, real-world testing on an intact structure would require that the procedure be performed on both sides of the joint, effectively doubling the test time.

Therefore a decision was made to reduce the number of points to be tested. This was accomplished by limiting testing to the even offsets plus centerline point at stations 1, 9, 17 and 25. This reduced the total number of test points N to 92 and TT to approximately 3 1/2 hours. These numbers presented a much more realistic balance in terms of test time versus accurate representation of the concrete moduli surrounding the joint.

One final detail needed to be decided before SPA testing could begin: the instrument's position over the point under test. The relationship between the IE and USW modes (outlined in Chapter 3) demonstrated that the data gathered for each required a different source-emitter combination. Therefore, the centerline of each test was necessarily different; the IE tests were centered between the source and near receiver, while the USW tests were centered between the source and far receiver. Because the difference between the two was known and consistent, it was decided to position the SPA so that the centerline of the USW test mode lay directly over the point under test. Furthermore a decision was reached to face the SPA so that the source was positioned away from the centerline (Figure 5.9). This would further minimize the finite surface effects of concern in Section 5.4.2.

Offsets Left　　　　　　　　　　**Offsets Right**
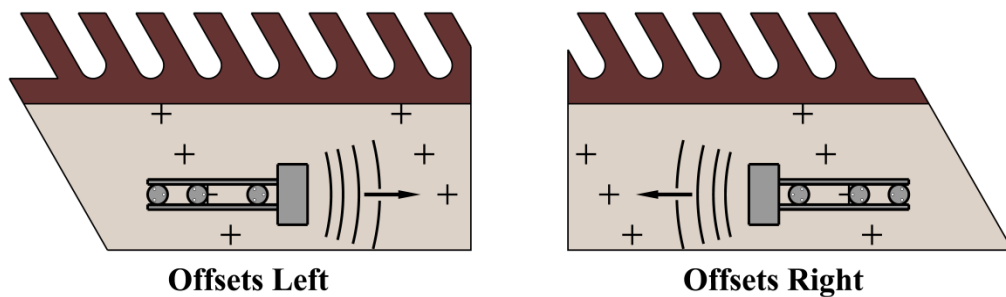
Figure 5.9. SPA positions for Left and Right Offsets.

Testing was begun by connecting the USB cable between the SPA and the Laptop. The appropriate file information and setup parameters were then established using the SPA Manager software. The instrument was then placed carefully over the first

test point - Station 1, Offset 22 Left - and the "TEST" button was pressed on the laptop screen. The SPA completed three sets of measurements, after which the test data was automatically reduced. This data was reviewed for consistency before acceptance; any major variances in the waveform, USW or IE graphs between the three individual measurements resulted in the instrument being repositioned over the test point and the measurements repeated. Otherwise, the SPA was placed over the next test point and the procedure repeated until data was collected on all 92 points. The typical position of the SPA over a test point is shown in Figure 5.10. Complete results of the individual test points are provided in Appendix B.
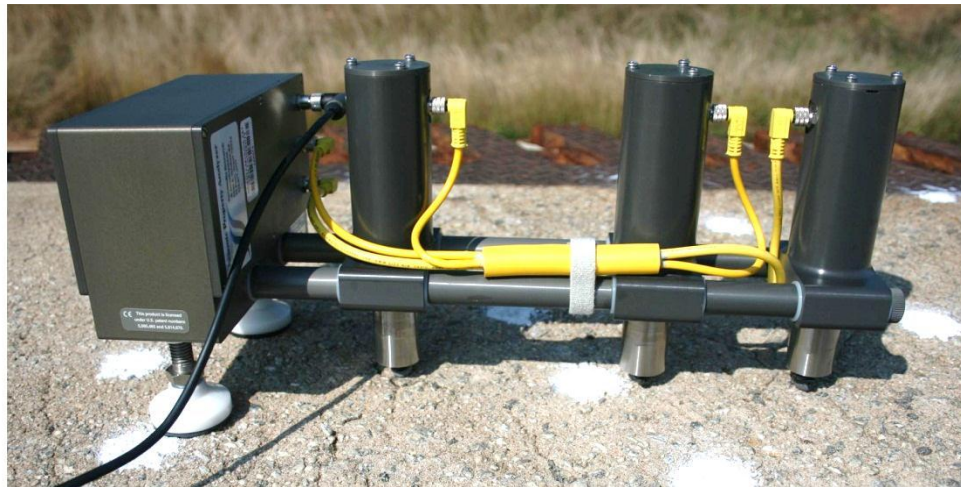
Figure 5.10. Typical SPA position over a test point.

CHAPTER 6

RESULTS AND DISCUSSION

6.1 HDS Results

6.1.1 Data Download and Processing

The Leica ScanStation described in Chapters 3 and 4 did not directly output data in a form that could be used directly in the field. The gathered data needed further processing before drawing any conclusions regarding the deck's surface topography. Two determinations needed to be made based upon this data:

1) The relative slopes of the deck surface in the vicinity of the joint.

2) The existence of any rutting or wear in the vicinity of the wheel paths.

Because much of the technology involved with HDS methods is "black box" – i.e. the internal processes are not open to inspection or intervention by the user – only a cursory explanation of the process will be given here.

Initial processing of the two point clouds (or *scan worlds*) was performed using Cyclone version 7.1.3 by Leica Geosystems. The two sets of data were matched or "indexed" using point data from the four targets described in Chapter 4. They were then combined into one point cloud, which was then converted into a Microstation CADD file. This point cloud was then edited to remove all points except for those within 4 ft. (1.2 m) of the joint interface. The remaining points were then rotated about the Z-axis until the joint interface lay parallel to the bottom of the computer screen. Finally, a Digital

Surface Model (DSM) was created using GeoPak (a Microstation add-on) and contours drawn at an interval of 0.1 ft. (30 mm). These contours are shown in Figure 6.1.
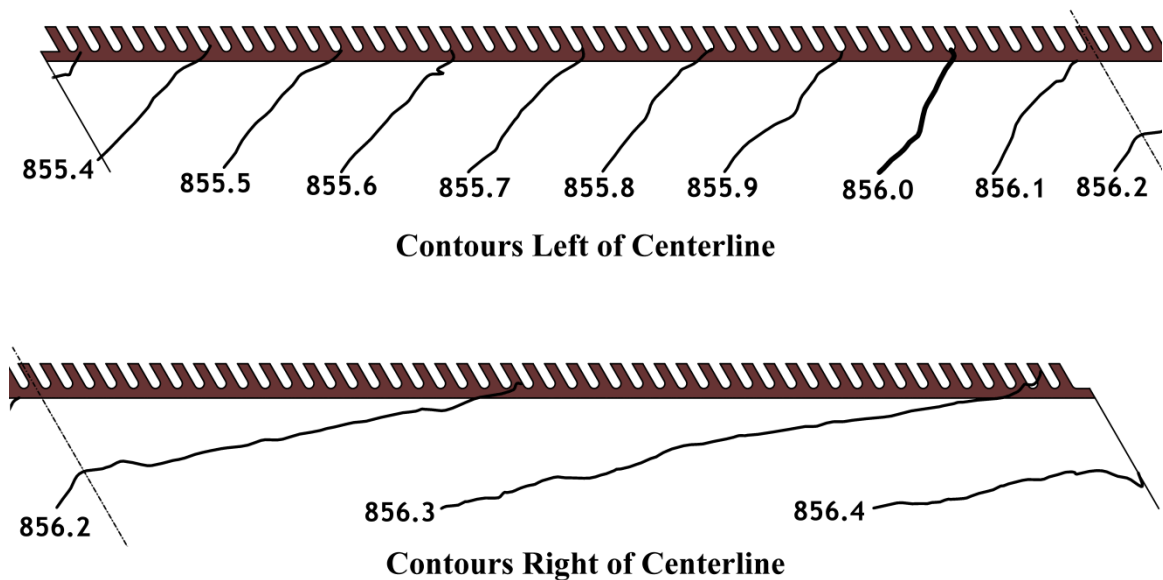
Figure 6.1. HDS-generated deck contours. Elevations are in US feet.

6.1.2 Analysis of HDS Data

The contours clearly show that the deck surface slopes downward along its longitudinal axis towards the joint. In addition, these contours show the differences in the deck slope (also known as superelevation) on either side of the centerline. Superelevation on most two-lane bridges is typically crowned, where both sides slope downward from the centerline to facilitate drainage. This crowning is existent on the Greyhound Court Bridge; however, the slopes on both sides of the centerline are such that the spacing of the contours to the left of the centerline indicates a steeper slope in

this area, suggesting that the deck was not level. This - coupled with the fact that the joint under study lies toward the extreme downhill end of the structure – suggests that the deck surface in the vicinity of the joint's left side was particularly susceptible to the effects of water ponding and possible seepage throughout its service life.

The contours also showed little or no evidence of rutting due to traffic or other such wear. These would have appeared as curves in the contours that bowed away from the joint and would have been located in the general vicinity of the wheel paths. Only the two contours at 855.9 ft. and 856.0 ft. display this effect; however, their positions are outside the areas where any wheel wear would be expected to occur.

6.2 GPR Results

6.2.1 Data Download and Initial Processing

While scan data could be viewed directly on the SSM's built-in screen, this approach suffered from several limitations. First, the screen's small size meant that only a small portion of any individual scan could be seen at once. This made it difficult to see any trends in the data that may have occurred gradually over longer scan distances. Another problem was the inability of the unit to produce directly useful output (other than a .bmp screenshot file) for detailed study or inclusion in a report. Furthermore, all scans were stored on the unit's SD card in the SSM's native – and proprietary - .DZT format, which was able to be read only by GSSI software. These three factors made it necessary to convert the raw data into a different format that would allow for more thorough analysis.

These difficulties were solved using GSSI's StructureScan Mini Viewer, a JAVA applet available on the GSSI website. It allowed the conversion of data from the SSM"s native .DZT format into a series of JPEG files. In addition, it provided processing capability that, while somewhat limited, greatly enhanced the ability of the researchers to draw conclusions on the gathered data.

The .DZT files for all scans were downloaded directly from the SSM to a desktop computer using the supplied USB cable. The StructureScan Mini Viewer was started in a web browser and the .DZT file for the first scan loaded. The chosen scan was then visible on the screen (Figure 6.2). Initial processing began by ensuring the applet's dielectric constant was set to 6.1 to match the number used in the SSM during the actual scanning. Next, the "Find Surface" button was selected to automatically remove the coupling area between the bottom of the SSM and the deck surface. The "Remove Background" button was selected to remove extraneous background noise from the image. Finally, the "Gain" slider was adjusted to achieve a readable image. The resulting image was then checked for errors before being stored as a .jpg file. This process was repeated for all of the remaining 13 scans.

A preliminary look at the scans revealed much about the bridge's structure (Figure 6.3). Scans closest to the joint under study revealed the relatively complex structure of the reinforcing steel in that area (see Appendix A, Stations 1 and 5). Echo signatures from the bottom of the slab were notably absent, possibly because of 1) interference from the reinforcing steel, 2) increased slab depth, and/or 3) the fact that the scan depth of the SSM was limited to 8 in. (203 mm). Images further from the joint

interface exhibited echo signatures from the bottom of the deck as well as the girder locations (see Appendix A, Stations 9, 13, 17, 21 and 25). This was considered as evidence of the SSM's ability to detect discernible patterns beneath the layers of reinforcing steel. These echo signatures were later used as the primary means of determining the maximum coring depth.

Of particular interest was the existence of several discolored or "ghosted" areas in the images. These were located primarily between the surface of the concrete and the upper layer of reinforcing steel. These apparent anomalies varied considerably in their intensity and were considered as possible evidence of delamination or other defects; many of these areas tended to sound hollow when struck with a hammer.
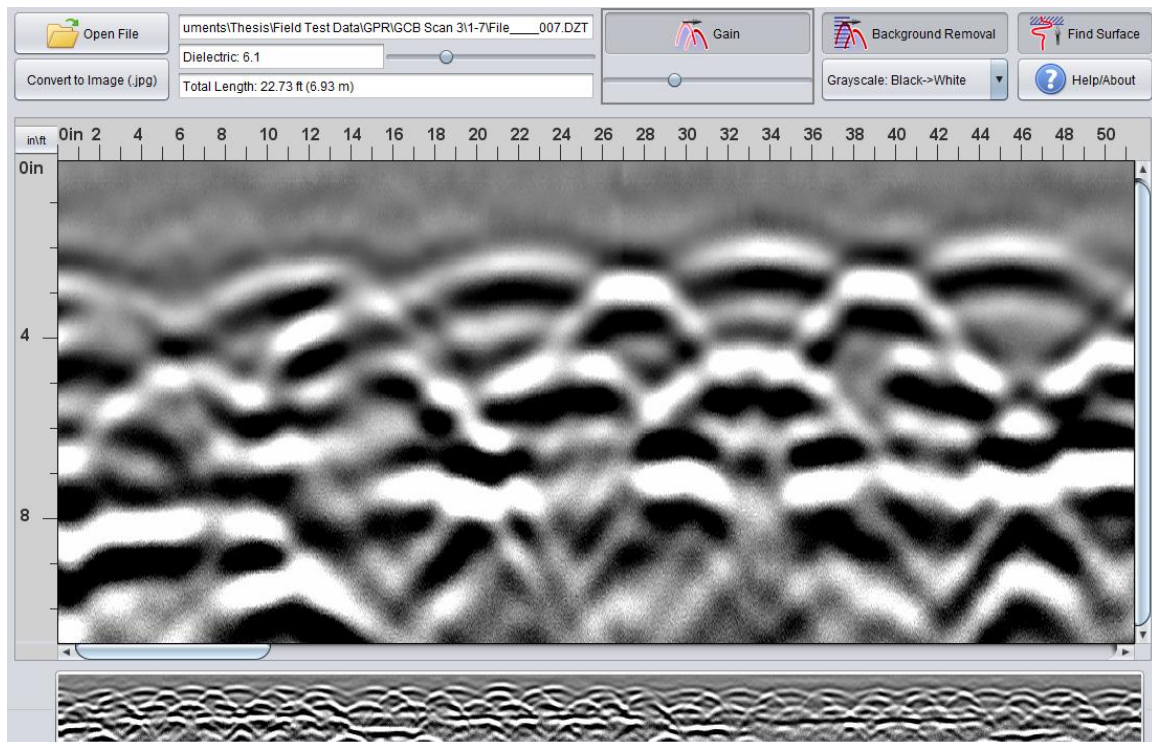
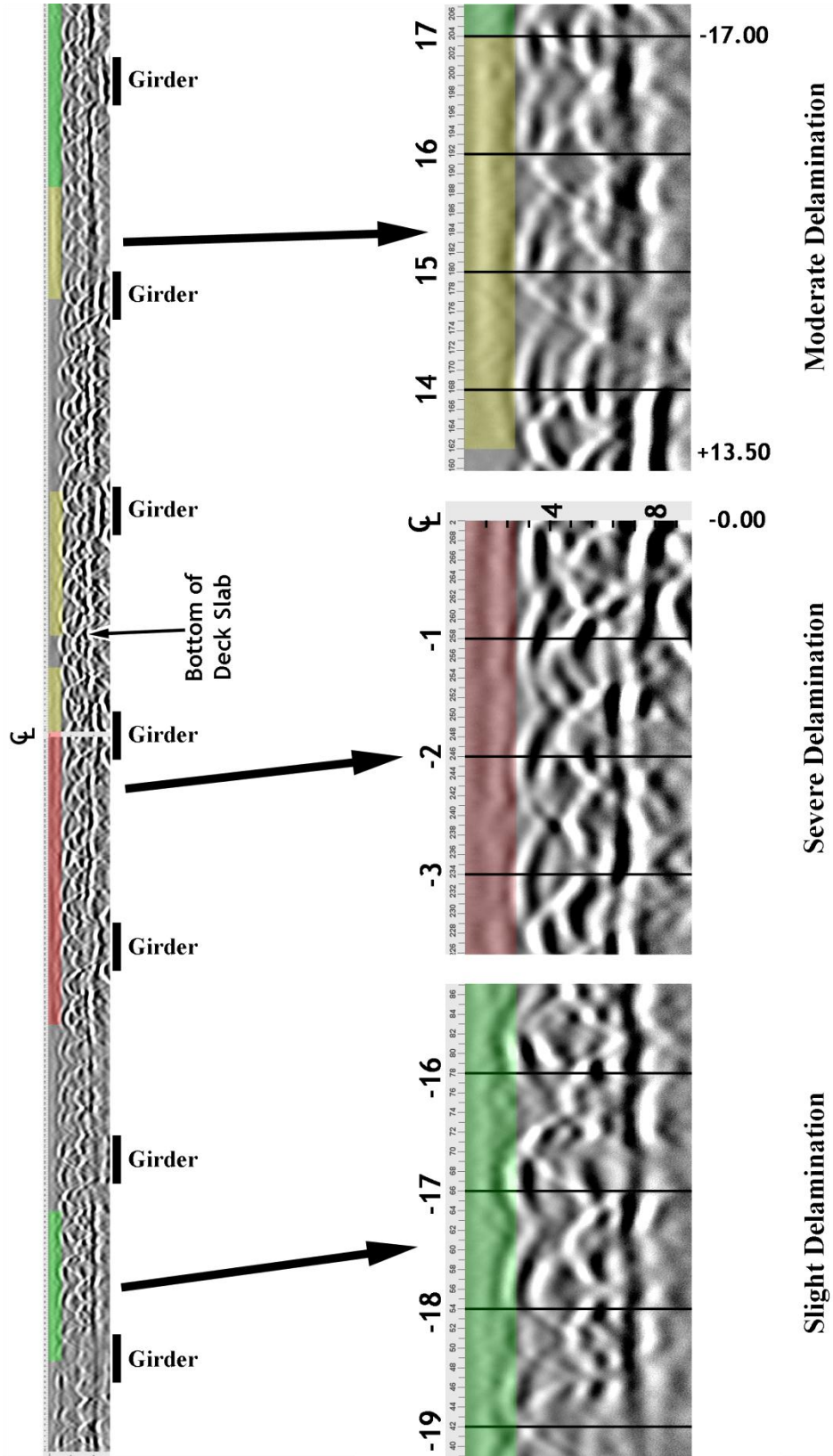**Figure 6.2. GSSI's StructureScan Mini Viewer.**

Figure 6.3. Typical GPR scan (Station 21 shown).

6.2.2 Detection of Anomalies in the Scan Data

The next step in processing the data was the detection and quantification of any suspected delamination. This was done visually by noting any extended areas of discoloration in each image that could not be accounted for by other objects such as reinforcing steel. A color-coded system was devised based upon the four-tier system used by Nazarian, et. al. in Chapter 2. Areas that exhibited little or no discoloration were not suspected to suffer from delamination and were therefore left uncolored. Areas which showed a linear ghosting effect were considered to be slightly delaminated and were tinted green. Ghosted areas which tended to exhibit dark edges above and below were labeled as moderately delaminated and tinted yellow, while areas suspected to suffer from severe delamination tended to exhibit rather well-defined dark boundaries; these were tinted red. All color coding was done using Adobe Photoshop Elements 9 and is illustrated in Figure 6.3. The complete set of scan data is given in Appendix A.

6.2.3 Scan Data Mapping

For the GPR testing, the ability to draw conclusions regarding the joint required that the results of the scan data be superimposed on a scale map of the deck surface. Again, this was accomplished by using Microstation. Each area of suspected delamination was drawn to its appropriate length using the data presented in Appendix A, then placed in its corresponding location on a scale outline of the joint area. The resulting delamination map is illustrated in Figure 6.4.

According to the GPR data, there appeared to be widespread evidence of damage to the concrete left of the deck's centerline. The areas most affected – those locations

where deterioration was rated as moderate or severe - appear to have occurred in the immediate vicinity of the joint interface and in those areas toward the centerline. Apparent deterioration tended to be less severe at the extreme left of the joint, although it was evidently just as widespread. There were isolated severe and moderate readings toward the left sidewalk at Stations 17 and 25, respectively. The region in the center of the travel lane showed much less evidence of deterioration; large portions of the scans at Stations 1, 5, 13, 17 and 21 Left revealed no visual anomalies that could be construed as evidence of damage.

The GPR data to the right of the centerline showed a similar pattern, although it was not as widespread. Areas of slight deterioration were detected immediately to the right of the centerline at Stations 1, 5, 17 and 25, while severe areas were detected at Stations 9 and 13. Unlike the readings on the left side, these generally extended only 2 to 3 ft. (0.6 to 0.9 m). With a few exceptions, the damage generally appeared to be light toward the centerline and more severe toward the right side of the joint.

The distribution of the GPR data on both halves of the deck suggests that the majority of the damage to the concrete appeared to lie in those areas directly in the vehicle wheel paths. This is evidenced by the relative scarcity of damage in the center of each lane. This fact correlates well with the outcome of the survey described in Chapter 2, where 100% of the respondents stated that damage to the armored joints was most apparent in these locations. However, the widespread nature of the suspected deterioration as shown by the GPR data suggests that it may be due to causes other than debonding of the joint.
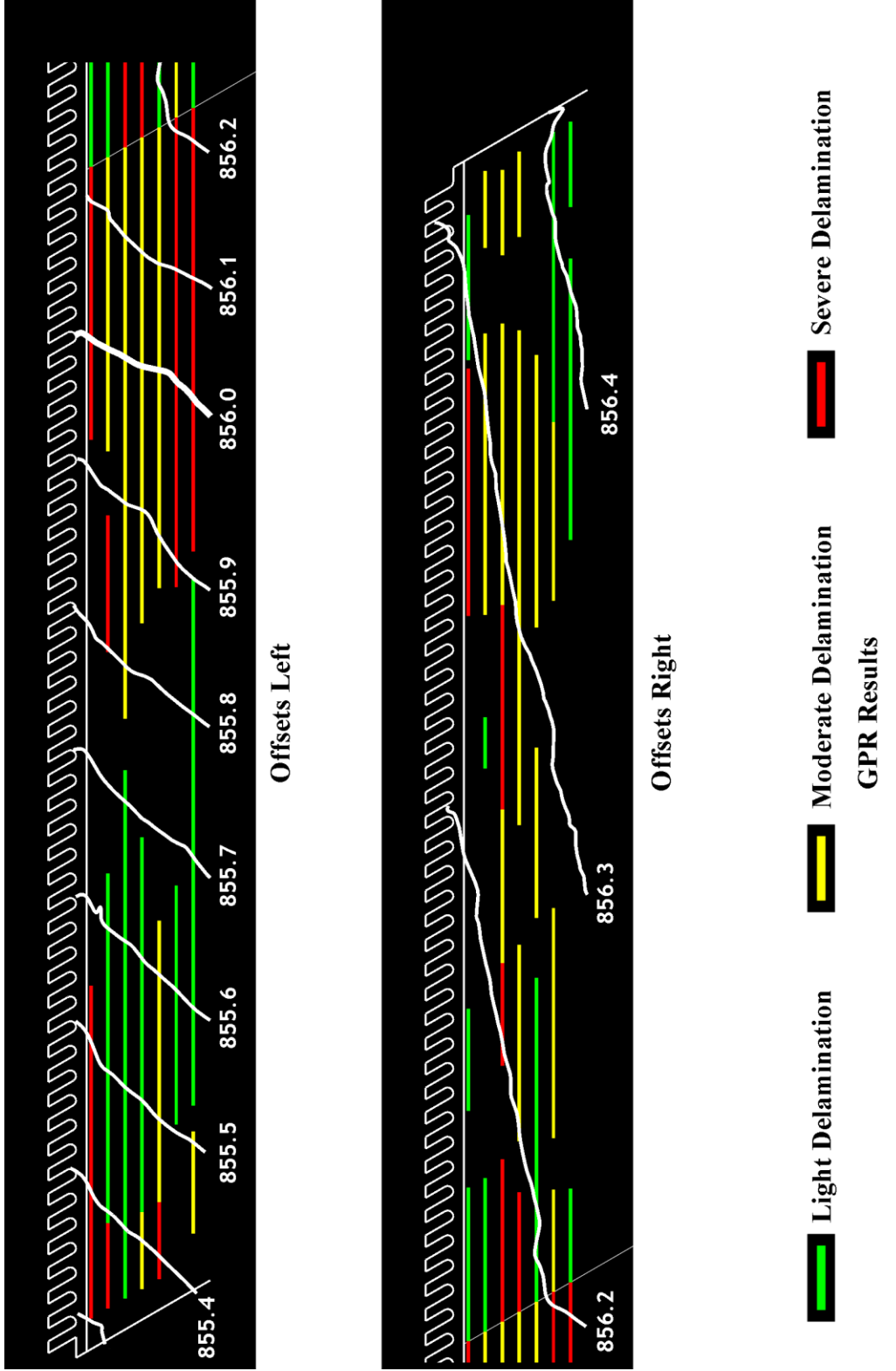
Offsets Left

Offsets Right

Light Delamination ■ **Moderate Delamination** ■ **Severe Delamination**

GPR Results

Figure 6.4. Deterioration map: HDS and GPR data.

99

6.3 SPA Results

6.3.1 Data Download and Initial Processing of Modulus Data

Mapping of the SPA modulus data was achieved using the SPA Manager and MATLAB. The SPA data was saved as a text report using the SPA Manager software. Since there were three average values for each test point, it was necessary to use some method of arriving at the most likely value to represent the modulus of a given point. Selecting the closest two modulus values for each test point then choosing the lower of the two as representative was considered, then rejected because of the potential for wide variability between readings on the same test point; some differed by as much as 1500 ksi (10.34 GPa). It was decided instead to use the average of the three individual modulus values, while paying attention to the standard deviation of each individual point.

Each data point was then assigned X and Y coordinates appropriate for its station and offset. These were saved in 92×1 vector matrices "X" and "Y" in MATLAB. A third 23×4 matrix "M" was created using the derived average modulus values for each point. This matrix was linked to the "X" and "Y" matrices to create a color contour plot. In an attempt to quantify any subsurface defects, the same four-tier scale was used as with the GPR scans. The suspected deterioration scale is shown in Table 6.1.

Table 6.1. Color-coding system for SPA data.

Damage Severity	Modulus Criteria	Color
None	> 3.5 ksi (> 24.1 MPa)	Blue
Slight	2.0-3.5 ksi (13.8-24.1 MPa)	Green
Moderate	1.0-2.0 ksi (6.9-13.8 MPa)	Yellow
Severe	≤ 1.0 ksi (≤ 6.9 MPa)	Red

6.3.2 Processing of IE Data

Initial review of the IE data verified that the deck was in poor overall condition. The IE signature for the majority of the test points displayed numerous high-amplitude echoes at varying depths, evidence of significant deterioration (Figure 6.5). This phenomenon was observed with reasonable consistency throughout the test area. An attempt was made to quantify and map this data, but no reasonable means to do so could be formulated. Therefore, the IE signature for each test point was reviewed individually and compared to the frequency and modulus plots.
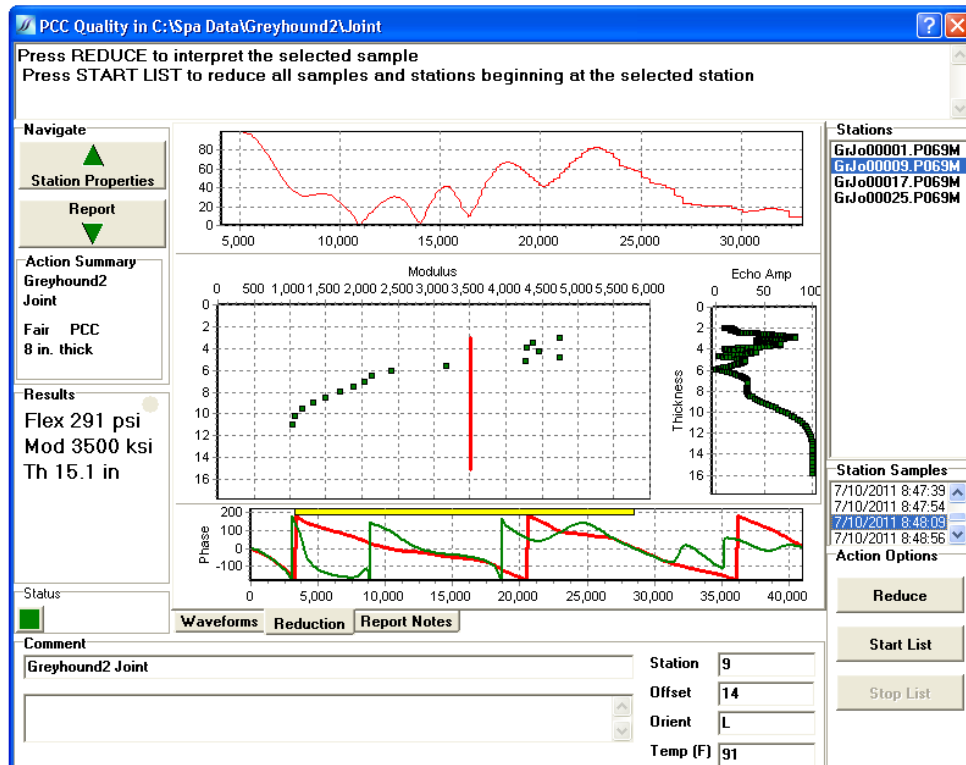

Figure 6.5. Screen capture of a typical SPA data reduction (Station 9, 14 ft, Right).
IE plot is at the middle right.

Another observed phenomenon was the apparent 2 in. (51 mm) offset in the thickness of the concrete. This offset must be subtracted from any reading on the scale in order to determine the correct depth of a given defect. The bottom "knee" of the IE graph indicates a depth of 8 in. (203 mm); subtracting 2 in. (51 mm) from this reading yields a total depth of 6 in. (0.15 m) in this location. This was subsequently verified during the process of collecting core samples.

6.3.3 Analysis of SPA Data

The deterioration map based upon the SPA data is given in Figure 6.6. According to this set of data, the majority of moderate to severe delaminations appear to lie in the area to the left of the centerline. The entire area approximately 7 ft. (2.1 m) to the right of the gutter appeared to be in relatively poor condition, with no reading over 2.0 ksi (13.8 MPa). The most severe deterioration appeared at the joint interface and in several intermittent areas toward the centerline. The remainder of the readings showed modulus values in the range of 2.0 to 3.0 ksi (13.8 to 20.7 MPa), with no reading over 3.5 ksi.

Similar results were obtained with data from the right half of the joint. While there were a few readings that indicated the presence of sound concrete (modulus > 3.5 ksi), the overall quality of the concrete was very poor. There were areas of severe, moderate and slight deterioration detected in the immediate vicinity of the joint interface. An extensive area of severe deterioration was detected beginning in the approximate center of the lane and extending toward the right sidewalk. Few readings were obtained over 1.0 ksi in this region, which extended lengthwise from the joint interface to the testing limits.
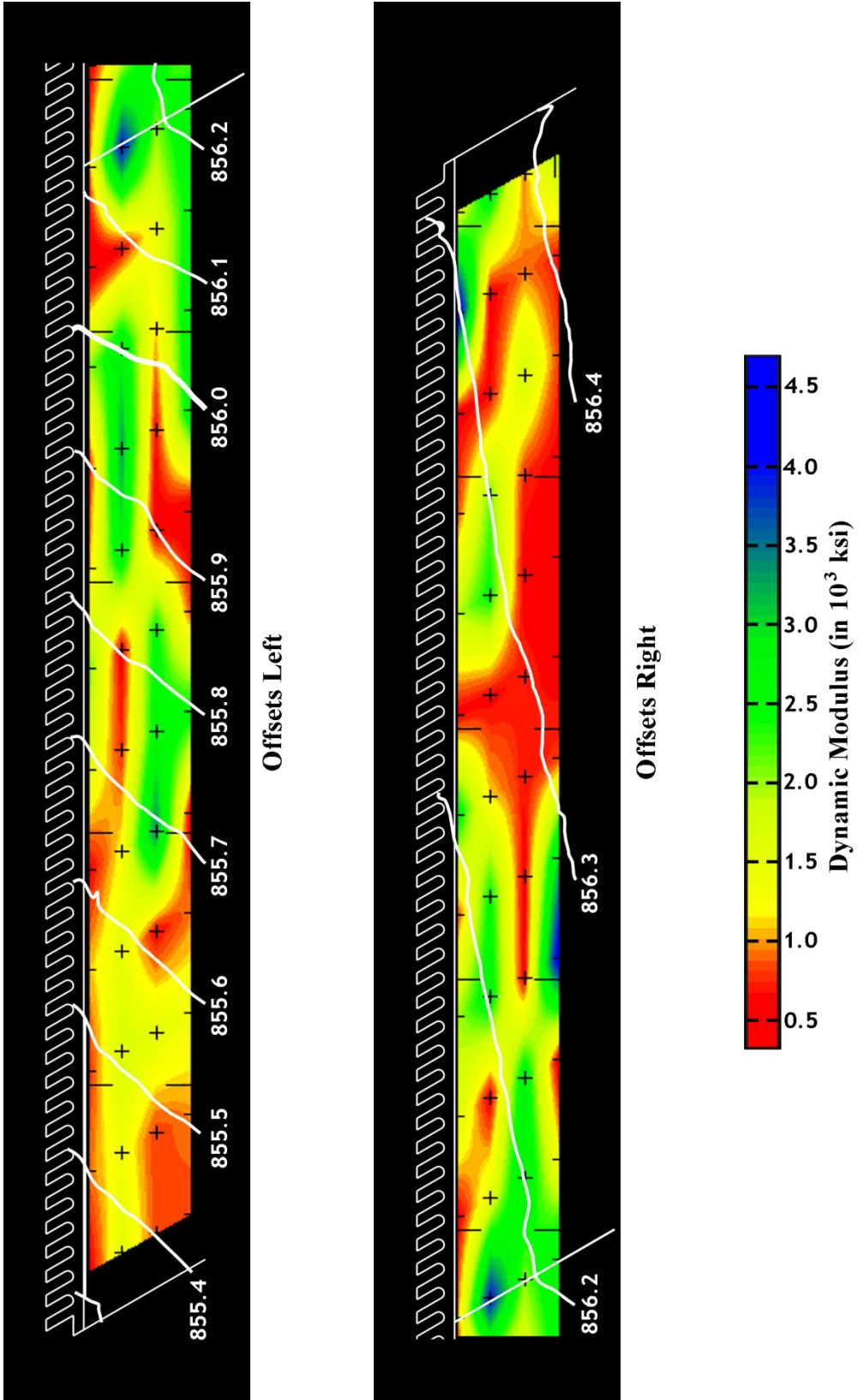
Offsets Left

Offsets Right

Dynamic Modulus (in 10³ ksi)

Figure 6.6. Deterioration map: HDS and SPA data.

Like the results gathered from the GPR data, the distribution and severity of the deterioration suggest that the damage in this vicinity was due to factors other than joint debonding. Unlike the GPR data, however, there seems to be no clear correlation between the damage as shown in the figure and vehicular wheel paths. Both of these appear to be supported by the IE data, which showed the deck surface to be in relatively poor condition throughout the test area.

6.4 Correlation of GPR and SPA Data

An attempt to draw a correlation between the GPR and SPA data began by superimposing the data from all three methods on a scale outline of the deck area (Figure 6.7). Conclusions that can be drawn from the figure include the following:

1) Overall correlation between the two sets of data was mixed. With regards to the actual *location* of suspected defects, the GPR and SPA data overlap reasonably well on the left half of the joint. Agreement between the two sets of data is much less apparent on the joint's right half.

2) The GPR data indicates no apparent deterioration at Station 17, Offset 12 Right. Moderate delamination was detected approximately 1 ft. (0.3 m) to either side of this point. The SPA data, however, indicated an extensive region of severe deterioration at this same location. Its size was noteworthy, as it extended approximately 16 ft. (4.9 m) from Offset 6 Right to Offset 22 Right, and from the joint interface to the limit of the test area.
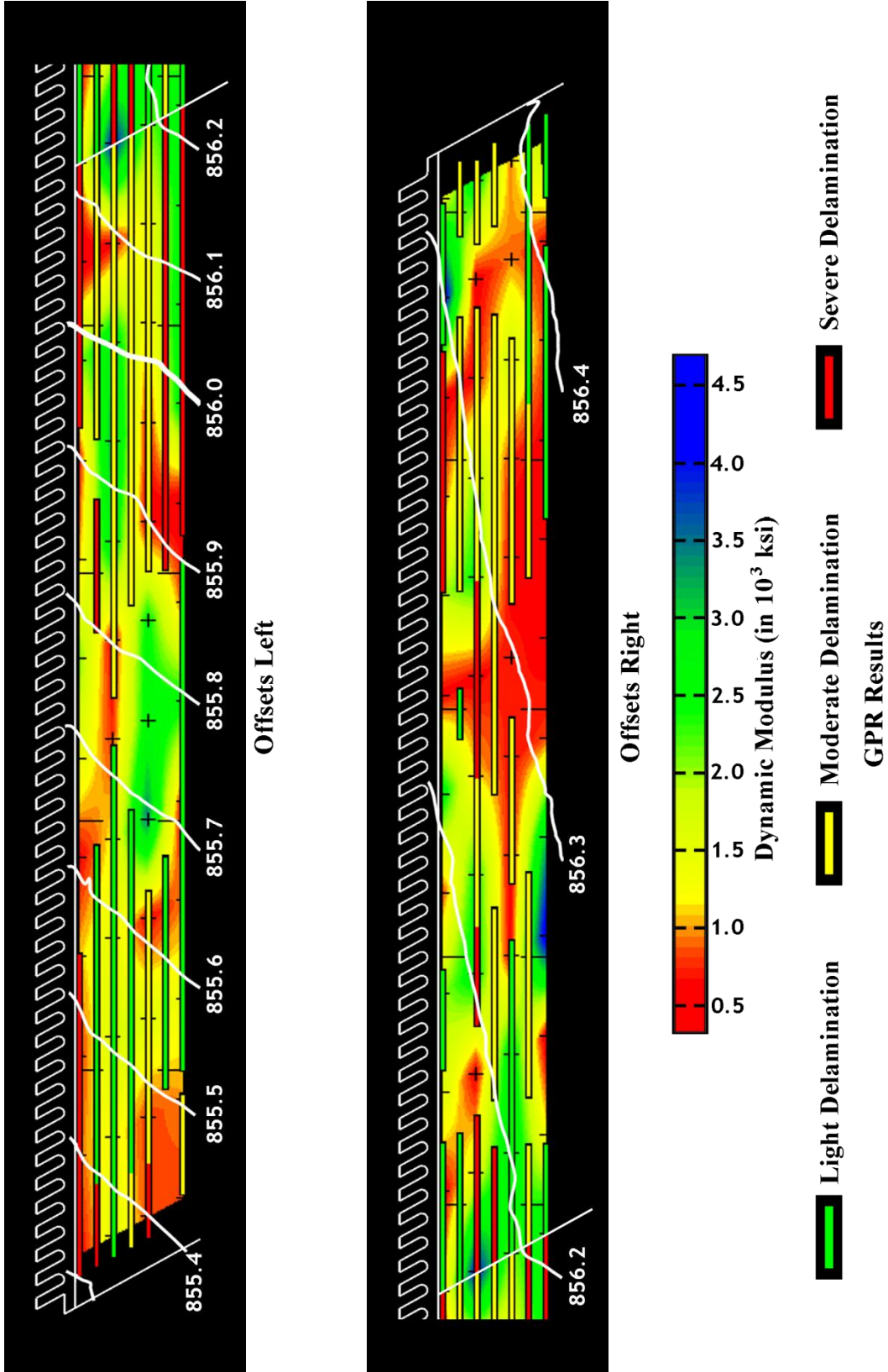
Offsets Left

Offsets Right

Dynamic Modulus (in 10³ ksi)

Light Delamination

Moderate Delamination

Severe Delamination

GPR Results

Figure 6.7. Deterioration map: HDS, GPR and SPA Data.

105

3) The GPR data detected severe deterioration immediately to the right of the centerline at Stations 9 and 13. Data from the SPA indicated the presence of only slight to moderate deterioration in this area.

4) One instance where the data correlated well was in the region centered around Station 17, Offsets 10, 12 and 14 Left. GPR data showed no apparent deterioration of the concrete in this area. The SPA data was in general agreement, with only light delamination detected.

5) Data agreement was poor in some areas along Station 25. GPR data indicated severe delamination along the first 8 ft. (2.4 m) to the left of the centerline, while the SPA data indicated only light deterioration first 6 ft. (1.8 m) of this same station. The reverse was true in the vicinity of Offset 16 Left. Likewise, the GPR data suggested no deterioration between Offset 2 and 14 Right; the SPA data indicated widely varying modulus values in this area.

6.5 Verification of Test Results by Coring

In order to verify the GPR and SPA results, six 4 in. (102 mm) diameter core samples were taken at random within the test area. Because of the bridge's location over live traffic, the core drill depth was limited to 5 in. (127 mm) to prevent penetration of the deck. One exception was at Station 1, 2 ft. Left, where the core depth was limited to 3 in. (76 mm). A summary of the coring results is given in Table 6.2, the location of each sample is shown in Figure 6.8 and a photograph of each core is shown in Figure 6.9. The particular details of each core specimen are described in the following sections.

6.5.1 Station 1, Offset 2 ft. Left

The GPR data at this location indicated severe delamination, while the SPA measured an average modulus of 347 ksi (2.39 GPa) with a standard deviation of 12 ksi (0.08 GPa). This corresponded to severe deterioration according to Table 6.1. The core sample proved that the concrete at this particular location was severely deteriorated; the only retrievable section of the core from this location was from the surface, a wedge-shaped disc of approximately $^1/_2$ in. (12 mm) maximum thickness. The remainder of the core consisted of coarse aggregate and small pieces of mortar which were impractical to piece together. These remnants exhibited discoloration indicative of extensive steel corrosion. The drill encountered severe resistance due to the large amount of reinforcing steel and was subject to binding; therefore the coring depth was limited to 3 in. (76 mm) to avoid damage to the coring bit.

6.5.2 Station 9, Centerline

The GPR data at this location indicated moderate to severe delamination, while the SPA measured a modulus of 4313 ksi (29.74 GPa) with a standard deviation of 236 ksi (1.63 GPa). This indicated good concrete (no deterioration) according to Table 6.1. The core sample appeared to be sound overall, except that during extraction the break occurred at a depth of 3 $^1/_4$ to 4 $^1/_4$ in. (83 to 108 mm). This was relatively shallow when compared to the actual 5 in. (127 mm) depth achieved by the coring bit. This fact, when combined with some slight fracturing of some of the coarse aggregate, is indicative of some degree of deterioration at this depth.

6.5.3 Station 9, Offset 16 ft. Right

The GPR data at this location indicated moderate delamination, while the SPA measured an average modulus of 2164 ksi (14.92 GPa) with a standard deviation of 2290 ksi (15.79 GPa). Although this indicates slight to moderate deterioration according to Table 6.1, the wide range in values suggests an error in the use of the SPA during data acquisition. Like the previous sample, this core appeared to be sound overall. During extraction the fracture occurred at the full 5 in. (127 mm) depth of the bit penetration. Some slight fracturing of the coarse aggregate was also present at the break, again suggesting that there was some deterioration at this depth.

6.5.4 Station 17, Offset 18 ft. Left

The GPR data at this location indicated moderate delamination, while the SPA measured an average modulus of 1663 ksi (11.47 GPa) with a standard deviation of 65 ksi (0.45 GPa). Although this indicates only moderate deterioration according to Table 6.1., this specimen fractured into at least five separate pieces during the actual coring (not during extraction). The mating faces of each piece exhibited extensive discoloration that indicated possible corrosion of the reinforcing steel. Remnants of the core below approximately 4 in. (102 mm) were similar to the remnants of the core at Station 1, Offset 2 ft. Left; these consisted of coarse aggregate and small pieces of mortar.

6.5.5 Station 17, Offset 2 ft. Right

The GPR data at this location indicated slight delamination, while the SPA measured a modulus of 3177 ksi (21.90 GPa) with a standard deviation of 68 ksi. (0.47 GPa). This indicated slight deterioration according to Table 6.1. This specimen appeared

to be in excellent shape overall, with no visible signs of delamination, discoloration or other defects. The fracture, while somewhat above the 5 in (127 mm) coring depth, was reasonably clean and generally in the same plane as the reinforcing steel. There was no evidence of aggregate fracturing, further suggesting that the concrete was sound at this depth.

6.5.6 Station 17, Offset 12 ft. Right

The GPR data at this location indicated no delamination (good concrete), while the SPA measured an average modulus of 800 ksi (5.52 GPa) with a standard deviation of 6 ksi (0.04 GPa). This indicated severe deterioration according to Table 6.1, yet this specimen appeared to be very similar to the one extracted from Station 9, Offset 16 Right. It appeared to be in excellent shape overall, with no visible signs of delamination, discoloration or other defects. The fracture was at the 5 in (127 mm) coring depth and was reasonably clean, with no visible signs of aggregate fracture.

Table 6.2. Summary of results for GPR, SPA and coring.

Location	GPR Results	SPA Results	Coring Results
Sta. 1, 2 Lt.	Severe	Severe	Severe
Sta. 9, Center	Moderate/Severe	Good	Moderate
Sta. 9, 16 Rt.	Moderate	Slight/Moderate	Slight
Sta. 17, 18 Lt.	Moderate	Moderate	Severe
Sta 17, 2 Rt.	Slight	Slight	Good
Sta. 17, 12 Rt.	Good	Severe	Good

Offsets Left

Offsets Right

Dynamic Modulus (in 10³ ksi)

GPR Results

■ **Light Delamination**   ■ **Moderate Delamination**   ■ **Severe Delamination**
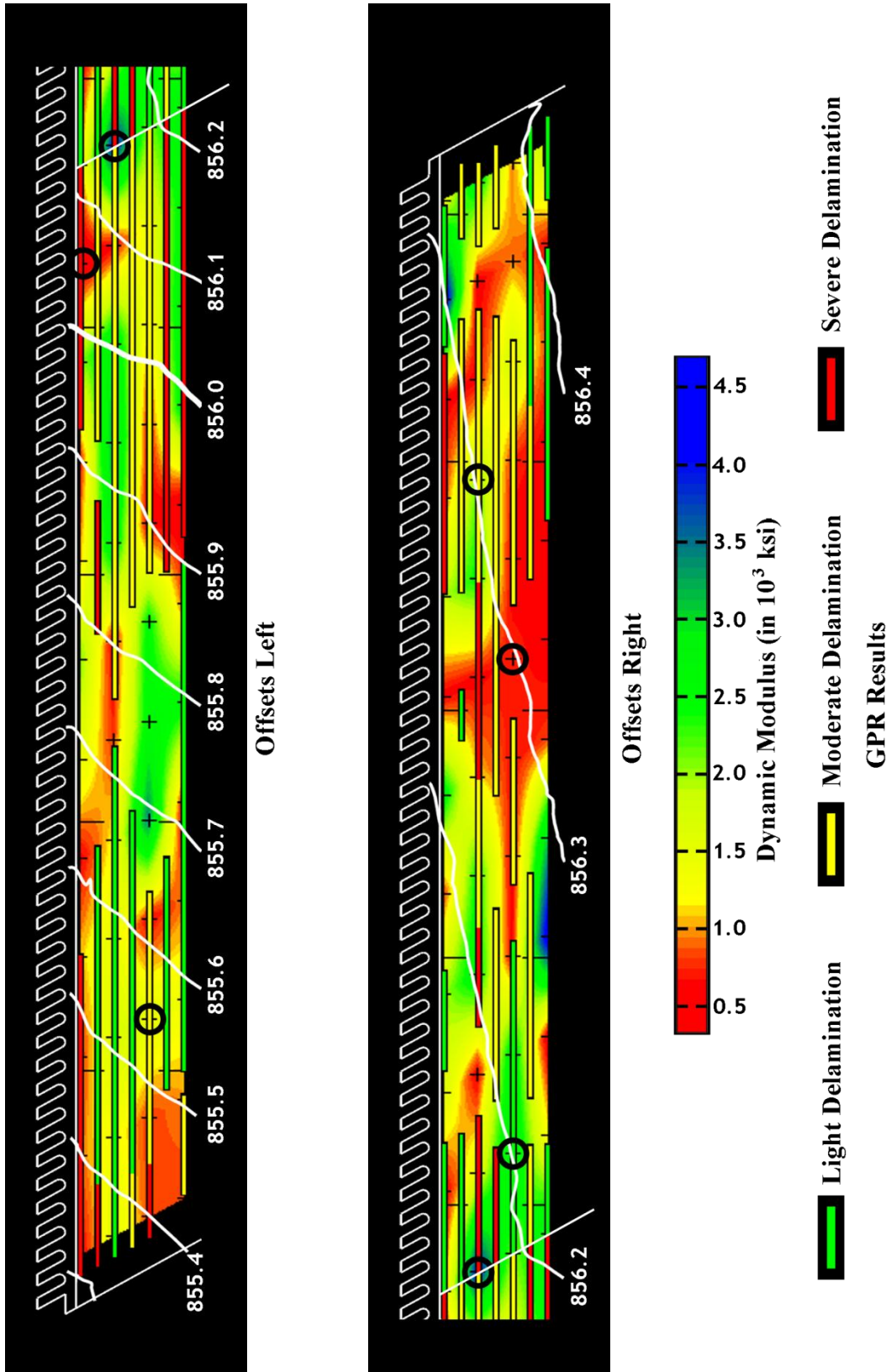
Figure 6.8. Locations of core samples taken for this study. Core locations are indicated by black circles.

110

Top View   **Side View**
Station 1, 2 ft. Left

Station 9, Centerline

Station 9, 16 ft. Right

Station 17, 18 ft. Left

Station 17, 2 ft Right

Station 17, 12 ft. Right
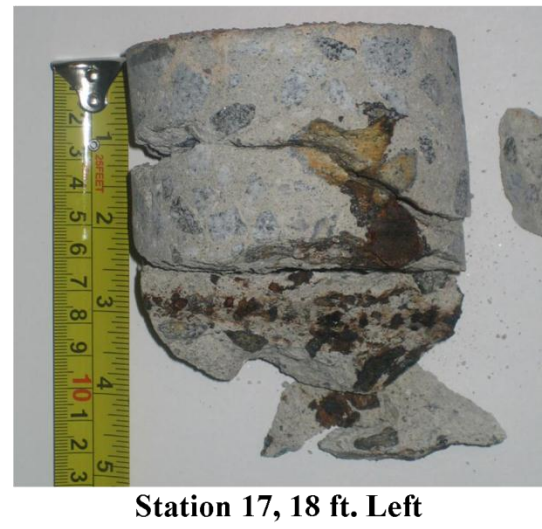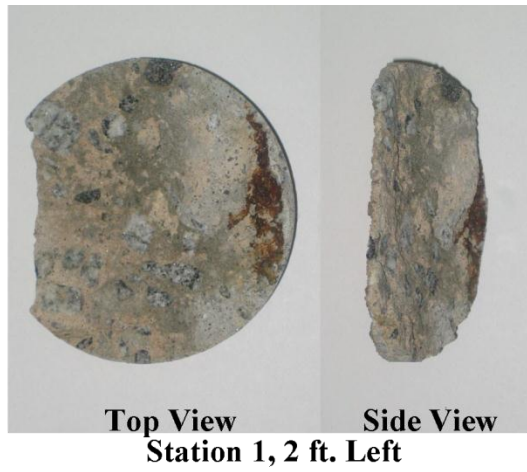
Figure 6.9.   Core sample photographs.

111

CHAPTER 7

CONCLUSIONS

7.1 Summary of Results

This research focused on developing methods and techniques for detecting debonding and delamination in armored bridge deck joints using portable NDT/E devices. The effectiveness of this equipment in detecting defects in the concrete surrounding deck joints was also investigated. Observations and conclusions drawn from the gathered data are summarized as follows:

1) Of the two actual NDT/E methods used in this study, GPR appeared to exhibit the greater potential for detecting subsurface deterioration due to delaminations or debonding of deck joint armor. This conclusion is based upon the favorable correlation between the data and actual core specimens.

2) The correlation between the SPA average modulus values and the core specimens was relatively poor.

3) Of the methods used in this study, HDS was the least useful. However, it does appear to have potential value in other NDT/E applications such as load testing.

4) Initial deployment of the HDS equipment was considerably more complex and time-consuming than the other two methods used in this study, but data collection and processing was relatively rapid.

5) The equipment for the GPR (SSM) and Acoustic methods (SPA) was quickly and easily deployed in the field, but the processing and mapping of the data was cumbersome and difficult.

6) The quality of the data gathered from all of the methods used – HDS, GPR and Acoustic – was *highly* dependent upon the quality of the surface under test. These methods may not be suitable for use on bridge decks where widespread delamination, severe weathering or other such deterioration is present.

7) The handheld GPR unit used in this study was very limited in its ability to detect delaminations or other anomalies below the first layer of reinforcing steel.

8) Development of a reference system specific to the bridge or joint under test is crucial for the accurate mapping of gathered data. Such a system should account for factors such as deck width, curbing and skew.

9) Accurate mapping of data is the key to representing the overall condition of the joint bonding areas at the time of testing.

10) The effective use of NDT/E methods for limited areas (such as deck joints) is currently hampered by the nonexistence of a comprehensive data processing, mapping and evaluation system.

11) NDT/E methods are only tools for assessing the current condition of the structural member under test. Their use is not a substitute for sound engineering judgment.

12) GPR appeared to be the only method upon which a decision to repair or replace a joint could be reasonably made.

7.2 Conclusions Based Upon the HDS Data

While the effectiveness of HDS as a deck joint evaluation tool was not specifically studied, the data gathered in this study indicated that HDS is of extremely limited value in this regard. The primary reason is that this technology is simply not a more effective alternative to VI. All other factors being equal, an experienced bridge inspector is easily capable of assessing a deck joint's condition with considerably greater speed and accuracy than HDS - and without its complexity and expense. Field deployment of the equipment is also somewhat awkward and unwieldy, although this is improving as the technology continues to mature.

HDS was also found to be of little value in detecting wear or rutting of concrete deck surfaces. It is possible that this could have been due to the overall poor surface quality of the bridge deck used in this study. A more likely possibility, however, could simply be that wear from traffic alone is negligible on concrete decks with a low ADT, even those over fifty years old. Deterioration of deck wearing surfaces is caused by numerous factors outside the scope of this study, and any structure exhibiting such damage is likely to have been improperly built, poorly maintained and at the end of its service life.

HDS does have great potential in other aspects of bridge management and maintenance, namely:

1) The development of three-dimensional models of bridges and other structures for inventory, management and maintenance purposes.

2) Deflection measurement of structural members during load testing.

3) The monitoring of long-term phenomena such as creep in structural members, swelling or subsidence of subgrade material in approaches, etc.

4) The inventory and preservation of historic bridges or those of high cultural value.

7.3 Conclusions Based Upon the GPR Data

Based upon the data, GPR appeared to be the most effective method used in this study with regard to detecting subsurface defects adjacent to deck joints. There appeared to be reasonable correlation between the data and the core specimens. It was the most easily and rapidly deployed device used in this study. This was due to the fact that it was entirely self-contained; all functions necessary to the proper use of the equipment (except for battery charging) were handled entirely by the on-board software, display and user interface. Additionally, it appeared to be relatively immune to the effects of vibration caused by traffic. This implies that the device can be reliably used in situations where live traffic is present on the structure under test.

Handheld GPR devices - such as the StructureScan™ Mini used in this study - show great promise as tools for detecting more extensive debonding in and around joint armor. Much more research and experimentation is necessary, however, before judgments regarding joint replacement can be made based upon their data. The

effectiveness of the GPR equipment in general appears to be significantly influenced by two key factors:

1) The overall condition of the deck surface, including the presence of chloride intrusion.

2) The relative complexity of the reinforcing steel in the vicinity of deck joints.

These were evidenced by the fact that the overwhelming majority of the suspected defects appeared to lie between the upper layer of reinforcing steel and the deck surface. Signatures from the various layers of reinforcing steel also made it difficult to detect any evidence of delaminations further toward the bottom of the deck slab.

7.4 Conclusions Based Upon the SPA Data

The primary advantage of the SPA as a bridge assessment tool lies in its ability to simultaneously assess the concrete's modulus and to detect subsurface defects at a particular point. While it is not entirely self-contained like the SSM, it is nonetheless easily deployed in the field. Another benefit is that its results for a particular point are displayed in real-time, without the need for further post-processing. The poor correlation between the SPA's data and the core specimens, however, suggests that much more work needs to be done before real engineering decisions can be made based upon its data *in this application*. The SPA's ability to gather valid data appeared to be severely impeded by the deck's poor condition. This affected the data in two ways.

The first involved the coupling issue described in Chapter 5 and illustrated in Figure 5.3. The extremely weathered condition of the deck surface made it very difficult

to obtain proper coupling of the source and receiver feet. Multiple attempts at positioning the SPA over the test point were sometimes necessary to achieve good results. In addition to increasing the necessary testing time, it also exacerbated the normal wear on the rubber coupling pads tied to the feet. It is important to note here that the poor deck surface also negatively affected the two stationary feet (beneath the electronics box), whose proper positioning was found to be just as crucial to obtaining good data as the three "active" feet.

The second involved the concrete's subsurface state. Major spalling of the deck surface due to corrosion of the upper layer of reinforcing steel had already occurred in several areas. This was noted in the inspection report and verified in the field. Hammer blows produced a distinct hollow sound at many of the SPA test points, evidence of severe delamination at the surface. The IE data further supports the evidence of this deterioration, and suggests that it had a negative effect on the wave propagation necessary to detect specific defects at lower depths.

From the standpoint of field deployment, there are three disadvantages to using the SPA:

1) Data gathering is extremely time-consuming when compared to the SSM.

2) Data gathered by the SPA is susceptible to corruption due to vibration from traffic. This implies that the structure under test should be completely closed to traffic while the unit is in operation.

3) The SPA contains rather delicate parts in its assembly that are subject to undue wear and/or maladjustment if used improperly [29].

7.5 Suggestions for Further Research

Although only the GPR data appeared to be sufficient for the purpose of determining the bonding status of this particular joint, the results from all three of the techniques described herein should still assist future researchers in further investigating the possibilities of GPR and Acoustic methods as tools for armored joint assessment. One research project should involve the same battery of tests that were involved in this study. These could be performed on a number of newer, in-service bridges where the quality of the wearing surface is not as suspect and where the joint bonding conditions are actually known. Such tests could verify the validity of advanced NDT methods under real-world conditions, and could further refine the procedures developed here.

NDT testing for joint debonding should also be performed under laboratory conditions. This would help establish thresholds for the detection of defects for each of the methods used. Full-scale mockups of both armored joint types should be constructed with several progressive stages of delamination. These should also include reproducing the complex matrix of reinforcing steel that is present in these areas.

During the course of this study, much more time was spent in arranging the data into a useable form than it took to actually collect it. It became apparent that some means of efficiently processing and mapping NDT data must be developed if these methods are to achieve any measure of success as tools for assessing limited areas of a structure. Therefore, the possibility of developing such a system should be investigated. It should be capable of accepting NDT data from a variety of sources (including GPS data), should

clearly present data from each method in a usable form and should allow the user to

define a reference system based upon the particulars of the test site.

REFERENCES

[1] Federal Highway Administration, "Our Nation's Highways 2010," U.S. Department of Transportation, Washington, D.C., Governmental Publication Publication Number FHWA-PL-10-023, 2010.

[2] American Society of Civil Engineers. (2009) Report Card for America's Infrastructure. [Online]. http://www.infrastructurereportcard.org/state-page/north-carolina

[3] North Carolina Department of Transportation. (2010, January) webstats.pdf. [Online]. http://www.ncdot.org/download/projects/ncbridges/webstats.pdf

[4] Ken Maser and Mark Bernhardt, "Statewide Bridge Deck Survey Using Ground Penetrating Radar," in *Structural Materials Technology IV - An NDT Conference*, Atlantic City, NJ, 2000, pp. 31-37.

[5] M. Scott et al., "A comparison of nondestructive evaluation methods for bridge deck assessment," *NDT&E International*, vol. 36, pp. 245-255, July 2002.

[6] North Carolina Department of Transportation, Division of Highways, Bridge Management Unit. (2010, September) Bridge Inspection Report, Rowan County Bridge Number 790143. PDF Document.

[7] North Carolina Department of Transportation. (June, 2010) statewidebridges. [Online]. http://www.ncdot.org/download/projects/ncbridges/statewidebridges.pdf

[8] Neal H. Bettigole and Rita Robison, *Bridge Decks: Design, Construction, Rehabilitation, Replacement*. New York, New York, United States of America: American Society of Civil Engineers, 1997.

[9] Petros P. Xanthakos, *Bridge Strengthening and Rehabilitation*. Upper Saddle River, New Jersey, United States of America: Prentice-Hall PTR, 1996.

[10] National Cooperative Highway Research Program, "NCHRP Synthesis 319: Bridge Deck Joint Performance," Transportation Research Board, Washington, DC, Transportation Research Board report ISBN 0-309-06957-2, 2003.

[11] North Carolina Department of Transportation. (2001, October) NCDOT 2006 Standard Specifications, Project Special Provision 22. PDF Document. [Online]. http://www.ncdot.org/doh/preconstruct/highway/structur/psp/newpsp06/PSP022.pdf

[12] North Carolina Department of Transportation. (2010, November) NCDOT 2006 Standard Specifications, Project Special Provision 21. PDF Document. [Online]. http://www.ncdot.org/doh/preconstruct/highway/structur/psp/newpsp06/PSP021.pdf

[13] North Carolina Department of Transportation. (2005, June) NCDOT 2006 Standard Specifications, Project Special Provision 20. PDF Document. [Online]. http://www.ncdot.org/doh/preconstruct/highway/structur/psp/newpsp06/PSP020.pdf

[14] Brent M. Phares, "Visual inspection techniques for bridges and other transportation

structures," in *Inspection and monitoring techniques for bridges and civil structures*, Gonkang Fu, Ed. Cambridge, England: Woodhead Publishing Limited, 2005, ch. 9.

[15] Fuat Guzaltan, "Deck Joints," in *Bridge Inspection and Rehabilitation*, Louis G. Silano and Arnold C. Henderson, Eds. New York, United States of America: John Wiley and Sons, Inc., 1993, ch. 11, pp. 221-240.

[16] Brent M. Phares, Dennis D. Rolander, Benjamin A. Graybeal, Glenn A. Washer, and Mark Moore, "Visual Inspection and Reliability Study," in *Structural Materials Technology IV - An NDT Conference*, Atlantic City, NJ, 2000, pp. 14-19.

[17] Stuart Gordon, Derek Lichti, and Mike Stewart, "APPLICATION OF A HIGH-RESOLUTION, GROUND BASED LASER SCANNER FOR DEFORMATION MEASUREMENTS," in *The 10th FIG International Symposium on Deformation Measurements*, Orange, California USA, 2001, pp. 23-32.

[18] ASTM International. (2011, March) ASTM International - SEDL Search. [Online]. http://www.astm.org/search/sedl-search.html?query=Ground%20Penetrating%20Radar#75124395

[19] Christopher L. Barnes, Jean-Francois Trottier, and Dean Forgeron, "Improved concrete bridge deck evaluation using GPR by accounting for signal depth-amplitude effects," *NDT&E International*, vol. 41, pp. 427-433, March 2008.

[20] ASTM International. (2010) Standard Test Method for Measuring the P-Wave Speed and the Thickness of Concrete Plates Using the Impact-Echo Method. PDF Document.

[21] ASTM International. (2010) Standard Practice for Evaluating the Condition of Concrete Plates Using the Impulse-Response Method. PDF Document.

[22] Manuel Celaya, Parisa Shokouhi, and Soheil Nazarian, "Assessment of Debonding in Concrete Slabs Using Seismic Methods," *Transportation Research Record: Journal of the Transportation Research Board*, vol. 2016, pp. 65-75, 2007.

[23] Manuel Celaya, Soheil Nazarian, Chetana Rao, and Harold Von Quintus, "Delamination Detection of HMA Airport Pavements with NDT Devices," in *2010 FAA Worldwide Airport Technology Transfer Conference*, Atlantic City, 2010.

[24] Hugh D. Young and Roger A. Freedman, *Sears ans Zemansky's University Physics*, 11th ed., Adam Black, Ed. San Francisco, CA, United States of America: Addison Wesley, 2004.

[25] Michael D. Gehrig, Derek V. Morris, and John T. Bryant, "Ground Penetrating Radar for Concrete Evaluation Studies," Bryant Consultants, Inc., Carrollton, TX,.

[26] David Prosper, "Automated Detection of Wave Velocities in Concrete Bridge Decks," Civil and Environmental Engineering, Massachusetts Institute of Technology, Boston, MA, United States, Master's Thesis 1998.

[27] North Carolina Department of Transportation, Division of Highways, Bridge Management Unit. (2008, July) Bridge Inspection Report, Forsyth County Bridge Number 330171. PDF Document.

[28] Geophysical Survey Systems, Inc. (2009) StructureScan Mini Quick Start Guide: A

Fast Chack List for Field Operation. PDF Document. [Online]. http://www.geophysical.com/structurescanmini.htm

[29] Geomedia Research and Development, *Portable Seismic Properties Analyzer PSPA & SPA Manager Manual*. El Paso, United States of America: Geomedia Research and Development, 2007.
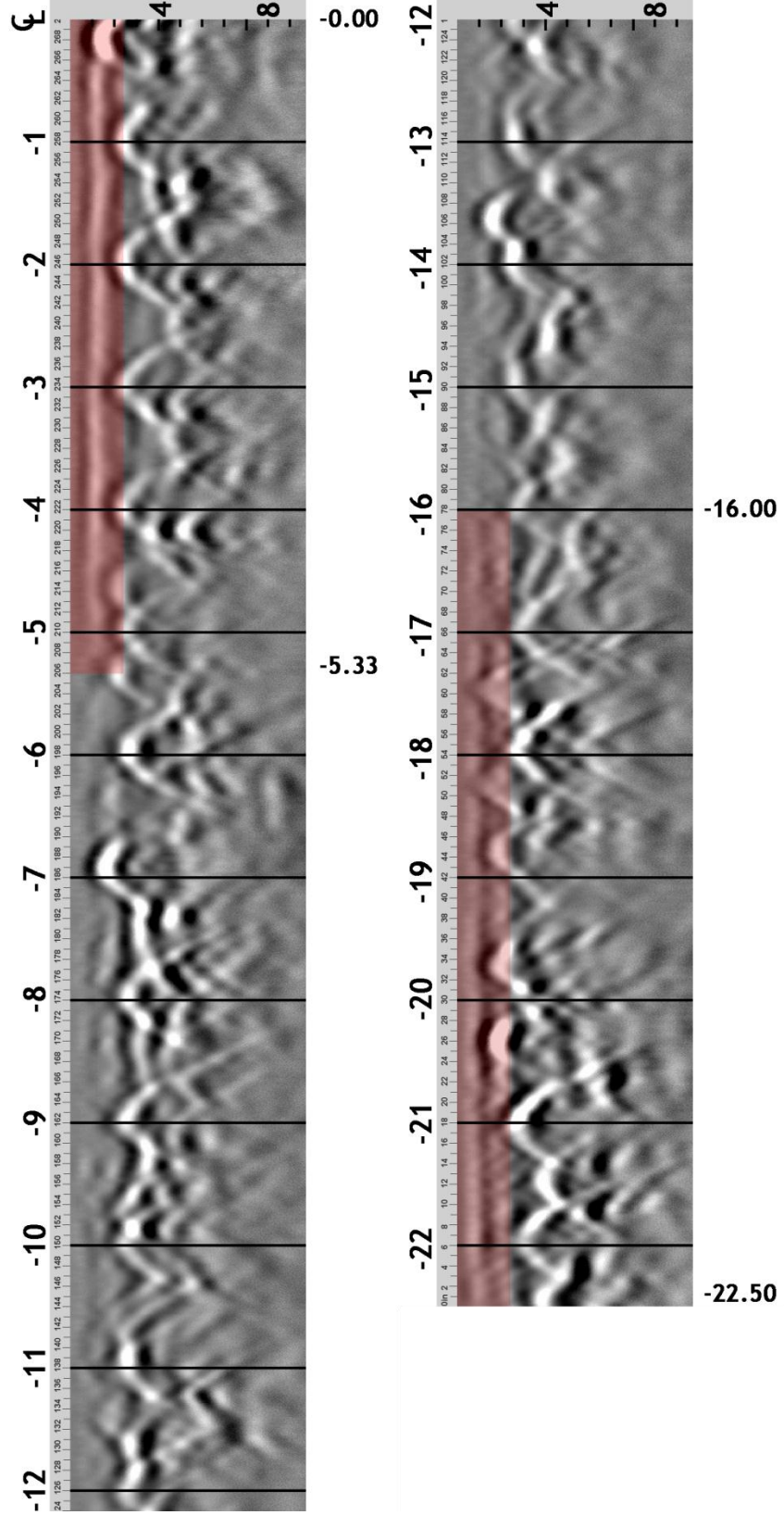
APPENDIX A

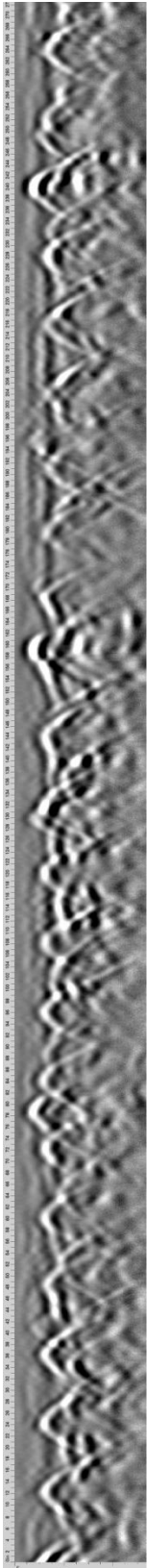# GPR SCAN DATA
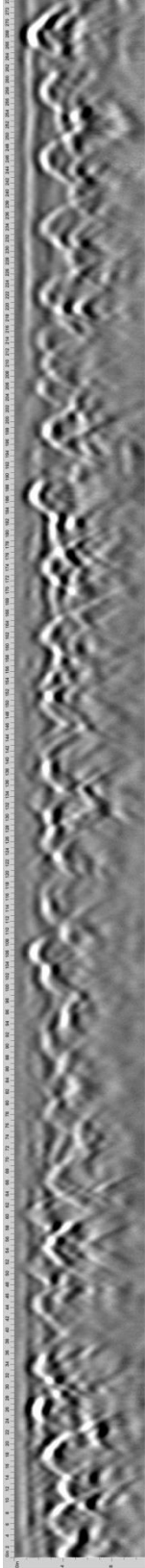
Original Scan

Station 1 Left

124

Original Scan

Station 1 Right

125

Original Scan

Station 5 Left

126
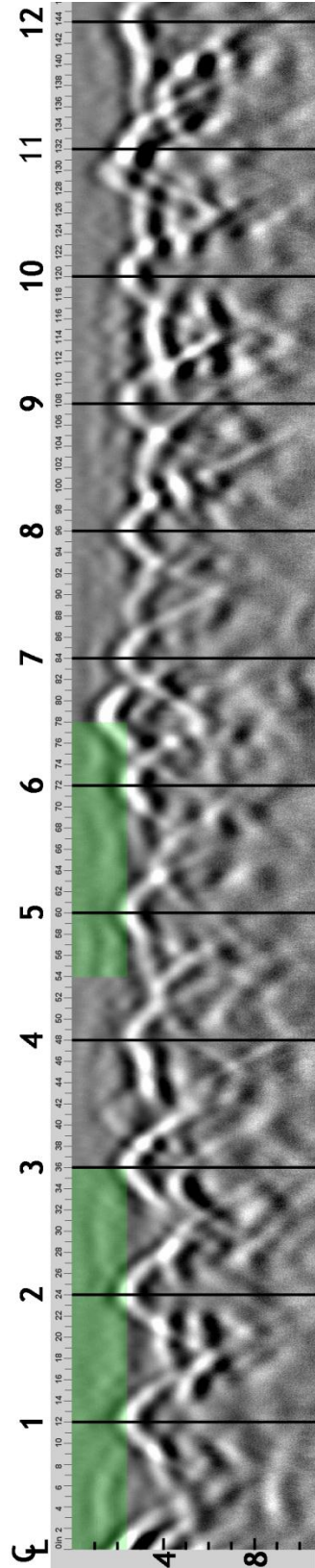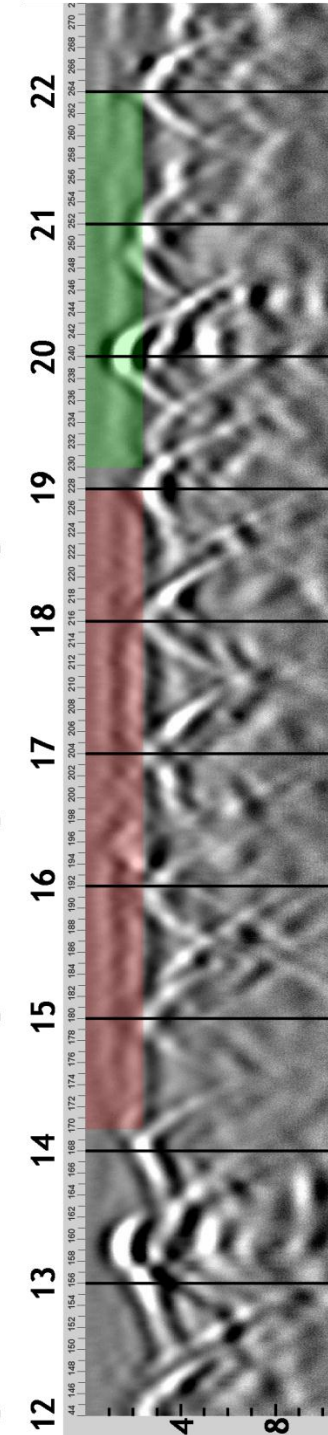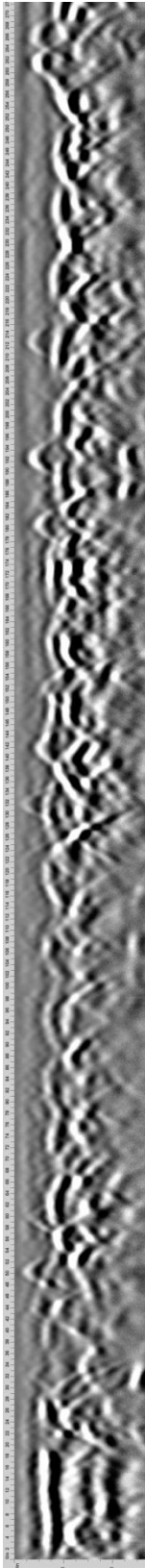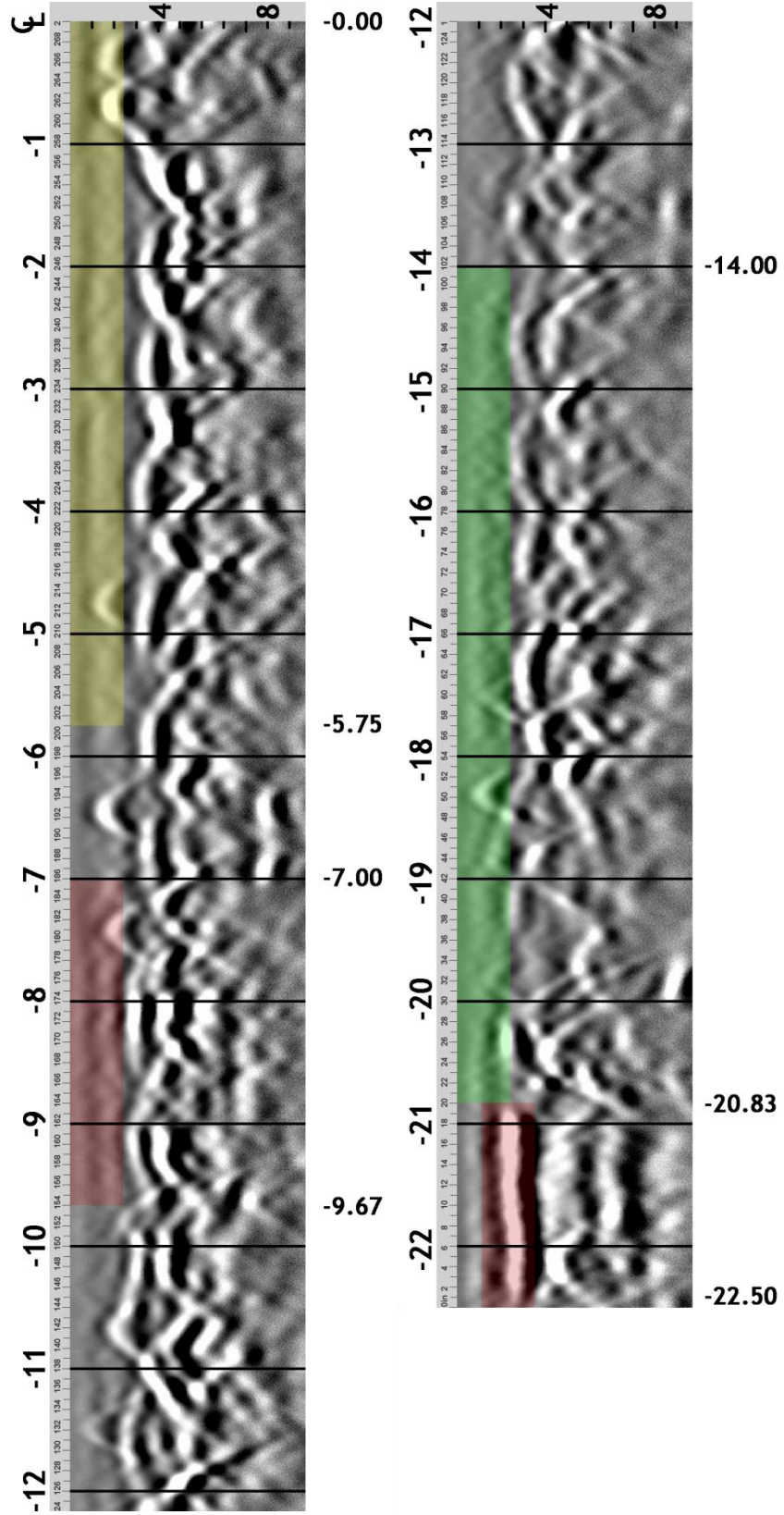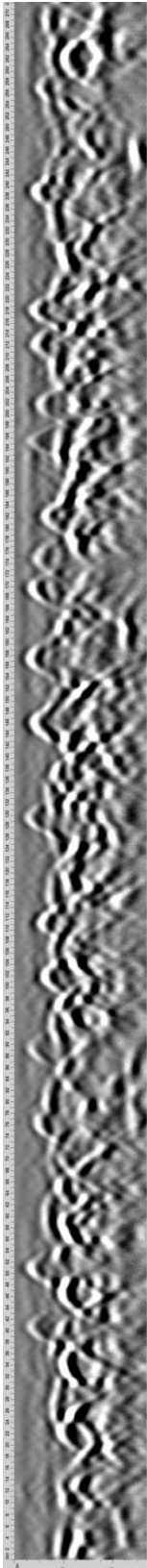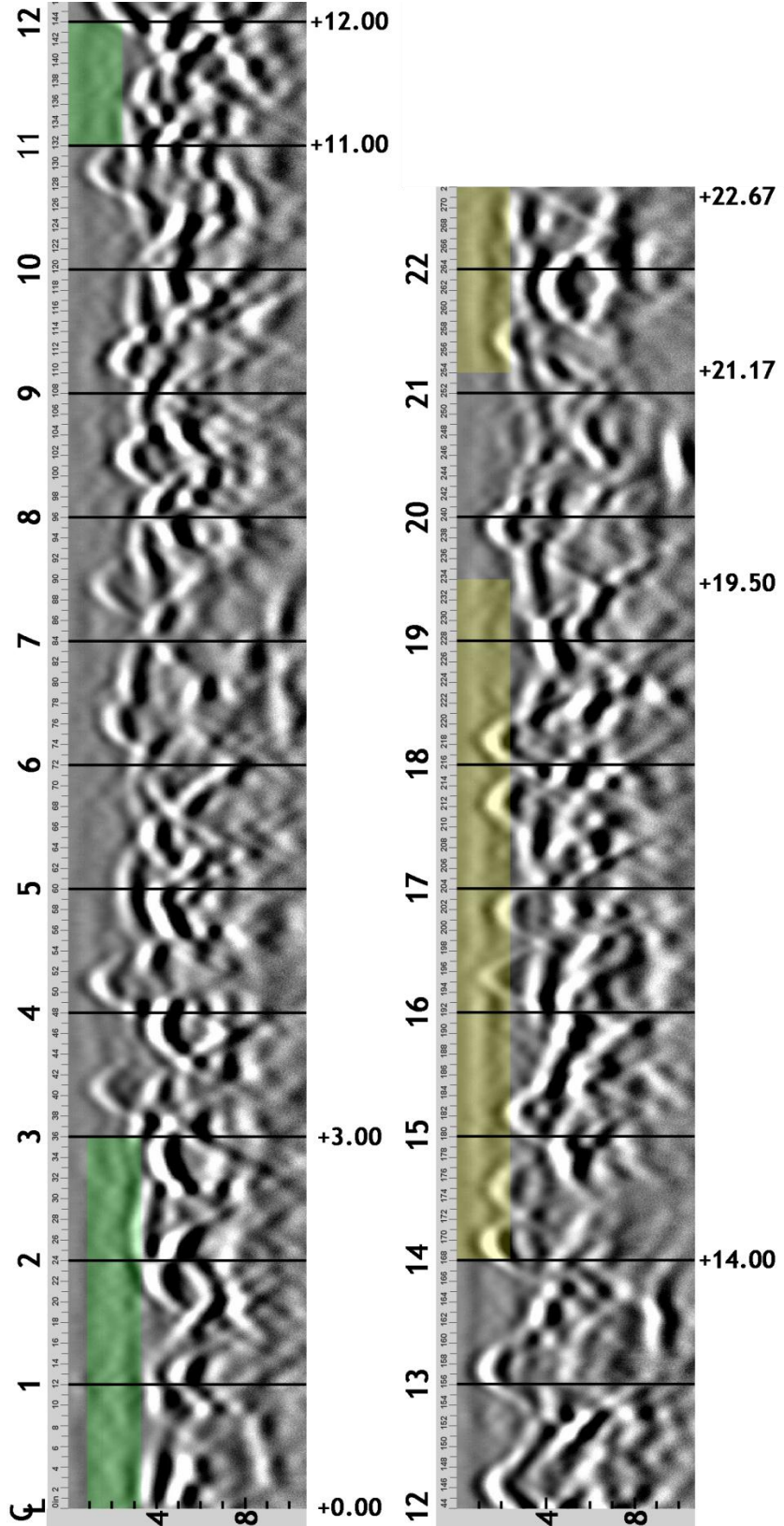
Original Scan

Station 5 Right
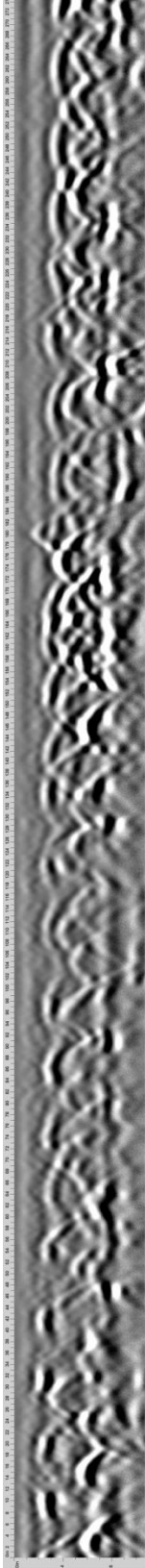
Original Scan
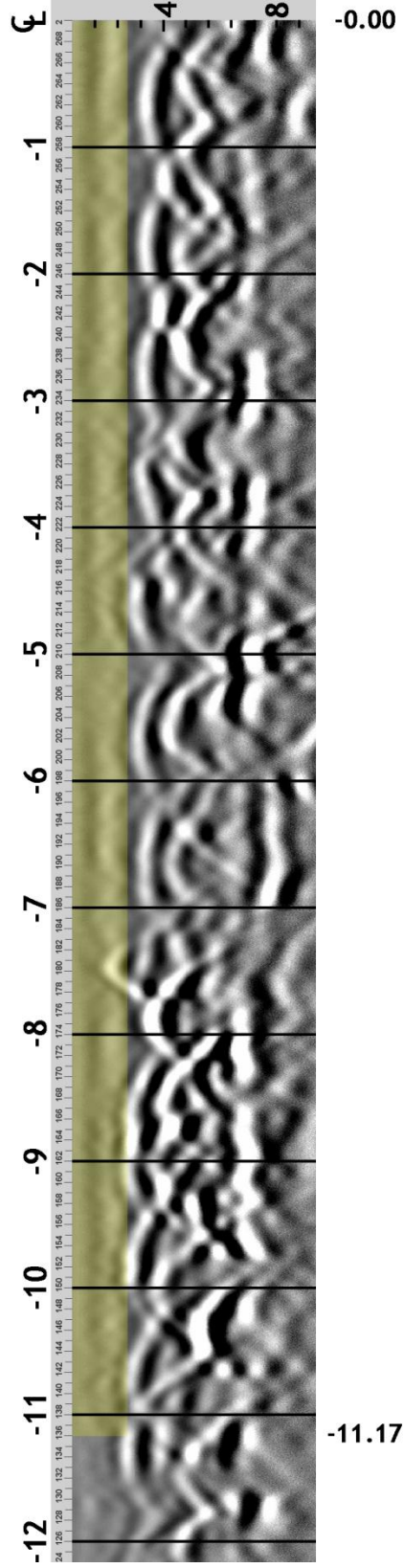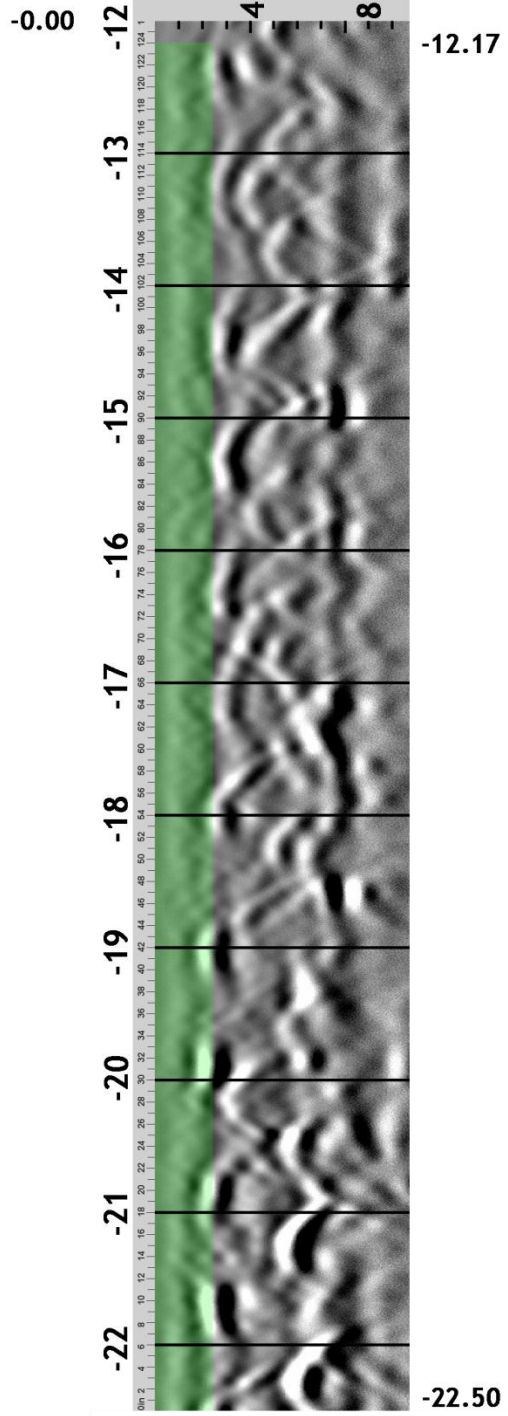
Station 9 Left
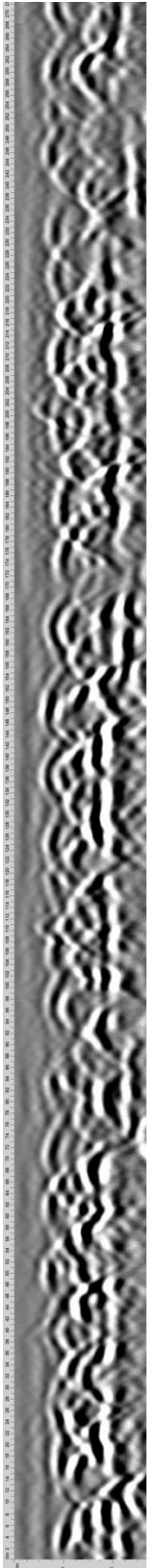
Original Scan
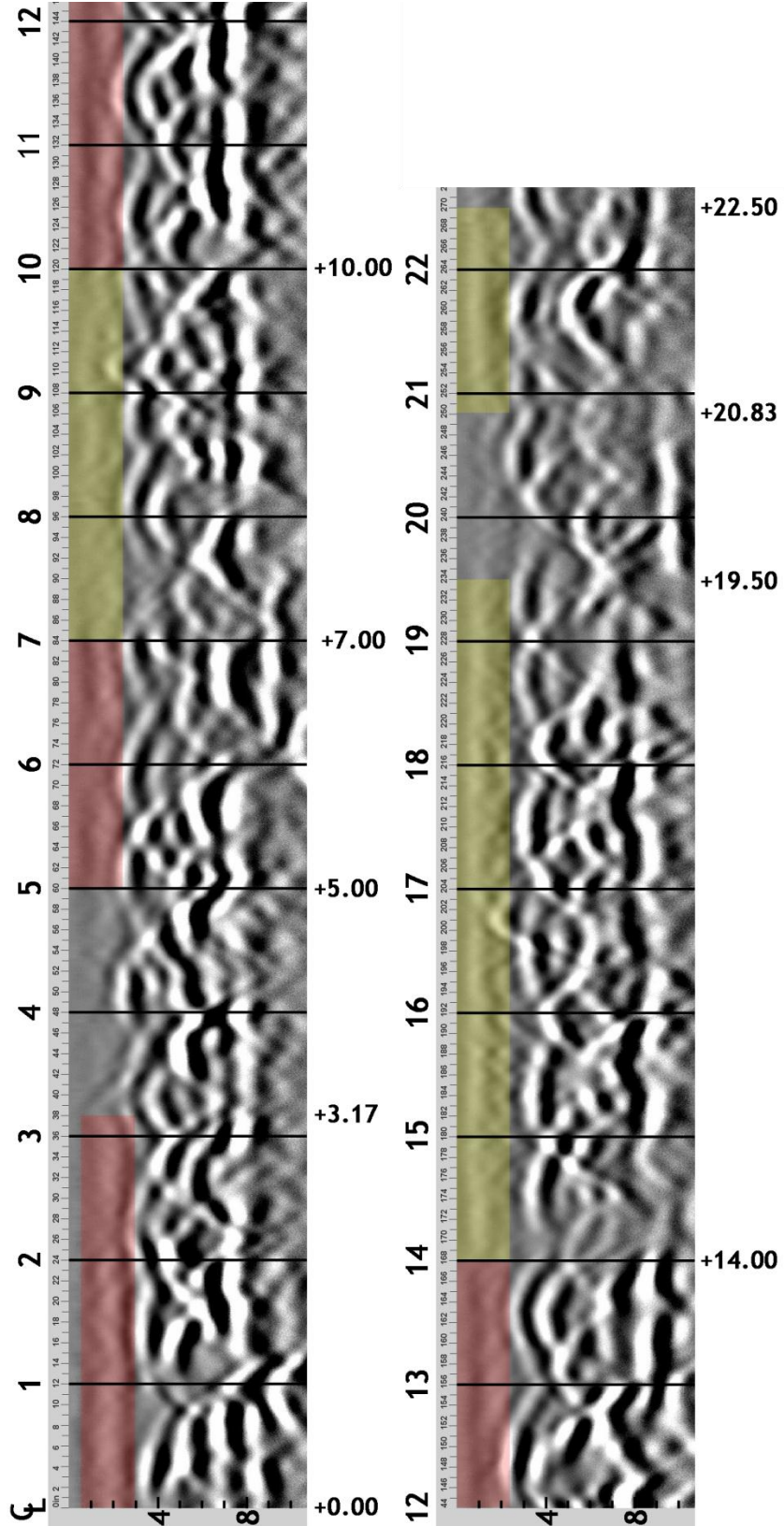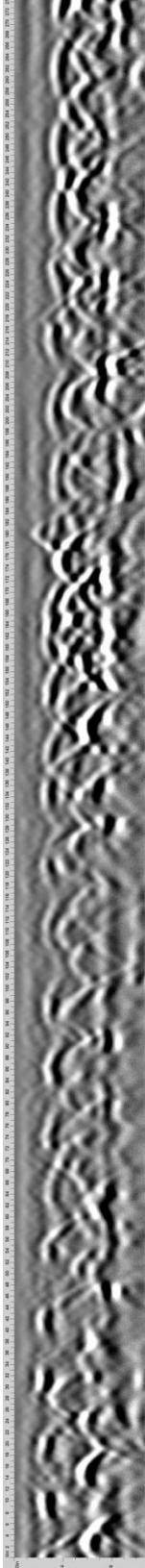
Station 9 Right
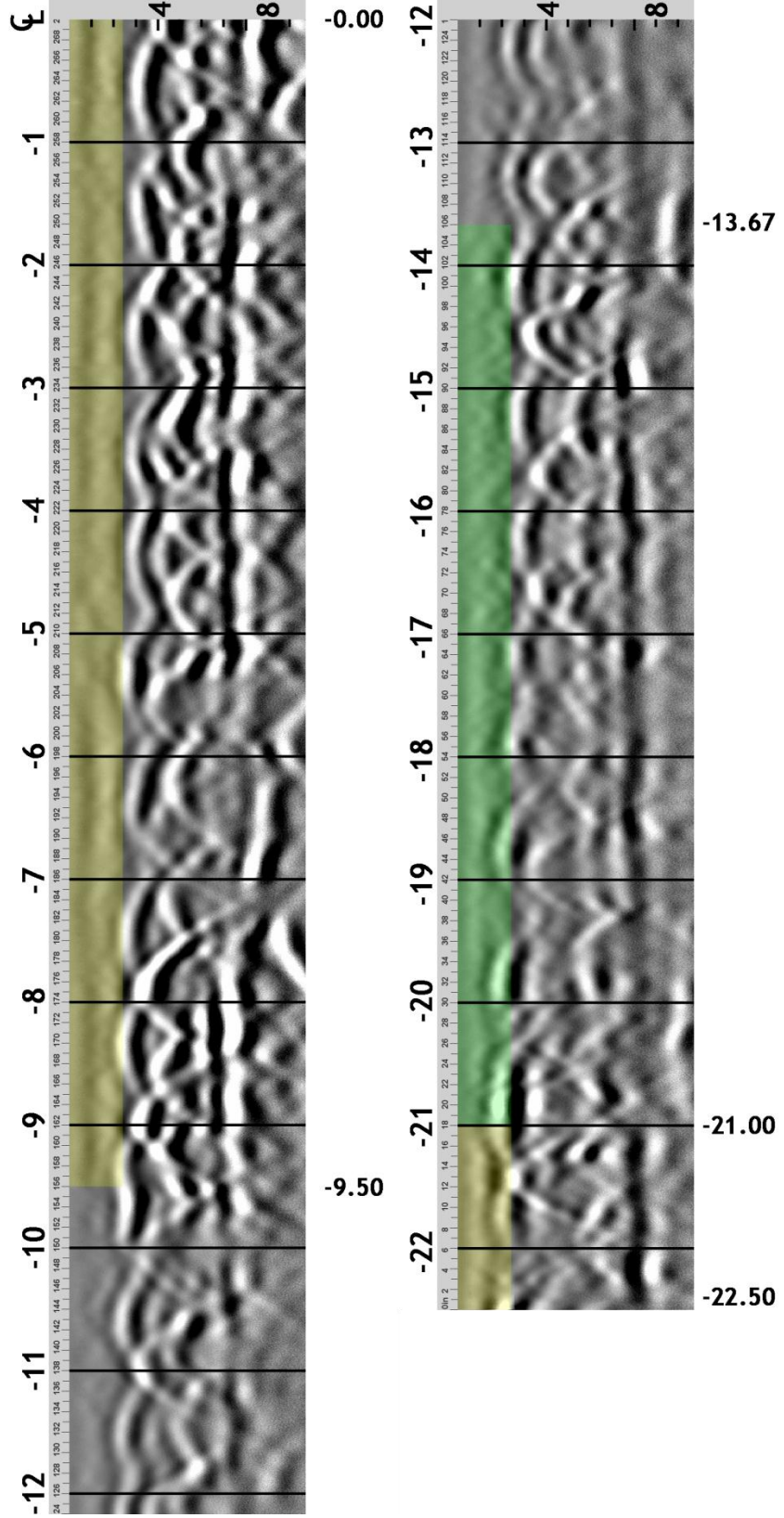
Original Scan

Station 13 Left

Original Scan

Station 13 Right

131
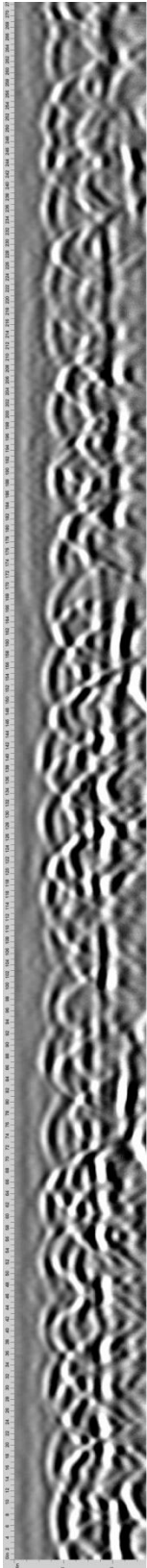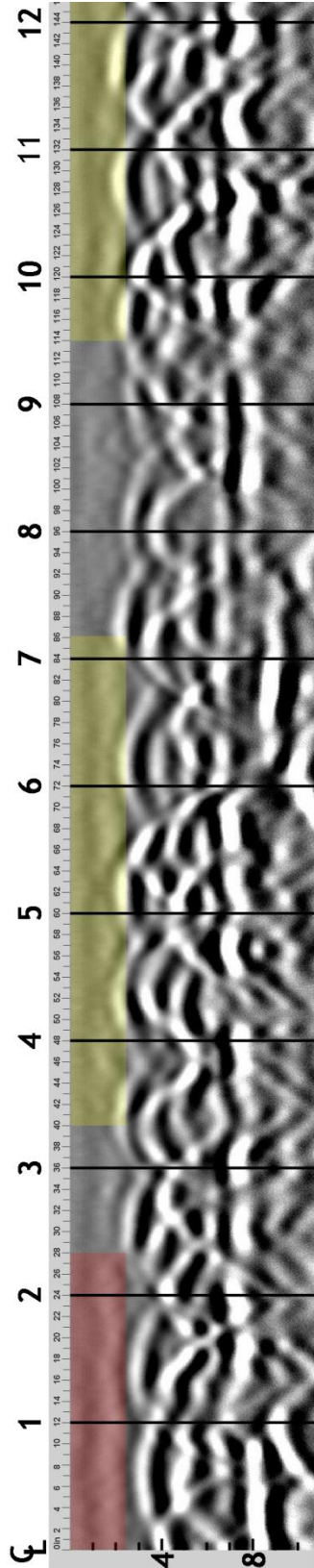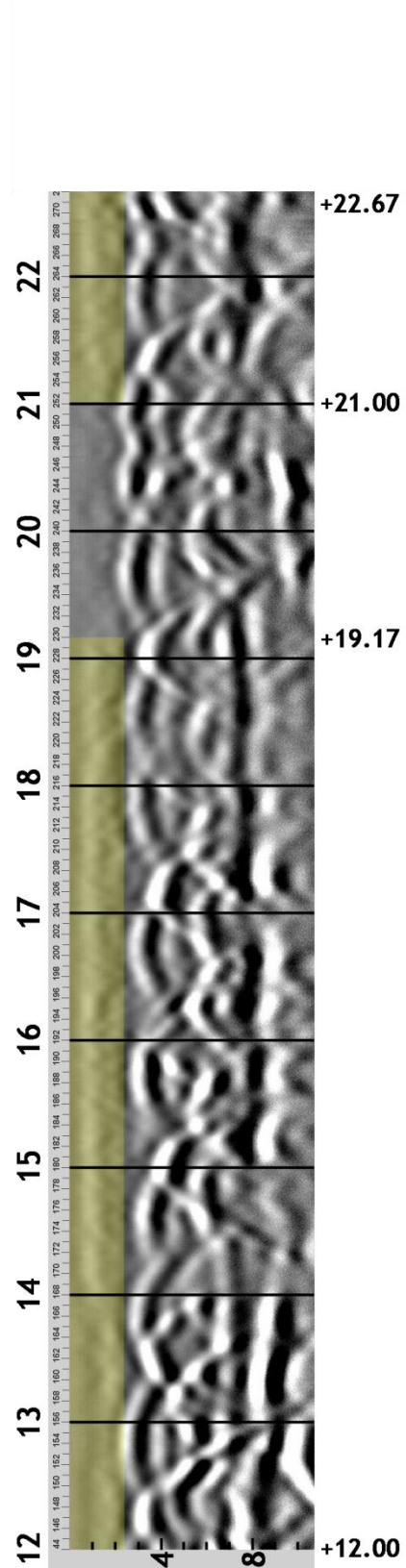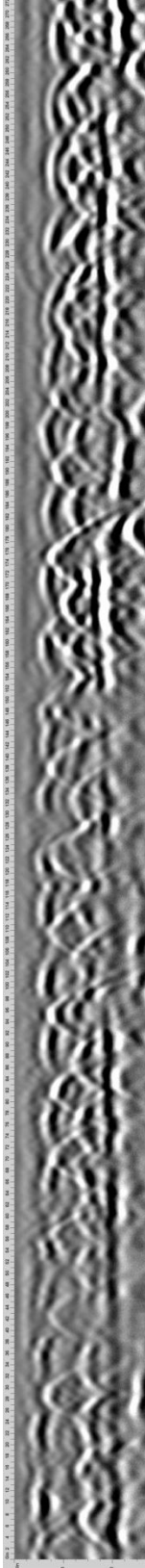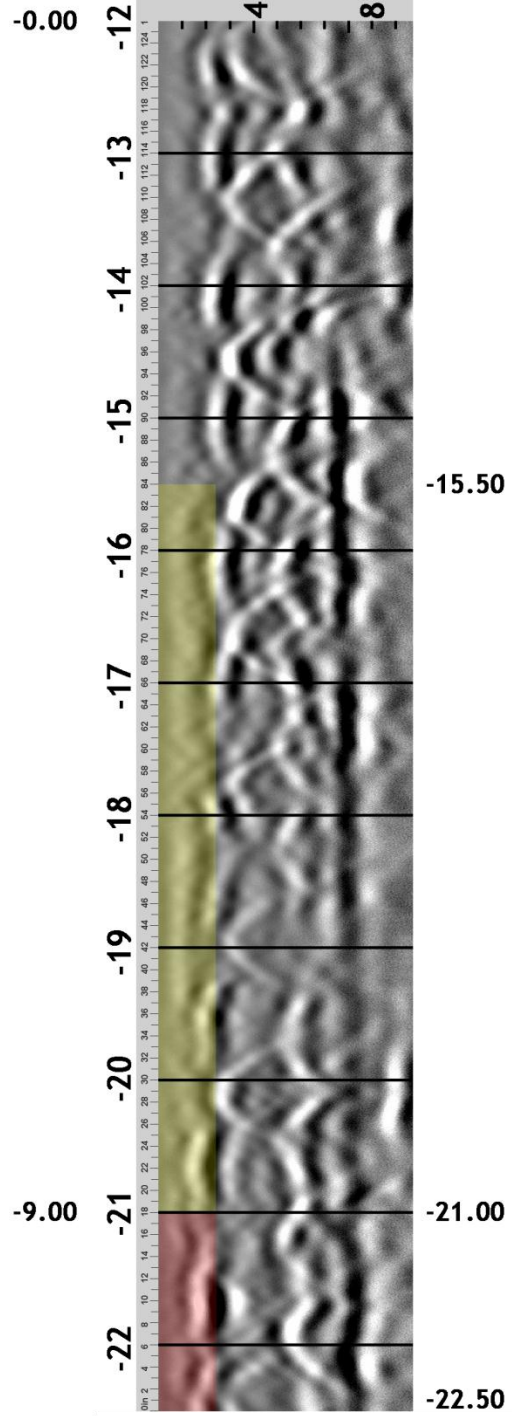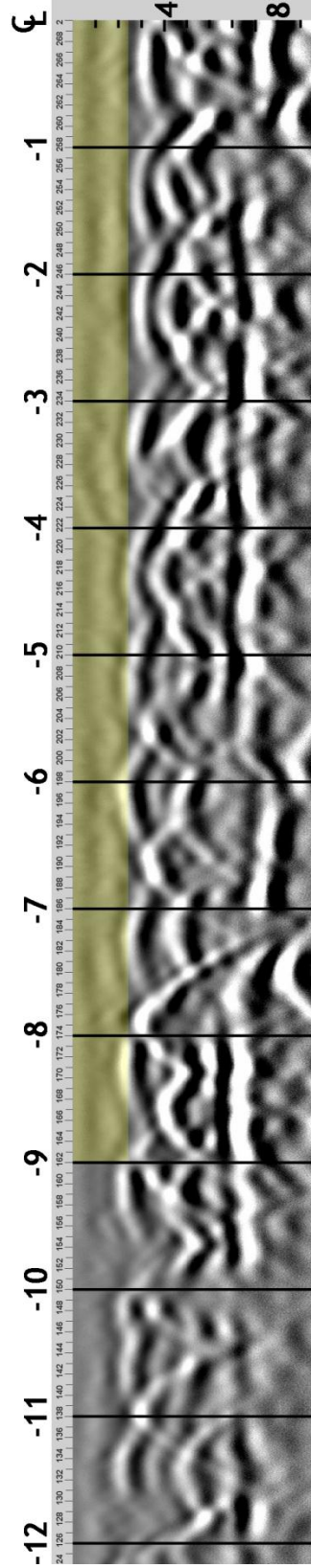
Original Scan

Station 17 Left
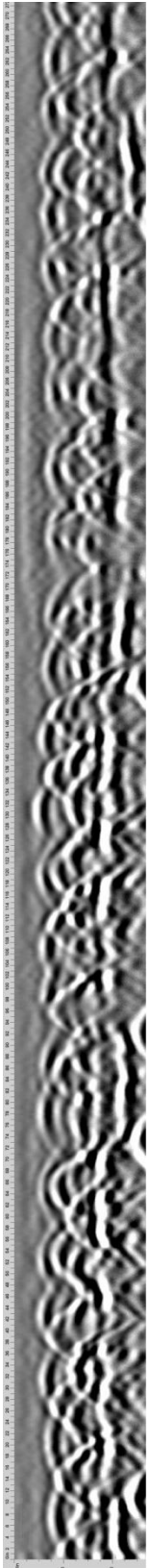
Original Scan
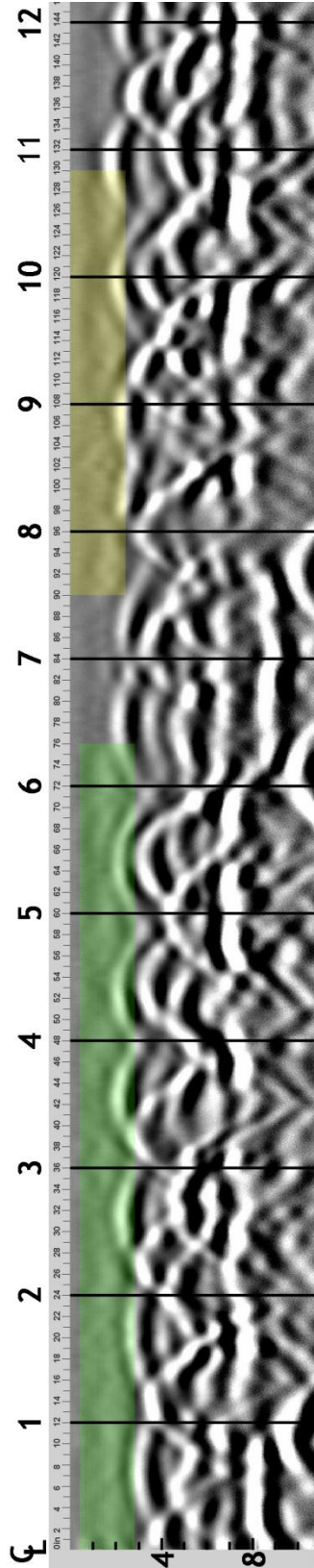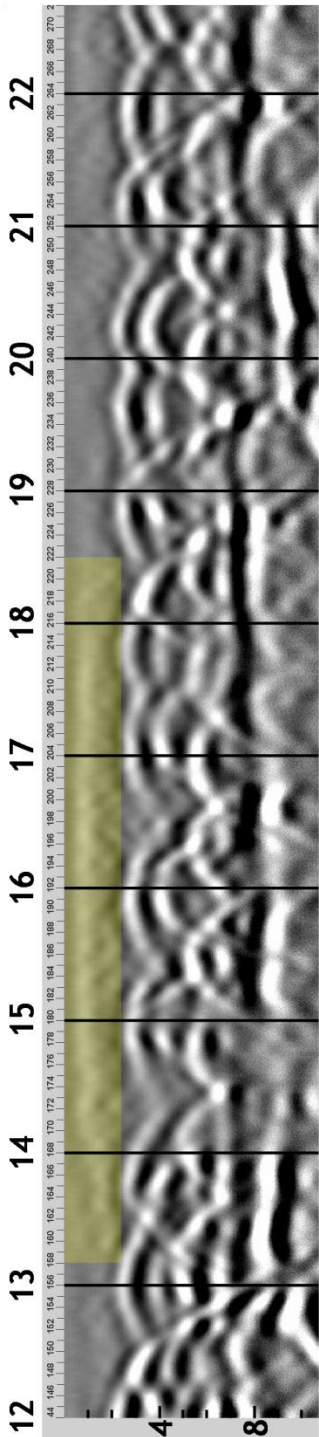
Station 17 Right

Original Scan

Station 21 Left

134

Original Scan

Station 21 Right

Original Scan

Station 25 Left

136
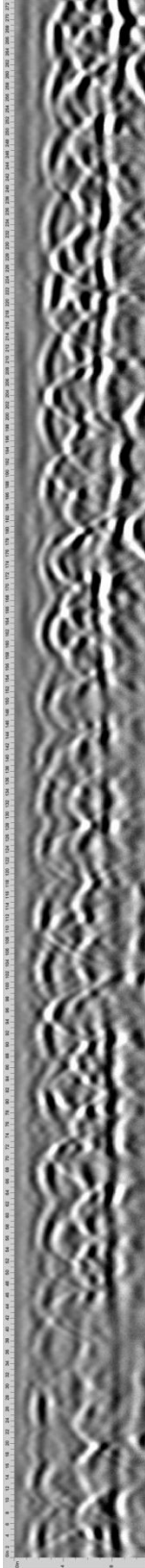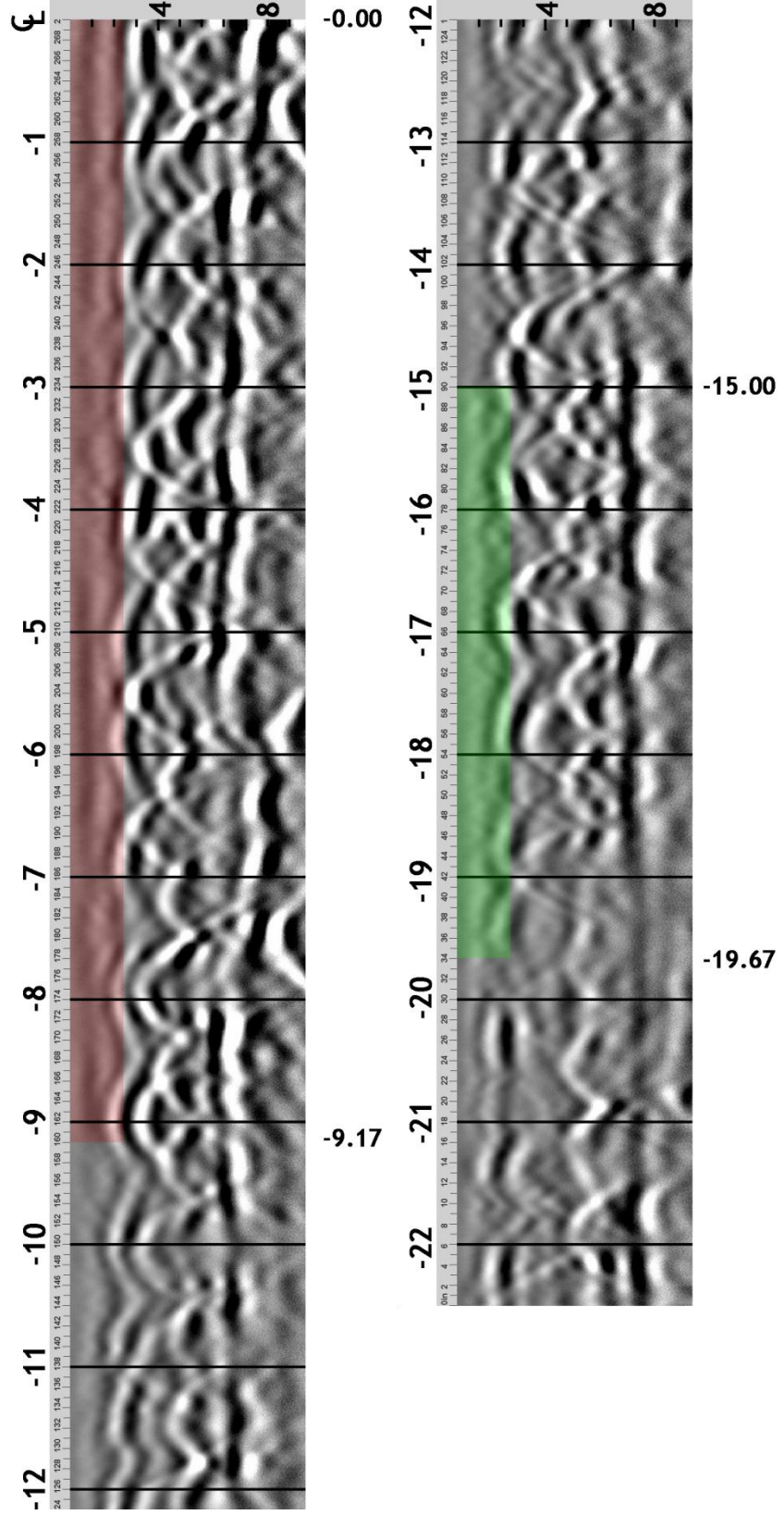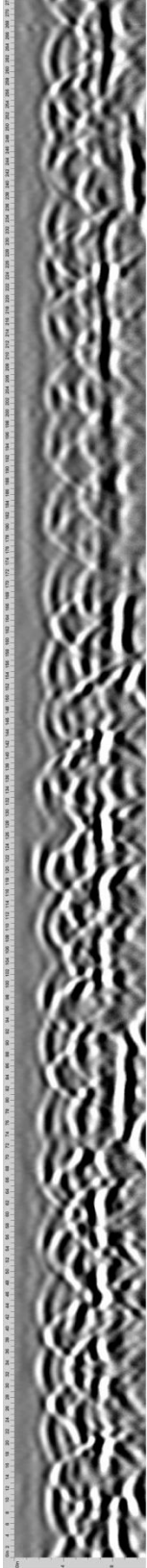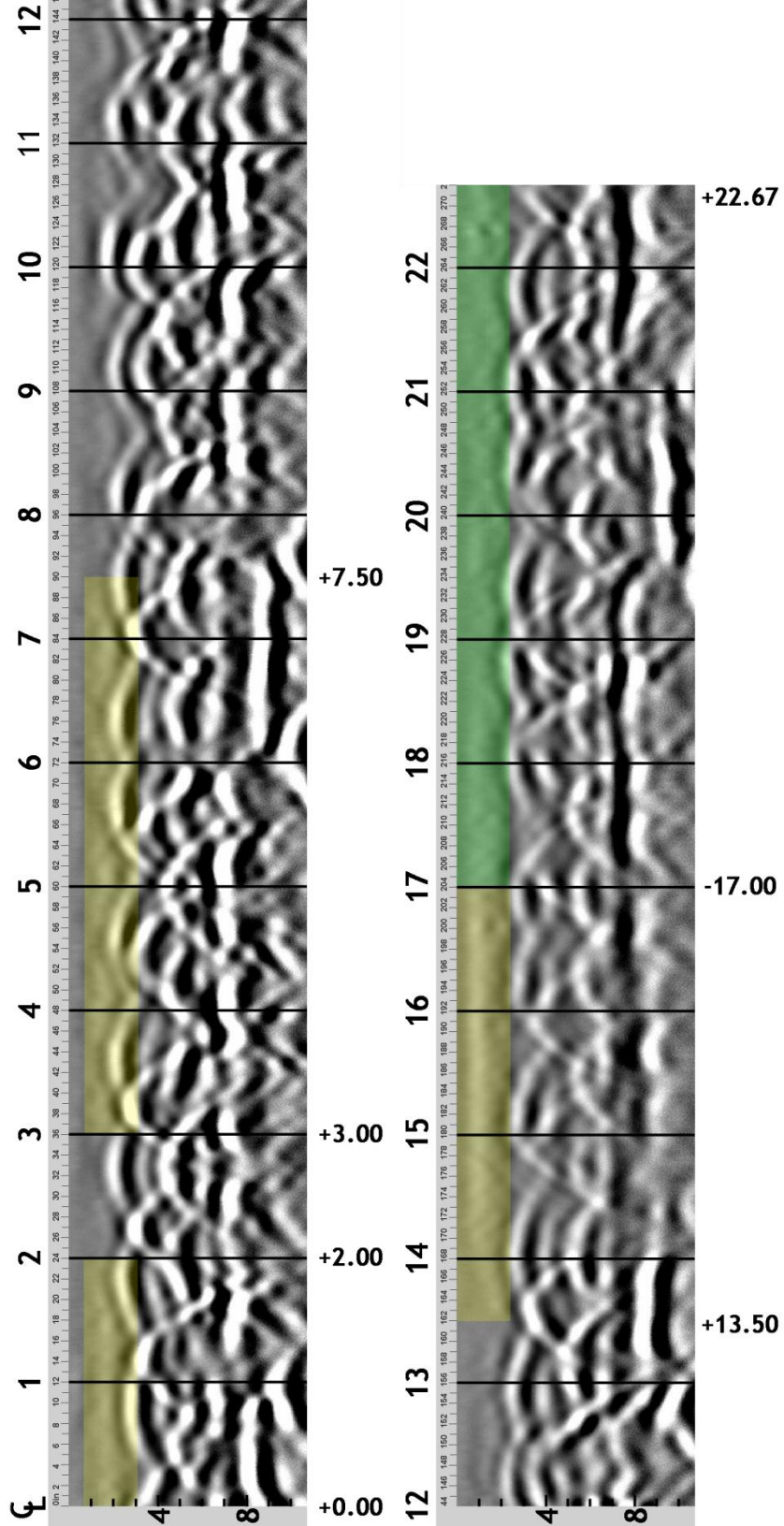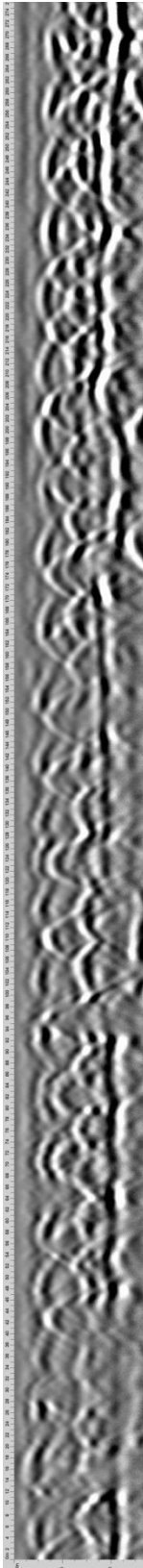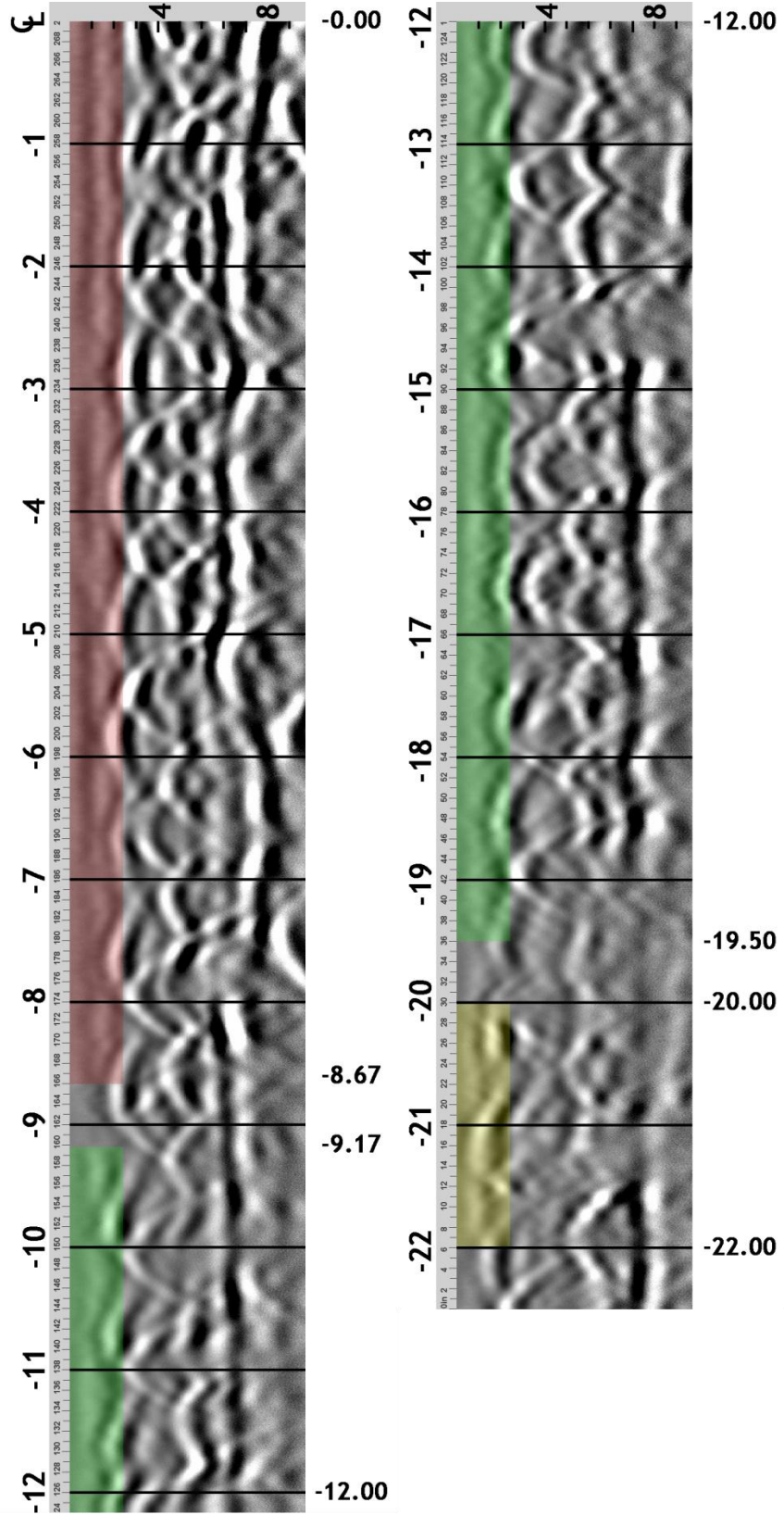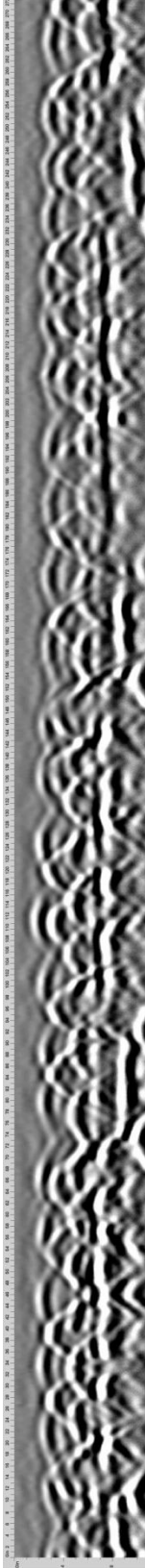
Original Scan

Station 25 Right

137
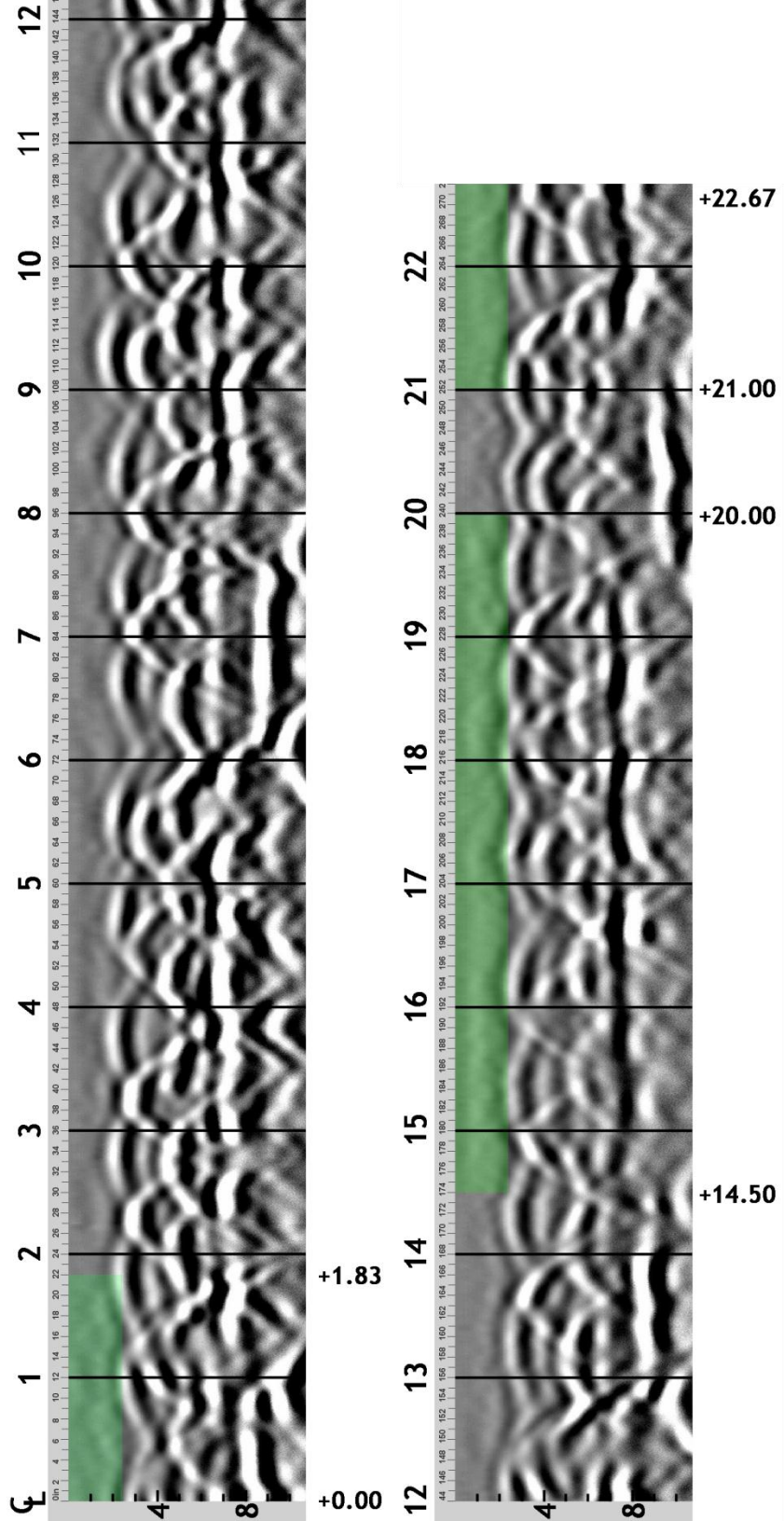
APPENDIX B

SPA DATA
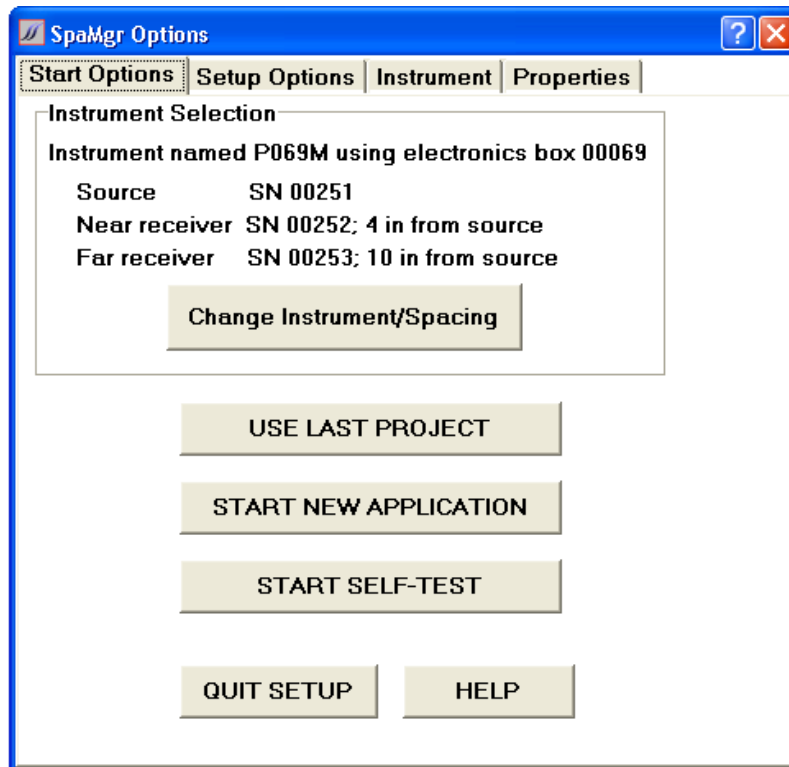
SPA Start Options Settings
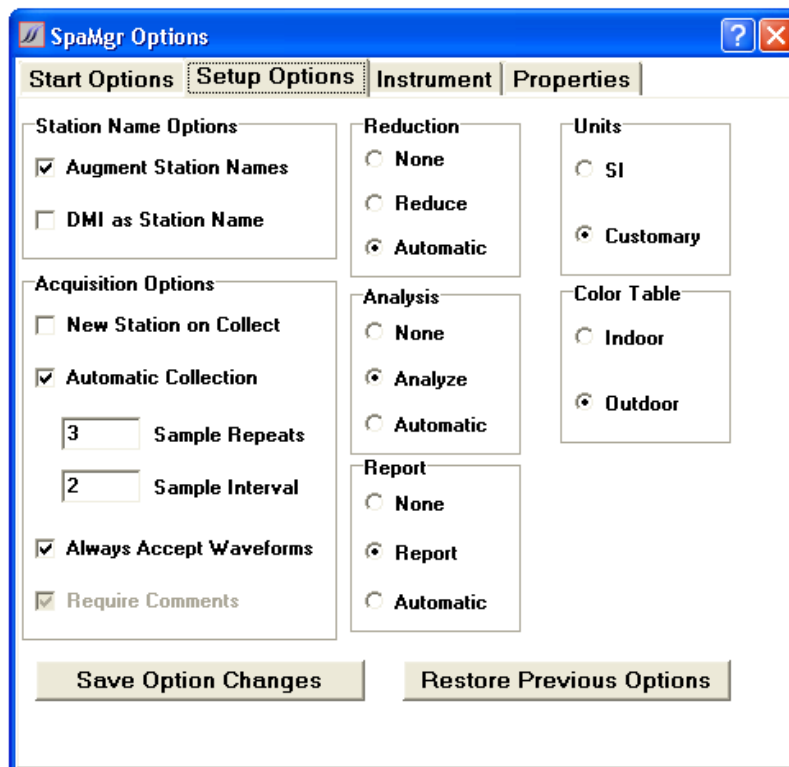
SPA Setup Options Settings

SPA Instrument Settings

SPA Material Properties Settings

141

Sta.	Time/Date	Offset	Modulus	Average	σ	Notes
1	7/10/2011 7:44	-22	610			
1	7/10/2011 7:44	-22	610			
1	7/10/2011 7:44	-22	370	530	139	N/A
1	7/10/2011 7:48	-20	730			
1	7/10/2011 7:48	-20	1390			
1	7/10/2011 7:48	-20	810	977	360	N/A
1	7/10/2011 7:50	-18	630			
1	7/10/2011 7:50	-18	840			
1	7/10/2011 7:50	-18	740	737	105	N/A
1	7/10/2011 7:51	-16	1220			
1	7/10/2011 7:51	-16	1710			
1	7/10/2011 7:51	-16	490	1140	614	N/A
1	7/10/2011 7:53	-14	550			
1	7/10/2011 7:53	-14	680			
1	7/10/2011 7:53	-14	580	603	68	N/A
1	7/10/2011 7:55	-12	1790			
1	7/10/2011 7:55	-12	830			
1	7/10/2011 7:55	-12	2530	1717	852	N/A
1	7/10/2011 7:56	-10	2310			
1	7/10/2011 7:56	-10	2120			
1	7/10/2011 7:56	-10	2750	2393	323	N/A
1	7/10/2011 7:58	-8	960			
1	7/10/2011 7:58	-8	1050			
1	7/10/2011 7:59	-8	930	980	62	N/A
1	7/10/2011 8:00	-6	380			
1	7/10/2011 8:00	-6	870			
1	7/10/2011 8:00	-6	350	533	292	N/A
1	7/10/2011 8:01	-4	2170			
1	7/10/2011 8:02	-4	2200			
1	7/10/2011 8:02	-4	2040	2137	85	N/A
1	7/10/2011 8:03	-2	360			
1	7/10/2011 8:03	-2	340			
1	7/10/2011 8:03	-2	340	347	12	Core Sample Taken
1	7/10/2011 8:04	0	360			
1	7/10/2011 8:04	0	1690			
1	7/10/2011 8:04	0	330	793	777	N/A
1	7/10/2011 8:05	2	380			
1	7/10/2011 8:06	2	770			
1	7/10/2011 8:06	2	400	517	220	N/A

Sta.	Time/Date	Offset	Modulus	Average	σ	Notes
1	7/10/2011 8:07	4	1720			
1	7/10/2011 8:07	4	1940			
1	7/10/2011 8:07	4	2040	1900	164	N/A
1	7/10/2011 8:08	6	2180			
1	7/10/2011 8:08	6	2020			
1	7/10/2011 8:08	6	2020	2073	92	N/A
1	7/10/2011 8:09	8	410			
1	7/10/2011 8:09	8	430			
1	7/10/2011 8:10	8	1350	730	537	N/A
1	7/10/2011 8:11	10	2310			
1	7/10/2011 8:11	10	3100			
1	7/10/2011 8:11	10	3300	2903	523	N/A
1	7/10/2011 8:12	12	1020			
1	7/10/2011 8:12	12	310			
1	7/10/2011 8:12	12	530	620	363	N/A
1	7/10/2011 8:13	14	2070			
1	7/10/2011 8:13	14	890			
1	7/10/2011 8:14	14	3040	2000	1077	N/A
1	7/10/2011 8:14	16	660			
1	7/10/2011 8:14	16	1190			
1	7/10/2011 8:15	16	460	770	377	N/A
1	7/10/2011 8:15	18	470			
1	7/10/2011 8:16	18	650			
1	7/10/2011 8:16	18	740	620	137	N/A
1	7/10/2011 8:16	20	5470			
1	7/10/2011 8:17	20	5330			
1	7/10/2011 8:17	20	4390	5063	587	N/A
1	7/10/2011 8:18	22	790			
1	7/10/2011 8:18	22	700			
1	7/10/2011 8:18	22	3380	1623	1522	N/A
9	7/10/2011 8:20	-22	1690			
9	7/10/2011 8:20	-22	1670			
9	7/10/2011 8:20	-22	1680	1680	10	N/A
9	7/10/2011 8:21	-20	1470			
9	7/10/2011 8:22	-20	1480			
9	7/10/2011 8:22	-20	1410	1453	38	N/A
9	7/10/2011 8:23	-18	1820			
9	7/10/2011 8:24	-18	1810			
9	7/10/2011 8:24	-18	1880	1837	38	N/A

Sta.	Time/Date	Offset	Modulus	Average	σ	Notes
9	7/10/2011 8:26	-16	1820			
9	7/10/2011 8:26	-16	1420			
9	7/10/2011 8:26	-16	1620	1620	200	N/A
9	7/10/2011 8:27	-14	2400			
9	7/10/2011 8:28	-14	720			
9	7/10/2011 8:28	-14	830	1317	940	N/A
9	7/10/2011 8:30	-12	840			
9	7/10/2011 8:30	-12	690			
9	7/10/2011 8:30	-12	980	837	145	N/A
9	7/10/2011 8:31	-10	450			
9	7/10/2011 8:32	-10	850			
9	7/10/2011 8:32	-10	570	623	205	N/A
9	7/10/2011 8:33	-8	2780			
9	7/10/2011 8:33	-8	3230			
9	7/10/2011 8:33	-8	3120	3043	235	N/A
9	7/10/2011 8:34	-6	4260			
9	7/10/2011 8:35	-6	4140			
9	7/10/2011 8:35	-6	2250	3550	1127	N/A
9	7/10/2011 8:36	-4	2850			
9	7/10/2011 8:36	-4	3130			
9	7/10/2011 8:36	-4	3150	3043	168	N/A
9	7/10/2011 8:37	-2	610			
9	7/10/2011 8:37	-2	690			
9	7/10/2011 8:37	-2	600	633	49	N/A
9	7/10/2011 8:38	0	4130			
9	7/10/2011 8:38	0	4580			
9	7/10/2011 8:39	0	4230	4313	236	Core Sample Taken
9	7/10/2011 8:40	2	1520			
9	7/10/2011 8:40	2	1790			
9	7/10/2011 8:41	2	1540	1617	150	N/A
9	7/10/2011 8:41	4	630			
9	7/10/2011 8:41	4	640			
9	7/10/2011 8:42	4	550	607	49	N/A
9	7/10/2011 8:42	6	4000			
9	7/10/2011 8:43	6	930			
9	7/10/2011 8:43	6	3690	2873	1690	N/A
9	7/10/2011 8:44	8	3800			
9	7/10/2011 8:44	8	750			
9	7/10/2011 8:44	8	3460	2670	1671	N/A

Sta.	Time/Date	Offset	Modulus	Average	σ	Notes
9	7/10/2011 8:45	10	1390			
9	7/10/2011 8:45	10	980			
9	7/10/2011 8:45	10	1230	1200	207	N/A
9	7/10/2011 8:46	12	650			
9	7/10/2011 8:46	12	620			
9	7/10/2011 8:47	12	660	643	21	N/A
9	7/10/2011 8:47	14	870			
9	7/10/2011 8:47	14	3580			
9	7/10/2011 8:48	14	3500	2650	1542	N/A
9	7/10/2011 8:48	16	640			
9	7/10/2011 8:49	16	1490			
9	7/10/2011 8:49	16	4740	2290	2164	Core Sample Taken
9	7/10/2011 8:51	18	650			
9	7/10/2011 8:51	18	780			
9	7/10/2011 8:51	18	570	667	106	N/A
9	7/10/2011 8:52	20	620			
9	7/10/2011 8:52	20	560			
9	7/10/2011 8:53	20	630	603	38	N/A
9	7/10/2011 8:53	22	2910			
9	7/10/2011 8:54	22	2910			
9	7/10/2011 8:54	22	2920	2913	6	N/A
17	7/10/2011 8:56	-22	1180			
17	7/10/2011 8:56	-22	300			
17	7/10/2011 8:56	-22	1210	897	517	N/A
17	7/10/2011 8:57	-20	850			
17	7/10/2011 8:58	-20	870			
17	7/10/2011 8:58	-20	870	863	12	N/A
17	7/10/2011 8:59	-18	1660			
17	7/10/2011 8:59	-18	1600			
17	7/10/2011 8:59	-18	1730	1663	65	Core Sample Taken
17	7/10/2011 9:00	-16	640			
17	7/10/2011 9:00	-16	670			
17	7/10/2011 9:00	-16	720	677	40	N/A
17	7/10/2011 9:01	-14	3630			
17	7/10/2011 9:01	-14	3760			
17	7/10/2011 9:02	-14	3640	3677	72	N/A
17	7/10/2011 9:02	-12	2700			
17	7/10/2011 9:03	-12	2950			
17	7/10/2011 9:03	-12	2780	2810	128	N/A

Sta.	Time/Date	Offset	Modulus	Average	σ	Notes
17	7/10/2011 9:04	-10	2720			
17	7/10/2011 9:04	-10	2870			
17	7/10/2011 9:04	-10	2570	2720	150	N/A
17	7/10/2011 9:05	-8	580			
17	7/10/2011 9:05	-8	620			
17	7/10/2011 9:05	-8	550	583	35	N/A
17	7/10/2011 9:06	-6	830			
17	7/10/2011 9:06	-6	640			
17	7/10/2011 9:07	-6	650	707	107	N/A
17	7/10/2011 9:07	-4	830			
17	7/10/2011 9:08	-4	1570			
17	7/10/2011 9:08	-4	1180	1193	370	N/A
17	7/10/2011 9:09	-2	1530			
17	7/10/2011 9:09	-2	1330			
17	7/10/2011 9:09	-2	1750	1537	210	N/A
17	7/10/2011 9:10	0	2990			
17	7/10/2011 9:10	0	1070			
17	7/10/2011 9:11	0	2630	2230	1021	N/A
17	7/10/2011 9:11	2	3100			
17	7/10/2011 9:12	2	3200			
17	7/10/2011 9:12	2	3230	3177	68	Core Sample Taken
17	7/10/2011 9:12	4	3710			
17	7/10/2011 9:13	4	2330			
17	7/10/2011 9:13	4	2860	2967	696	N/A
17	7/10/2011 9:14	6	580			
17	7/10/2011 9:14	6	580			
17	7/10/2011 9:14	6	670	610	52	N/A
17	7/10/2011 9:15	8	580			
17	7/10/2011 9:15	8	630			
17	7/10/2011 9:16	8	620	610	26	N/A
17	7/10/2011 9:16	10	680			
17	7/10/2011 9:17	10	900			
17	7/10/2011 9:17	10	640	740	140	N/A
17	7/10/2011 9:17	12	800			
17	7/10/2011 9:18	12	800			
17	7/10/2011 9:18	12	790	797	6	Core Sample Taken
17	7/10/2011 9:19	14	600			
17	7/10/2011 9:20	14	600			
17	7/10/2011 9:20	14	580	593	12	N/A

Sta.	Time/Date	Offset	Modulus	Average	σ	Notes
17	7/10/2011 9:20	16	1070			
17	7/10/2011 9:21	16	650			
17	7/10/2011 9:21	16	700	807	229	N/A
17	7/10/2011 9:22	18	1450			
17	7/10/2011 9:22	18	1900			
17	7/10/2011 9:22	18	2430	1927	491	N/A
17	7/10/2011 9:23	20	1170			
17	7/10/2011 9:23	20	900			
17	7/10/2011 9:23	20	1050	1040	135	N/A
17	7/10/2011 9:24	22	950			
17	7/10/2011 9:24	22	1300			
17	7/10/2011 9:25	22	940	1063	205	N/A
25	7/10/2011 9:26	-22	830			
25	7/10/2011 9:26	-22	880			
25	7/10/2011 9:26	-22	860	857	25	N/A
25	7/10/2011 9:27	-20	1100			
25	7/10/2011 9:27	-20	1030			
25	7/10/2011 9:27	-20	1050	1060	36	N/A
25	7/10/2011 9:28	-18	1530			
25	7/10/2011 9:28	-18	1390			
25	7/10/2011 9:29	-18	1440	1453	71	N/A
25	7/10/2011 9:29	-16	970			
25	7/10/2011 9:29	-16	1110			
25	7/10/2011 9:30	-16	1000	1027	74	N/A
25	7/10/2011 9:31	-14	600			
25	7/10/2011 9:31	-14	620			
25	7/10/2011 9:31	-14	600	607	12	N/A
25	7/10/2011 9:32	-12	2780			
25	7/10/2011 9:33	-12	2870			
25	7/10/2011 9:33	-12	2610	2753	132	N/A
25	7/10/2011 9:34	-10	960			
25	7/10/2011 9:34	-10	910			
25	7/10/2011 9:34	-10	850	907	55	N/A
25	7/10/2011 9:35	-8	360			
25	7/10/2011 9:36	-8	400			
25	7/10/2011 9:36	-8	400	387	23	N/A
25	7/10/2011 9:37	-6	2780			
25	7/10/2011 9:37	-6	3150			
25	7/10/2011 9:37	-6	2840	2923	199	N/A

Sta.	Time/Date	Offset	Modulus	Average	σ	Notes
25	7/10/2011 9:38	-4	3090			
25	7/10/2011 9:39	-4	3030			
25	7/10/2011 9:39	-4	3060	3060	30	N/A
25	7/10/2011 9:40	-2	2740			
25	7/10/2011 9:40	-2	2710			
25	7/10/2011 9:40	-2	2940	2797	125	N/A
25	7/10/2011 9:41	0	3080			
25	7/10/2011 9:41	0	3170			
25	7/10/2011 9:42	0	3190	3147	59	N/A
25	7/10/2011 9:43	2	1360			
25	7/10/2011 9:43	2	1400			
25	7/10/2011 9:43	2	1330	1363	35	N/A
25	7/10/2011 9:44	4	560			
25	7/10/2011 9:44	4	510			
25	7/10/2011 9:44	4	510	527	29	N/A
25	7/10/2011 9:45	6	4770			
25	7/10/2011 9:45	6	4380			
25	7/10/2011 9:46	6	4690	4613	206	N/A
25	7/10/2011 9:46	8	3230			
25	7/10/2011 9:47	8	3360			
25	7/10/2011 9:47	8	3300	3297	65	N/A
25	7/10/2011 9:48	10	850			
25	7/10/2011 9:48	10	780			
25	7/10/2011 9:48	10	960	863	91	N/A
25	7/10/2011 9:49	12	580			
25	7/10/2011 9:49	12	620			
25	7/10/2011 9:49	12	620	607	23	N/A
25	7/10/2011 9:50	14	560			
25	7/10/2011 9:51	14	560			
25	7/10/2011 9:51	14	620	580	35	N/A
25	7/10/2011 9:52	16	660			
25	7/10/2011 9:52	16	620			
25	7/10/2011 9:52	16	630	637	21	N/A
25	7/10/2011 9:53	18	910			
25	7/10/2011 9:53	18	870			
25	7/10/2011 9:53	18	870	883	23	N/A
25	7/10/2011 9:54	20	640			
25	7/10/2011 9:54	20	680			
25	7/10/2011 9:55	20	780	700	72	N/A

Sta.	Time/Date	Offset	Modulus	Average	σ	Notes
25	7/10/2011 9:55	22	3440			
25	7/10/2011 9:56	22	2510			
25	7/10/2011 9:56	22	630	2193	1432	N/A

APPENDIX C

MATLAB SCRIPT FOR MAPPING SPA DATA

```matlab
%joint_plot.m

%Plot of Joint Area

%Larry L. Rickard, Jr.

%31 July 2011

clc

X=[1.27, 3.27, 5.27, 7.27, 9.27, 11.27, 13.27, 15.27, 17.27, 19.27, 21.27, 23.27, 25.27,
27.27, 29.27, 31.27, 33.27, 35.27, 37.27, 39.27, 41.27, 43.27, 45.27; 1.65, 3.65, 5.65,
7.65, 9.65, 11.65, 13.65, 15.65, 17.65, 19.65, 21.65, 23.65, 25.65, 27.65, 29.65, 31.65,
33.65, 35.65, 37.65, 39.65, 41.65, 43.65, 45.65; 2.04, 4.04, 6.04, 8.04, 10.04, 12.04,
14.04, 16.04, 18.04, 20.04, 22.04, 24.04, 26.04, 28.04, 30.04, 32.04, 34.04, 36.04, 38.04,
40.04, 42.04, 44.04, 46.04; 2.42, 4.42, 6.42, 8.42, 10.42, 12.42, 14.42, 16.42, 18.42,
20.42, 22.42, 24.42, 26.42, 28.42, 30.42, 32.42, 34.42, 36.42, 38.42, 40.42, 42.42, 44.42,
46.42];

Y=[-0.083, -0.083, -0.083, -0.083, -0.083, -0.083, -0.083, -0.083, -0.083, -0.083, -0.083, -
0.083, -0.083, -0.083, -0.083, -0.083, -0.083, -0.083, -0.083, -0.083, -0.083, -0.083, -
0.083; -0.75, -0.75, -0.75, -0.75, -0.75, -0.75, -0.75, -0.75, -0.75, -0.75, -0.75, -0.75, -0.75,
-0.75, -0.75, -0.75, -0.75, -0.75, -0.75, -0.75, -0.75, -0.75, -0.75; -1.417, -1.417, -1.417, -
1.417, -1.417, -1.417, -1.417, -1.417, -1.417, -1.417, -1.417, -1.417, -1.417, -1.417, -
1.417, -1.417, -1.417, -1.417, -1.417, -1.417, -1.417, -1.417, -1.417; -2.083, -2.083, -
2.083, -2.083, -2.083, -2.083, -2.083, -2.083, -2.083, -2.083, -2.083, -2.083, -2.083, -
2.083, -2.083, -2.083, -2.083, -2.083, -2.083, -2.083, -2.083, -2.083, -2.083];
```

M=[0.530, 0.977, 0.737, 1.140, 0.603, 1.717, 2.393, 0.980, 0.533, 2.137, 0.347, 0.793,

0.517, 1.900, 2.073, 0.730, 2.903, 0.620, 2.000, 0.770, 0.620, 5.063, 1.623; 1.680, 1.453,

1.837, 1.620, 1.317, 0.837, 0.623, 3.043, 3.550, 3.043, 0.633, 4.313, 1.617, 0.607, 2.873,

2.670, 1.200, 0.643, 2.650, 2.290, 0.667, 0.603, 2.913; 0.897, 0.863, 1.663, 0.677, 3.677,

2.810, 2.720, 0.583, 0.707, 1.193, 1.537, 2.230, 3.177, 2.967, 0.610, 0.610, 0.740, 0.797,

0.593, 0.807, 1.927, 1.040, 1.063; 0.857, 1.060, 1.453, 1.027, 0.607, 2.753, 0.907, 0.387,

2.923, 3.060, 2.797, 3.147, 1.363, 0.527, 4.613, 3.297, 0.863, 0.607, 0.580, 0.637, 0.883,

0.700, 2.193];

XI=interp2(X,6);

YI=interp2(Y,6);

MI=interp2(M,6);

axis normal;

contourf(XI,YI,MI,100,'edgecolor','none');

hold on;

plot(X,Y,'+k');

set(gcf,'Colormap',jointcmap);

hold off;

APPENDIX D

NCDOT DECK JOINT SURVEY

NCDOT Bridge Deck Joint Survey

Types of Armored Joints

Please choose the deck joint type that is found most in your area.

1. Which type of armored deck joint is used the most in your area?

○ Armored "Evazote" seals

○ Armored gland-type seals with "hold-down" bars

[Next]

NCDOT Bridge Deck Joint Survey

Armored "Evazote" Seals

The following questions apply to poured-in-place ("Evazote") seals ONLY.

2. In your experience, what is the most common way for the armor of "Evazote"-type seals to fail? Please choose all that apply.

☐ Debonding or delamination of the concrete anchoring the joint from the surrounding bridge deck.

☐ Debonding of the steel anchor studs from the surrounding concrete

☐ Actual fracture or shearing of the steel anchor studs

Other (please explain)

3. What are the methods you use the most to detect failure of the joint armor in "Evazote"-type seals? Please choose all that apply.

☐ Visual evidence (cracked steel or concrete, visible movement of the armor plate)

☐ Audible evidence during direct testing (for example, using chain-drag or hammer)

☐ Audible evidence from live traffic (for example, listening for a "clank" as traffic passes over the joint)

Other (please explain)

154

Armored "Evazote" Seals

4. At what point is the decision made to replace this type of joint?

○ At the very first sign of damage to the armor plate (in other words, when cracked steel or concrete is first seen, or when "clanking" is first heard)

○ At the very first sign that the watertight integrity of the joint is compromised (in other words, when it becomes apparent that the joint is beginning to leak)

○ When it is clear that the joint has failed completely and that loosened members of the joint may present a hazard to traffic

Other (please explain)

[   ]

Prev   Next

Armored Neoprene or "Gland"-type Seals

The following three questions are regarding armored "gland"-type seals with hold-down bars ONLY.

5. For armored "gland"-type seals with hold-down bars only: In your experience, what is the most common way for the armor to fail? Please choose all that apply.

☐ Breakage of the hold-down bars

☐ Breakage of the bolts that fasten the hold-down bars

☐ Debonding or delamination of the anchoring concrete from the surrounding bridge deck

☐ Debonding of the steel studs from the surrounding concrete

☐ Breakage or shearing of the anchor studs

Other (please explain)

[   ]

Exit this survey

Armored Neoprene or "Gland"-type Seals

6. For armored "gland"-type seals with hold-down bars only: What are the methods you use the most to detect failure of the joint armor? Please choose all that apply.

☐ Visual evidence (cracked steel or concrete, visible movement of the armor plate)

☐ Audible evidence during direct testing (for example, using chain-drag or hammer)

☐ Audible evidence from live traffic (for example, listening for a "clank" as traffic passes over the joint)

Other (please explain)

[   ]

7. In your experience, at what point is the decision made to replace the joint? Please choose only ONE.

○ At the very first sign of damage to the armor plate (in other words, when cracked steel or concrete is first seen, or when "clanking" is first heard)

○ At the very first sign that the watertight integrity of the joint is compromised (in other words, when it becomes apparent that the joint is beginning to leak)

○ When it is clear that the joint has failed completely and that loosened members of the joint may present a hazard to traffic

Other (please explain)

[   ]

Prev   Next

NCDOT Bridge Deck Joint Survey

Exit this survey

Location of Damage

*8. In your experience, where do you most commonly see defects in armored deck joints (regardless of type)?

○ At the gutterline or extreme outer ends of the joint

○ At the deck centerline

○ In the wheel pathways

○ other

Prev   Next

NCDOT Bridge Deck Joint Survey

Exit this survey

Education and Experience

*9. Please choose your level of education from the choices below.

○ High school graduate (or equivalent)

○ 2-year degree (Associates degree or equivalent)

○ 4-year degree (Bachelor's or equivalent)

○ Graduate degree (Master's, Doctorate or other post-graduate study)

*10. How many years' experience do you have in the field of highway bridge maintenance, management or inspection?

○ 1-5

○ 5-10

○ 10-15

○ 15-20

○ 20 or more

Prev   Done

1. Which type of armored deck joint is used the most in your area?	Create Chart	Download

	Response Percent	Response Count
Armored "Evazote" seals	77.8%	7
Armored gland-type seals with "hold-down" bars	22.2%	2
	answered question	9
	skipped question	0

2. In your experience, what is the most common way for the armor of "Evazote"-type seals to fail? Please choose all that apply.	Create Chart	Download

	Response Percent	Response Count
Debonding or delamination of the concrete anchoring the joint from the surrounding bridge deck.	57.1%	4
Debonding of the steel anchor studs from the surrounding concrete	57.1%	4
Actual fracture or shearing of the steel anchor studs	57.1%	4
	Other (please explain)	0
	answered question	7
	skipped question	2

3. What are the methods you use the most to detect failure of the joint armor in "Evazote"-type seals? Please choose all that apply.	Create Chart	Download

	Response Percent	Response Count
Visual evidence (cracked steel or concrete, visible movement of the armor plate)	85.7%	6
Audible evidence during direct testing (for example, using chain-drag or hammer)	14.3%	1
Audible evidence from live traffic (for example, listening for a "clank" as traffic passes over the joint)	85.7%	6
	Other (please explain)	0
	answered question	7
	skipped question	2

4. At what point is the decision made to replace this type of joint?

Create Chart ⬇ Download

		Response Percent	Response Count
At the very first sign of damage to the armor plate (in other words, when cracked steel or concrete is first seen, or when "clanking" is first heard)	▬▬▬▬	42.9%	3
At the very first sign that the watertight integrity of the joint is compromised (in other words, when it becomes apparent that the joint is beginning to leak)		0.0%	0
When it is clear that the joint has failed completely and that loosened members of the joint may present a hazard to traffic	▬▬▬▬▬	57.1%	4
	Other (please explain) Show Responses		1
	answered question		7
	skipped question		2

PAGE: ARMORED NEOPRENE OR "GLAND"-TYPE SEALS

5. For armored "gland"-type seals with hold-down bars only: In your experience, what is the most common way for the armor to fail? Please choose all that apply.

Create Chart ⬇ Download

		Response Percent	Response Count
Breakage of the hold-down bars	▬▬▬	40.0%	2
Breakage of the bolts that fasten the hold-down bars	▬▬▬▬▬▬	80.0%	4
Debonding or delamination of the anchoring concrete from the surrounding bridge deck	▬▬▬▬	60.0%	3
Debonding of the steel studs from the surrounding concrete	▬	20.0%	1
Breakage or shearing of the anchor studs	▬▬▬▬	60.0%	3
	Other (please explain) Show Responses		1
	answered question		5
	skipped question		4

159

6. For armored "gland"-type seals with hold-down bars only: What are the methods you use the most to detect failure of the joint armor? Please choose all that apply.

⬤ Create Chart   ⬇ Download

		Response Percent	Response Count
Visual evidence (cracked steel or concrete, visible movement of the armor plate)		60.0%	3
Audible evidence during direct testing (for example, using chain-drag or hammer)		20.0%	1
Audible evidence from live traffic (for example, listening for a "clank" as traffic passes over the joint)		100.0%	5
	Other (please explain) Show Responses		1
	answered question		5
	skipped question		4

7. In your experience, at what point is the decision made to replace the joint? Please choose only ONE.

⬤ Create Chart   ⬇ Download

		Response Percent	Response Count
At the very first sign of damage to the armor plate (in other words, when cracked steel or concrete is first seen, or when "clanking" is first heard)		0.0%	0
At the very first sign that the watertight integrity of the joint is compromised (in other words, when it becomes apparent that the joint is beginning to leak)		0.0%	0
When it is clear that the joint has failed completely and that loosened members of the joint may present a hazard to traffic		100.0%	5
	Other (please explain) Show Responses		1
	answered question		5
	skipped question		4

160

8. In your experience, where do you most commonly see defects in armored deck joints (regardless of type)? 🥧 Create Chart ⬇ Download

		Response Percent	Response Count
At the gutterline or extreme outer ends of the joint		0.0%	0
At the deck centerline		0.0%	0
In the wheel pathways	▬▬▬▬▬▬▬	100.0%	6
other		0.0%	0
	answered question		6
	skipped question		3

9. Please choose your level of education from the choices below. 🥧 Create Chart ⬇ Download

		Response Percent	Response Count
High school graduate (or equivalent)	▬▬▬▬▬	50.0%	3
2-year degree (Associates degree or equivalent)		0.0%	0
4-year degree (Bachelor's or equivalent)	▬▬▬	33.3%	2
Graduate degree (Master's, Doctorate or other post-graduate study)	▬	16.7%	1
	answered question		6
	skipped question		3

10. How many years' experience do you have in the field of highway bridge maintenance, management or inspection? 🥧 Create Chart ⬇ Download

		Response Percent	Response Count
1-5	▬	16.7%	1
5-10	▬	16.7%	1
10-15	▬	16.7%	1
15-20		0.0%	0
20 or more	▬▬▬▬	50.0%	3
	answered question		6
	skipped question		3